Chemically Modified Ceramic Membranes- Study of Structural and Transport Properties

Graduation committee:

Chairman:	Prof.dr. ir. A. Bliek	University of Twente
Promotor:	Prof. dr. ing. D.H.A. Blank	University of Twente
Assistant promotor:	Dr. ir. J.E. ten Elshof	University of Twente
Members:	Prof. dr. ing. M. Wessling	University of Twente
	Prof. dr. A.B. de Haan	University of Twente
	Prof. dr. F. Kapteijn	Delft University of Technology
Referent:	Dr. A.J.A. Winnubst	University of Twente
	Dr. J. Vente	ECN, Petten, The Netherlands

The research described in this thesis was carried out in the Inorganic Materials Science group at the University of Twente. Financial support was provided by the Dutch Technology Foundation STW in the framework of the programme, "Hydrophobic Silica Membranes for Molecular Filtration of Air, Hydrogen and Water vapour", Project no. TFC.5426.

Chemically Modified Ceramic Membranes – Study of Structural and Transport Properties
Ashima Sah
ISBN 90-365-2311-7

Printed by PrintPartners Ipskamp, The Netherlands.

CHEMICALLY MODIFIED CERAMIC MEMBRANES – STUDY OF STRUCTURAL AND TRANSPORT PROPERTIES

DISSERTATION

to obtain
the doctor's degree at the University Twente,
on the authority of the rector magnificus,
prof. dr. W.H.M. Zijm,
on account of the decision of the graduation committee,
to be publicly defended
on Friday 3rd March 2006 at 15.00

by

Ashima Sah

born on 13th March 1977

in Bareilly, India

The dissertation is approved by the promotor
Prof. dr. ing. D.H.A. Blank and the assistant promotor Dr. ir. J.E. ten Elshof

Summary vii

Samenvatting ix

Chapter 1 General Introduction 1
1.1. Introduction 1
1.2. Overview of the existing state-of-the-art ceramic membranes 3
1.3. Challenges in ceramic membrane development 4
1.4. Goal of the work described in this thesis 5
1.5. Outline of the thesis 6
1.6. References 7

Chapter 2 Theoretical and Experimental Background 9
2.1. Sol-gel Chemistry of Silica 9
2.2. Membrane preparation: Description of the composite membrane system. 15
2.3. Experimental techniques 15
2.3.1. Particle sizing 15
2.3.2. Surface area and Porosity 16
2.3.3. Permporometry 19
2.3.4. XPS (X-ray photoelectron spectroscopy) 21
2.3.5. Solvent permeation experiments 21
2.3.6. Gas Permeation 22
2.4. References 24

Chapter 3 Hydrophobisation of mesoporous γ-Al_2O_3 with organochlorosilanes – efficiency and structure 27
3.1. Abstract 27
3.2. Introduction 28
3.3. Experimental 30
3.3.1. Materials preparation 30
3.3.2. Materials characterisation 31
3.4. Results and Discussion 31
3.4.1. Extent of modification 31
3.4.2. Physical structure 33
3.4.3. Hydrophobicity and surface polarity 40
3.5. Conclusions 40
3.6. References 41

Chapter 4 Hydrophobic modification of γ-alumina membranes with organochlorosilanes 43
4.1. Abstract 43
4.2. Introduction 44
4.3. Experimental 46
4.3.1. Membrane preparation 46
4.3.2. Membrane characterization 47
4.4. Results and discussion 47
4.5. Conclusions 56
4.6. References 57

Chapter 5 Development of sol-gel derived microporous organosilica hybrid materials 59
5.1. Abstract 59
5.2. Introduction 60
5.3. Experimental 63
5.3.1. Synthesis 63
5.3.2. Characterization Techniques 64
5.4. Results and discussion 66
5.4.1. NMR studies 66
5.4.2. Mass Spectrometry 68
5.4.3. Sol stability 71
5.4.4. Influence of pH 71
5.4.5. Influence of molar ratio of [BTESE]/ [MTES] 72
5.4.6. Influence of hydrolysis ratio 73
5.4.7. Influence of reflux time 74
5.4.8. Adsorption and density experiments 75
5.4.9. Chemical Stability of the hybrid powders 76
5.5. Conclusions 77
5.6. References 77

Chapter 6 Development of hybrid inorganic-organic silica membranes and study of transport properties. 79
6.1. Abstract 79
6.2. Introduction 80
6.3. Experimental 81
6.3.1. Membrane synthesis 81
6.3.2. Characterization Techniques 82
6.4. Results and Discussion 84
6.5. Conclusions 93
6.6. References 93

Chapter 7 Conclusions and Recommendations 95
7.1. Grafting 95
7.2. In Situ Modification 95
7.3. Future outlook for hybrid materials 97
7.4. References 97

List of Publications 99

Acknowledgements 101

Summary

This PhD thesis describes the development and separation properties of the composite membrane system α-alumina(macroporous)/γ-alumina(mesoporous)/hybrid silica (microporous).
The influence of chemical modification of the surface and pores of the mesoporous and microporous layers of the membrane by covalently bonded organic groups was studied.

Two synthesis strategies to make more hydrophobic layers have been followed in this regard. The first is grafting of the surface of the intermediate mesoporous layer with organochlorosilanes, the second one is the in situ hydrolysis and condensation of organosilane precursors to prepare microporous top layers.

The grafting of γ-alumina powders and membranes with organochlorosilanes was addressed. The effects of covalently bonded bulky long chain organosilanes and multifunctional organosilanes on the efficiency of the grafting process were investigated. Solvent and temperature effects were also investigated. The unsupported powders were characterized by nitrogen and CO_2 adsorption techniques, thermogravimetric analysis and SEM.
The effect of modification of the γ-alumina membranes with the abovementioned organochlorosilanes was studied by XPS, permporometry, and solvent permeation experiments.
Characterization of unsupported modified γ-alumina powder and the results obtained on the modified γ-alumina membranes substantiate each other. The multifunctional precursors formed a polymerized network inside the mesopores which imparted greater resistance to flow of solvents as well as a more hydrophobic character.

In order to develop a more hydrophobic microporous material than silica, a new hybrid sol prepared from 1,2-bis(triethoxysilyl)ethane and methyltriethoxy silane precursor molecules was developed. Characterization was carried out by means of dynamic light scattering measurements and mass spectrometry to determine particle size. Nanosized sols consisting of particles of 2-8 nm in ethanol were obtained. The particle size of the sol could be tuned to meet the requirements for defect-free thin film formation by varying the preparation parameters of the sol like hydrolysis ratio, pH, and molar ratio of the two precursors. In situ ^{29}Si NMR of the sols gave an insight into the development of the sol upon water addition to alcoholic solutions of the precursors.

The pore sizes and porosity of unsupported microporous powders derived from these sols were characterized by sorption of nitrogen, CO_2 and acetylene. This information helps in understanding the transport and sieving behaviour of membranes prepared from these sols.

The particle size of the sol plays a definite role in the formation of a defect-free thin film on supported γ-alumina membranes. When the particle size of the sol was small, penetration of sol particles into the underlying layers occurred, which suffocated these pores. A low flux and low separation factors were consequently observed. The use of sols made of larger nanoparticles that could not penetrate into the γ-alumina layer resulted in defect-free continuous films. The resulting hybrid silica membranes were characterized by using SEM, XPS, permporometry, gas permeation and pervaporation.
It was not possible to obtain membranes with a uniform double coated organic-inorganic hybrid silica layer. It was seen that the ethanol-based second organosilica coating did not wet the calcined first layer. This shows that the surface tension of the calcined hybrid silica membrane is small, which may be indicative of a hydrophobic surface.
The hydrophobicity of the membrane was also seen in gas permeation experiments. The membrane pores appear to provide a hydrophobic environment, as the permeance of H_2 containing water vapour at various partial pressures remained unaffected by the presence of water, unlike standard silica. Therefore it can be concluded that no adsorption of water vapour on the inner walls of the pore had taken place.

The organic-inorganic hybrid silica membranes exhibited enhanced hydrothermal stability than silica in pervaporation of a 97.5 wt% n-butanol / 2.5 wt% water mixture. It was possible to carry out this process with an organosilica membrane coated on a one meter long tube of 14 mm outer diameter at the high temperature of 150°C for an extended period (>3 months) without deterioration of the membrane. In comparison with the maximum working temperature of 95°C of standard silica membranes, this presents a significant improvement.

Samenvatting

Dit proefschrift beschrijft de ontwikkeling en scheidingseigenschappen van het composiet membraan α-alumina (macroporeus)/γ-alumina (mesoporeus)/hybride silica (microporeus). De invloed van chemische modificatie van het oppervlak en de poriën van de mesoporeuze en microporeuze lagen van het membraan door middel van covalent gebonden organische groepen is bestudeerd

Twee parallelle syntheseroutes voor het maken van hydrofobe lagen zijn gevolgd. De eerste is het zgn. graften ('enten') van het oppervlak van de intermediaire mesoporeuze laag met organochlorosilanen. De tweede betreft de in situ hydrolyse en condensatie van organofunctionele silicium alkoxide precursors voor het maken van microporeuze toplagen.

Bij het graften van γ-alumina poeders en membranen met organochlorosilanen werd het effect van covalent gebonden grote organosilanen en multifunctionele organosilanen op de efficiency van het graft-proces onderzocht. Ook werd de invloed van oplosmiddel en temperatuur bestudeerd. De poeders zijn gekarakteriseerd door middel van stikstof- en CO_2-adsorptie technieken, thermogravimetrische analyse en scanning electron microscopie (SEM). Het effect van modificatie van de γ-alumina membranen met de bovengenoemde organochlorosilanen is onderzocht met behulp van X-ray photoelectron spectroscopy (XPS), permporometrie en vloeistofpermeatie-experimenten. De resultaten die verkregen zijn op de gemodificeerde γ-alumina poeders en de gemodificeerde γ-alumina membranen zijn onderling in overeenstemming. De multifunctionele precursors vormen een gepolymeriseerd netwerk in de poriën. Dit veroorzaakt een grotere weerstand tegen vloeistoftransport, maar geeft het membraan ook een hydrofober karakter.

Om een meer hydrofoob microporeus materiaal dan silica te kunnen maken, is een nieuw hybride sol ontwikkeld, gemaakt van de precursors 1,2-bis(triethoxysilyl)ethaan en methyltriethoxysilaan. Nano-solen, bestaande uit deeltjes van 2-8 nm diameter in ethanol, zijn op deze manier verkregen. De solen zijn gekarakteriseerd door middel van dynamic light scattering experimenten en massaspectrometrie. Door aanpassing van de synthese-parameters van de sol, met name hydrolyse-ratio, pH en molaire verhouding van de twee precursors, kon de deeltjesgrootte van de sol worden aangepast om aan de eisen voor vorming van een defect-vrije dunne film te kunnen voldoen. In situ ^{29}Si NMR analyse aan deze solen verschafte inzicht in de ontwikkeling van de sol na toevoeging van water aan alcoholische oplossingen van de precursors. Uit deze solen zijn microporeuze poeders gemaakt waarvan de poriegrootte en porositeit is bepaald door middel van sorptie van stikstof, CO_2 en acetyleen. Hierdoor

kon de permeabiliteit en het scheidingsgedrag van membranen die van dezelfde solen waren gemaakt, beter worden begrepen.

De deeltjesgrootte van de sol bleek een belangrijke rol te spelen bij de vorming van defect-vrije dunne lagen op gedragen γ-alumina membranen. Als de deeltjesgrootte van de sol erg klein was, trad penetratie van de soldeeltjes in de onderliggende laag op, waardoor de poriën in die laag verstopt raakten. Deze membranen vertoonden een lage flux en lage scheidingsfactoren. Door gebruik te maken van solen met grotere nanodeeltjes kon doordringing in de onderliggende γ-alumina laag worden voorkomen, en dit resulteerde in defect-vrije continue films. Deze hybride silica membranen zijn vervolgens gekarakteriseerd met SEM, XPS, permporometrie, gaspermeatie en pervaporatie.

Het bleek niet mogelijk te zijn om membranen dubbel te coaten met de organisch-anorganische hybride silica laag. Het bleek namelijk dat de ethanol-gebaseerde tweede organosilica sol niet vloeide op de gecalcineerde eerste laag. Dit betekent dat de oppervlaktespanning van de gecalcineerde hybride silica film klein is, en dat toont mogelijk het hydrofobe karakter van dit oppervlak aan. De hydrofobiciteit van het membraan werd ook waargenomen in gaspermeatie-experimenten. De poriën van het membraan bleken een hydrofobe omgeving te verschaffen, aangezien de permeatie van H_2 met verschillende concentraties waterdamp niet werd beïnvloed door de aanwezigheid van water. Bij normale microporeuze silica membranen gebeurt dit wel, en wordt de permeatie van waterstof dientengevolge kleiner. Hieruit kon worden geconcludeerd dat in organosilica geen adsorptie van water op het binnenoppervlak van de poriën plaatsvond.

De ontwikkelde organisch-anorganische hybride silica membranen hebben een betere hydrothermale stabiliteit dan silica in de pervaporatie van een 97.5 gewicht% n-butanol / 2.5 gewicht% watermengsel. Het bleek mogelijk om dit proces uit te voeren met een microporeus organosilica membraan, aangebracht op een één meter lange buis van 14 mm buitendiameter, op een temperatuur van 150°C. Na meer dan 3 maanden continue operatie was geen duidelijke verslechtering van de kwaliteit van het membraan meetbaar. In vergelijking met de maximale werkingstemperatuur van 95°C van standaard silica membranen betekent dit een significante verbetering.

Chapter 1 General Introduction

1.1. Introduction

This thesis deals with membranes. A membrane is a semipermeable barrier which prevents contact between two phases. The barrier is permselective, i.e., it exhibits preferential permeation of one component with respect to other components of a mixture. Porous membranes have a porous top layer on a porous support, usually of a metal oxide (1). Dense metal or oxide tubes are examples of symmetric membranes, which posses a single layer of a structured material. Single walled symmetric systems have a considerable thickness for mechanical strength. In order to obtain larger fluxes the thickness of the separation layers must be reduced as much as possible. This is achieved by using asymmetric membranes which consist of a support with large pores on top of which are layers with gradually decreasing pore size.

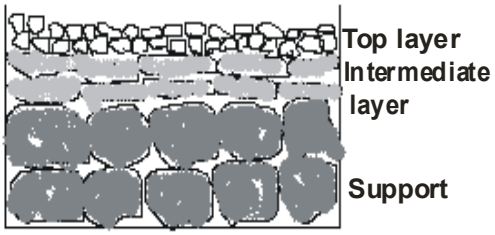

Figure 1 Schematic diagram of a composite membrane.

The pore size or pore width is the distance between two opposite walls of the pore.
According to IUPAC-definitions, pore diameters are defined as follows:

- Macropores: width > 50 nm
- Mesopores: width between 50 and 2 nm
- Micropores: width < 2 nm (supermicropores > 0.7 nm; ultramicropores < 0.7 nm).

The maximum size of ultramicropores corresponds to a bilayer thickness of nitrogen molecules adsorbed on a solid surface (2×0.354 nm).

Figure 1 depicts an asymmetric ceramic membrane with layers of decreasing thickness, used in the separation of gases and liquids by a microporous top layer. The composite membrane system of

interest in this thesis is an α-alumina (macroporous)/γ-alumina (mesoporous)/hybrid silica (microporous) stacked membrane. The macroporous support has a thickness of 1-2 mm. On top of the support is the intermediate mesoporous layer, which is 200 - 3000 nm thick. Its main purpose is to provide sufficient smoothness for deposition of an ultrathin top layer. The microporous top layer has a thickness of 30 -100 nm, and is responsible for the separation properties of the membrane.

Inorganic membranes differ from polymer membranes in having a relatively high thermal and chemical stability, biocompatibility with specific moieties, and considerable resistance to erosion. However, the production of ceramic membranes is more complicated and expensive than that of polymers.

The field of organic-inorganic hybrids as suitable oxide materials for membranes has gained recognition in recent years in advanced applications that require materials with properties that exceed those of conventional materials (2).

Hybrid materials can be made by a combination of inorganic and organic materials (3). The organic and inorganic components interpenetrate each other from the sub-micronic range down to the nanometer level. They can be divided in two classes:

- Hybrids in which organic molecules, oligomers or low molecular weight polymers exist in an inorganic network to which they are held by weak hydrogen or Van der Waals bonds.

- Hybrids in which the organic and inorganic components are bonded by strong covalent or partially covalent bonds.

In this thesis the development of new hybrid inorganic-organic membranes from silsesquioxanes as starting precursors is discussed. Silsesquioxanes are described by the formula $(RSiO_{1.5})_n$. They derive the name from the fact that each silicon atom is linked on an average to one and a half (sesqui) oxygen (ox) atoms and to one hydrocarbon group (ane). They are obtained by hydrolytic condensation of trifunctional silanes, e.g., alkoxysilanes, silanols and silanolates. By careful control of the reaction kinetics, incorporation of surfactants or organic molecules as templates, the porosity as well as the periodicity of the materials can be tuned according to requirements. The hydrocarbon groups can vary and impart optical as well as dielectric properties in the material (2). Thus the hybrids act as a bridge between inorganic and organic materials.

1.2. Overview of the existing state-of-the-art ceramic membranes

This section describes the state of the art silica-based membranes and their transport properties as reported by different authors, briefly.

The state-of-the-art microporous silica based membranes have shown good separation properties in gas separation but suffer from water adsorption at room temperature due to the hydrophilicity of the silica surface. De Lange et al. (4) studied polymeric silica and mixed SiO_2/ TiO_2, SiO_2/ ZrO_2 and SiO_2/ Al_2O_3 sols for ceramic membranes. These sols were analysed by small angle X-ray scattering. The authors found that prehydrolysis of the silica precursor TEOS was the best method to synthesize polymeric binary systems. They concluded that the consolidation of weakly branched polymers would result in microporous materials.

Nair (5) has also studied silica based membranes based on TEOS, from varying compositions of water, acid and aging time. Gas transport through these membranes was studied. They found that the flux of N_2 molecule was insignificant through selective pores of the membrane whereas He molecules showed activated diffusion. The size of such pores was reported to be 3 Å. The authors also studied pervaporation of methanol/methyltert-butylether at 323 K. They have reported separation factors as high as 300 and fluxes around 0.3 kg/(m^2.h).

An alternative approach to make stable pervaporation membranes was pursued by Sekulic et al. (6), who developed and studied doped silica membranes for alcohol dehydration by pervaporation. The aim of the work was to develop inorganic membranes that would broaden the application of pervaporation technology in industry. The systems SiO_2-Al_2O_3-TiO_2-ZrO_2-MgO were investigated for chemical stability and pervaporation performance in alcohol dehydration processes. It was found that, depending on the nature and amount of dopant, composite membranes with improved pervaporation characteristics and chemical stability were obtained. The study was carried out because in silica based systems the most mature membrane is the stacked system α-alumina-γ-alumina-silica (7), but its operation window is limited, particularly at a combination of high temperature and high pH (8). Both mesoporous γ-alumina and microporous silica show a limited chemical stability at extreme pH values. The authors concluded that doping silica with zirconium or titanium led to a moderate improvement of the chemical stability, while cations with a lower valency led to a reduction of the chemical stability of the silica matrix. Microporous silica doped with small amounts of zirconium showed improved performance in pervaporation, compared with undoped silica material. The flux was significantly reduced when ~10 mol% Al was present, while the other systems showed fluxes similar to silica itself.

The presence of very small concentrations of Al in the silica layer may be beneficial for the separation performance, however. Sekulic et al. (9) studied the pervaporation properties of two microporous three-layer ceramic membranes that differ only in the nature of the mesoporous interlayer. The membrane system α-alumina/γ-alumina/microporous silica was found to have a higher selectivity for dewatering of alcohols than the corresponding membrane with a mesoporous anatase layer. The difference was attributed to the presence of acidic Al^{3+} sites in the silica layer when γ-alumina was used as intermediate layer material. It was concluded that this increased the hydrophilicity of the silica top layer.

De Vos et al. (10) developed hydrophobic silica membranes for gas separation. The authors proposed a method for reducing water molecule interaction by in situ synthesis using a hydrophobic precursor. The standard silica membranes were prepared by dip-coating supported γ-alumina membranes in a diluted sol, followed by thermal treatment at 400°C. The standard silica sol was prepared by acid-catalysed hydrolysis and condensation of tetra-ethyl-ortho-silicate (TEOS) in ethanol (11). In order to make the silica material more hydrophobic, methyl-tri-ethoxy-silane (MTES) was incorporated at a certain stage of sol preparation. The final membranes prepared from a combination of TEOS and MTES showed very high gas permeance for small molecules such as H_2, CO_2, N_2, O_2 and CH_4. For a double-coated silica membrane layer, the authors reported a total thickness of 60 nm and a pore size of 0.6 nm. The membranes were found to be 10 times more hydrophobic than the state-of-the-art silica membranes, based on measurements of the hydrophobicity index. The hydrophobicity index is defined by the ratio $HI= x_{octane}/x_{water}$. In this method, the samples were dried at 250 °C in an Ar stream. After that an Ar stream containing defined and equal concentrations of water and octane was used to load the sample until saturation at 30 °C. The values of x_{octane} and x_{water} were obtained by integration of the breakthrough curves of individual components obtained by gas chromatography (12).

1.3. Challenges in ceramic membrane development

- Conventional ceramic microporous and mesoporous membranes are hydrophilic by nature. The hydroxyl groups present in the structure and on the pore surface are the main sources of hydrophilicity as they promote the adsorption of water. This may lead to pore blocking at ambient conditions. The operating conditions, such as temperature and the environment under which the membranes are used, are affected. In industry, where reactions are done on a large scale, it would be energy and cost conserving if the temperatures could be lowered.

- The silica structure that is most commonly used to make a microporous layer consists of siloxane bridges (Si-O-Si) and terminal hydroxyl groups, which can interact with water, leading to deterioration of the membrane and ultimately to loss of separation properties. The stability of the membrane is limited to certain maximum temperatures and water vapour concentrations beyond which the membrane microstructure will break down. Increasing the hydrothermal stability of microporous silica is therefore a challenge. Campaniello et al. found that the incorporation of covalently bonded methyl groups in microporous silica membranes enhanced the service time in dehydration of a butanol-water mixture at 96 °C from a few weeks to more than 18 months with a water flux of about 4 kg m^{-2} h^{-1} and a separation factor between 500 and 20000 (13). However, the maximum concentration of methyl groups relative to silicon atoms in this membrane was only 30%. A higher content of methyl groups led to a collapse of the siloxane network.

1.4. Goal of the work described in this thesis

The goal is to increase the hydrophobicity of the membrane, so that capillary condensation of water vapour is inhibited and operating temperatures can be lowered, and simultaneously hydrothermal stability of silica can be increased. This can be done by incorporating hydrocarbon groups, resulting in hybrid organosilica. Increase of membrane hydrophobicity and improvement of hydrothermal stability may be achieved by the same strategy and the improvement of both properties will help in widening the window of operation of silica based membranes.

The following approaches describe the steps towards reaching the goal.

- The first strategy is to post-modify a mesoporous inorganic membrane by grafting the internal pore surface with organosilanes. A hydrolysable group of the organosilane undergoes coupling with the surface hydroxyl groups of the mesoporous oxide layer, forming a chemically bound monolayer that imparts the desired hydrophobicity.
- Another route is to make a hydrophobic layer by in situ hydrolysis and condensation of alkoxide precursors with hydrophobic side groups, such as organosilanes or bridged silsesquioxanes. The advantages in the latter case being a homogeneous distribution of organic groups in the network, as the organic groups reside in the walls of the material.

Both strategies are discussed in this thesis. The modification of state of the art mesoporous ceramic membranes by organofunctional groups, and the development of a microporous hybrid inorganic organic membrane for gas and liquid separation processes are described.

1.5. Outline of the thesis

Chapter 2 gives an introduction to the sol gel chemistry of silica, the state of the art composite membrane system that is used in this study, and presents a description of the experimental techniques that have been used in this thesis for the characterization of structural and transport properties of membranes.

Chapter 3 is a detailed nitrogen and carbon dioxide adsorption study of the effect of grafting mono-, di- and trifunctional chlorosilanes on the pore structure of mesoporous γ-alumina powders. The parameters affecting the extent of grafting like length of the hydrocarbon group, functionality, and reactions conditions, i.e., type of solvent and temperature, are discussed. It was found that methylchlorosilanes are most effective in bringing about a homogeneous modification, as it presents the least steric hinderance.

Chapter 4 discusses the hydrophobic modification of γ-alumina membranes with organochlorosilanes.The effect of monofunctional, difunctional, trifunctional precursors in forming a polymerized layer and the steric influence of bulky side groups in affecting the grafting process are compared. It is seen that the surface concentration on the membrane and also the extent to which the hydrophobic moiety enters the pores determines the permeability towards solvents.

Chapter 5 describes the development of sols for hybrid silica membranes from silsesquioxane precursors. The effect of various processing parameters on the particle size and morphology of the sol are discussed. The pore structure of calcined powders directly derived from these sols is studied by vapour adsorption. It is shown that microporous powders with pore sizes smaller than 0.28 nm and almost no pore sizes larger than 0.30 nm were obtained.

Chapter 6 is a continuation of the work described in Chapter 5. It discusses the development of the formation of uniform thin supported membranes from the hybrid sols described in Chapter 5, and several transport measurements carried out on the resulting supported hybrid silica membranes.

In Chapter 7 the conclusions of this work and recommendations for future study and application are discussed.

1.6. References

1) A. J. Burggraaf, “Important Characteristics of Inorganic Membranes”; pp. 21-34 in Fundamentals of Inorganic Membrane Science and Technology, Vol., 4 , Edited by A. J. Burggraaf and L. Cot, Elsevier Science, Amsterdam,1996.

2) K. J. Shea and D. A. Loy, Chem. Mater. 2001, 13, 3306-3319.

3) A. C. Pierre, “New types of Sol-Gel Derived Materials”; pp. 251-278, in: Introduction to Sol-Gel Processing, Kluwer Academic Publishers group, Dordrecht, The Netherlands, 1998.

4) R. S. A. de Lange, J. H. A. Hekkink, K. Kiezer and A. J. Burggraaf, Journal of Non- Crystalline Solids 191, 1995, 1-16.

5) Balagopal N. Nair, PhD thesis, ” Structure-Property Relationships in Silica sols, Gels and Molecular- sieving Membranes”, University of Twente, The Netherlands, Enschede, 1998.

6) J. Sekulic, M. W. J. Luiten, J. E. Ten Elshof, N. E. Benes, K.Keizer, Desalination 148, 2002, 19-23.

7) H. M. van Veen, Y. C. van Delft, C. W. R. Engelen and P. P. A. C. Pex, Sep. Purification Technol., 22-23, 2001, 361-366.

8) R. K. Iler, The Chemistry of Silica; Solubility, Polymerisation, Colloid and Surface Properties and Biochemistry, Wiley, New York, 1979.

9) J. Sekulic, J. E. ten Elshof, D. H. A. Blank, J. Membr. Sci., 254, 2005, 267-274.

10) R. M. de Vos, W. F. Maier, H. Verweij, J. Membr. Sci., 158, 1999, 277-288.

11) R. M. de Vos, H. Verweij, J. Membr. Sci. 143, 1998, 37.

12) R. de Vos, High-Selectivity, High-Flux Silica Membranes for Gas Separation, PhD thesis, University of Twente, Enschede, The Netherlands, 1998.

13) J. Campaniello, C. W. R. Engelen, W. G. Haije, P. P. A. C. Pex and J. F. Vente, Chem. Commun., 2004, 834-835.

Chapter 2 Theoretical and Experimental Background

2.1. Sol-gel Chemistry of Silica

A common method to prepare ceramic membranes is by the sol gel process. Sol-gel processing can generate materials with controlled pore structures between 0.3 and 500 nm. The sol-gel process offers higher purity and homogeneity, and lower processing temperatures compared to traditional ceramic methods. The properties of sol-gel materials are governed by numerous reaction parameters like temperature, starting concentration of precursors, hydrolysis ratio, acid concentration, and reflux time. Hydrolysis ratio is defined as the molar ratio of water to precursor. The pore structure and permeability of the porous network can be tuned to meet requirements.

Solution chemistry of metal alkoxide precursors

Sol-gel processing does not refer to a particular technique, but to a broad set of procedures that are central to a single scheme as shown in Figure 2.1. There are two general routes to sol-gel processing.

One involves formation of colloids in aqueous media where agglomeration of particles is prevented by mutual repulsion of similar electrostatic charges at the particle surfaces. The other route involves the use of metal-organic precursors in alcoholic media. The polymeric particles remain separated in solution because of their small size (1). Both routes yield nano-sized particles from which porous membranes and materials can be produced. The colloidal route yields rather dense nanoparticles, which can serve as building blocks for mesoporous materials: Since the packing of spherical nanoparticles will leave some pores between them that are too large for making microporous materials, they end up in the final body as mesopores. The polymeric route, on the other hand, is very useful for making microporous materials.

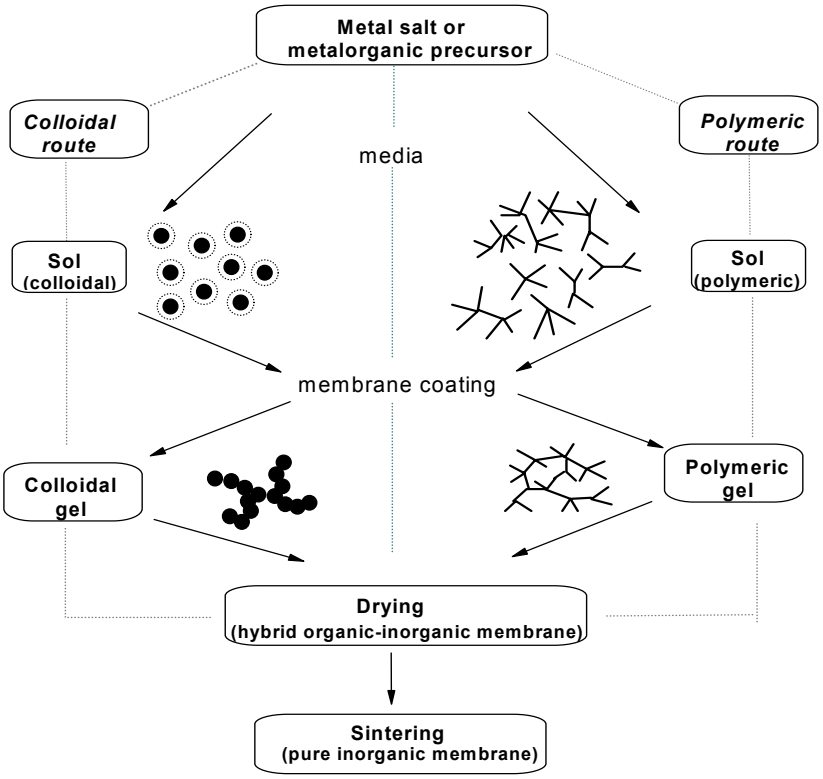

Figure 2.1 Diagram showing two sol-gel routes used in ceramic membrane preparation (2).

The advantages of metal alkoxide precursors like $Si(OC_2H_5)_4$ and CH_3-$Si(OCH_3)_3$ over metal salts are their high purity and the absence of interference by anions (e.g., Cl^-, NO_3^-) during the sol gel reactions. With metal alkoxides the residuals products of sol gel reactions are alcohols, which can be easily removed.

The first step in a sol gel process is selecting the precursors of the desired material. It is the precursor, which by its chemistry, leads to the formation of either colloidal particles or polymeric gels depending on reaction conditions (3).

The main steps in sol gel reactions are hydrolysis and condensation as shown schematically below.

Hydrolysis $Si(OR)_4 + n\ H_2O \rightleftharpoons Si(OR)_{4-n}(OH)_n + nROH$

Condensation $\equiv Si\text{-}OH + RO\text{-}Si \equiv \rightleftharpoons \equiv Si\text{-}O\text{-}Si \equiv + ROH$ (alcohol)

$\equiv Si\text{-}OH + HO\text{-}Si \equiv \rightleftharpoons \equiv Si\text{-}O\text{-}Si \equiv + H_2O$ (water)

The factors influencing the hydrolysis of metal alkoxides are the nature of the metal cation M, the nature of the alkyl group R, the nature of the solvent, the species concentration, water to alkoxide ratio $[H_2O]/[M]$, temperature, and acid/base catalyst, which are discussed later.

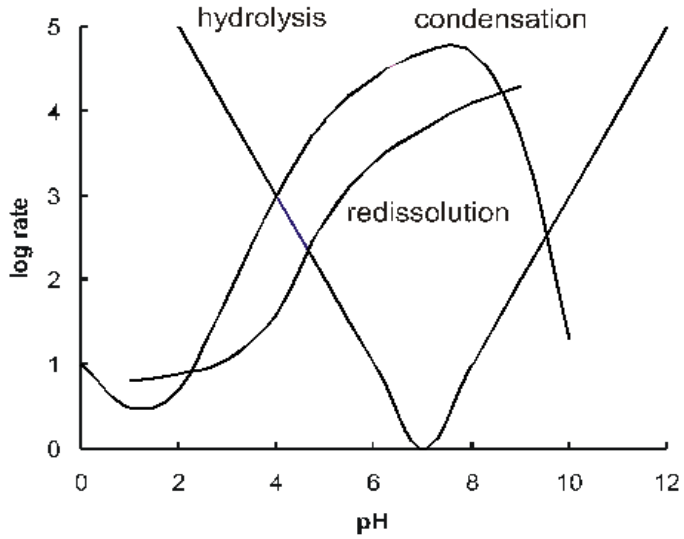

Figure 2.2 Rates of hydrolysis, condensation and redissolution of TEOS as a function of pH (4).

Figure 2.2 shows the progress of hydrolysis, condensation and redissolution of TEOS (tetraethylorthosilicate) as pH is varied. As hydrolysis and condensation proceed, a three-dimensional network is built up that ultimately forms a solid phase. The process is accelerated by heat as the rates of the hydrolysis and condensation reactions increase with temperature. The kinetics of hydrolysis and condensation, and formation of polymers are dependent on pH and a variety of materials with different structures can be obtained. The materials can be polymeric or dense colloidal particles or small particles with less weakly bonded cross-linked clusters of polymers. For silicon alkoxides, the three main reaction steps, i.e., hydrolysis, condensation and redissolution, are in eternal competition with one another. The final composition of the sols depends on the kinetics of these reactions and they vary according to pH.

Factors affecting reactivity of metal alkoxides

Influence of ligand

Table 2.1 Variation of hydrolysis rate constant with –R group (3).

$Si(OR)_4$ R	hydrolysis rate constant (10^{-2} l/mol s H^+)
- C_2H_5	5.1
- C_4H_9	1.9
- C_6H_{13}	0.83

The above table shows the variation of hydrolysis rate constant with –R group. In general, bulkier alkyl groups lead to slower rates of hydrolysis.

Replacement of alkyl groups R' for alkoxy groups OR increases the electron density of the silicon atom. Van Bommel et al. (5) found that the addition of small amounts of an alkyl-substituted ethoxysilane $R'Si(OR)_3$ to a mixture of TEOS (tetraethylortho silicate), ethanol and water has a large effect on the hydrolysis and condensation of the TEOS (tetraethylorthosilicate) mixture. It was found that MTES (methyl triethoxysilane) hydrolyses 7 times faster than TEOS under the same conditions.

Influence of water-to-alkoxide ratio

The stoichiometry of the net reaction of TEOS into silica requires two moles of water per mole of TEOS. The overall reaction is given below:

$Si(OCH_2CH_3)_4$ (liq.) + $2H_2O$ (liq.) = SiO_2 (solid) + $4HOCH_2CH_3$ (liq.)

In practice, this amount of water leads to incomplete reaction, and weak, cloudy aerogels. Most aerogel recipes, therefore, use a higher water ratio than is required by the balanced equation (anywhere from 4-30 equivalents).

The hydrolysis ratio is defined here as the molar ratio of water to precursor.

Hydrolysis ratio <<4 slow hydrolysis (non-Si)

Hydrolysis ratio ~ 4 fast hydrolysis and gelation (3D network)

Hydrolysis ratio >> 4 dilution effect: slower condensation (colloidal synthesis)

Acid catalysed hydrolysis of silicon alkoxide

Under acid catalyzed sol-gel conditions the first step is a fast protonation of the alkoxy group. The alkoxy group is substituted by water according to an S_N2 reaction accompanied by inversion of the silicon tetrahedron.

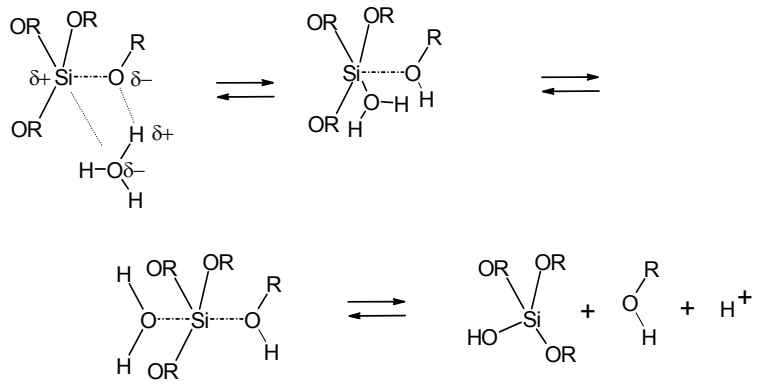

Figure 2.3 Mechanism of acid catalysed hydrolysis of silicon alkoxides (3).

Acid catalysed condensation

Acid catalyzed condensation leads to the formation of an oxo bridge (Si-O-Si), resulting in the formation of mainly linear polymers.

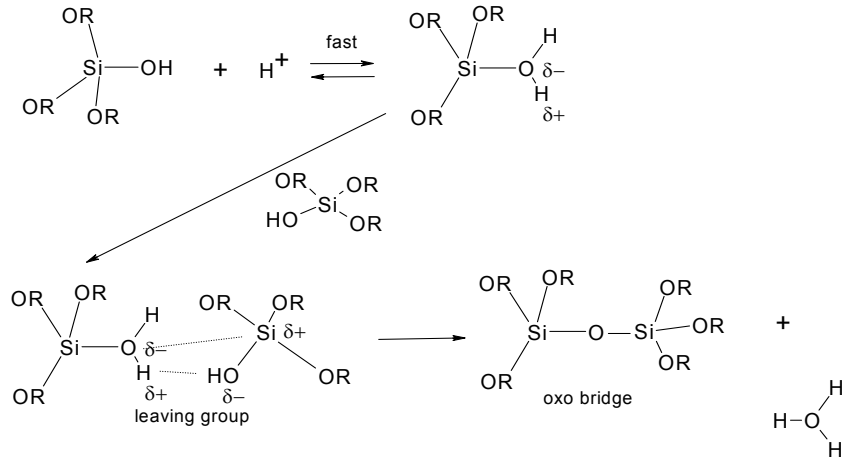

Figure 2.4 Acid catalysed condensation of silicon alkoxides (3).

Base catalysed hydrolysis

The hydrolysis reaction in basic conditions proceeds via a pentavalent negatively charged intermediate.

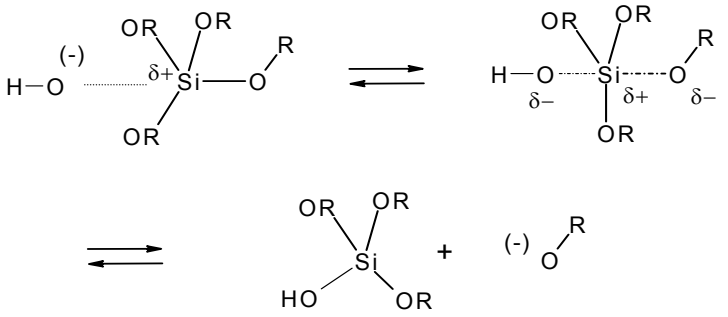

Figure 2.5 Base catalysed hydrolysis of silicon alkoxides (3).

Base catalysed condensation

Under basic conditions, condensation is much faster than under acidic conditions, and the reactivity increases with a decreasing number of alkoxy groups. A nucleophilic hydroxyl anion interacts with the silicon of the alkoxysilane.

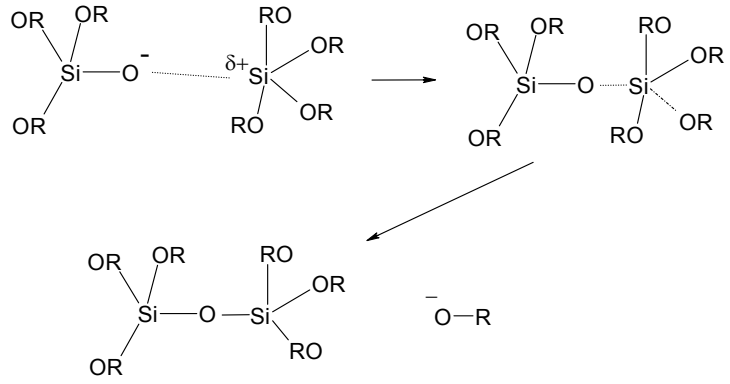

Figure 2.6 Base catalysed condensation of silicon alkoxides (3).

Acid catalysis is associated with fast hydrolysis rates and relatively long gel times whereas under basic conditions hydrolysis is slow and condensation rates are faster, giving rise to shorter gel times. Acid catalyzed condensation leads to the formation of an oxo bridge (Si-O-Si), resulting in the formation of mainly linear polymers. Condensation of silanols under basic conditions results in highly branched dense polymers.

2.2. Membrane preparation: Description of the composite membrane system.

The membrane consists of a macroporous α-alumina support and a thin mesoporous γ-alumina layer. The α-alumina supports are made by colloidal filtration of well-dispersed 0.4 μm α-alumina particles (AKP-30, Sumitomo). The dispersion is stabilized by peptizing with nitric acid. After drying at room temperature, the filter compact is sintered at 1100ºC. Mesoporous γ-alumina membranes are prepared by dip coating the above mentioned porous α-alumina supports in a boehmite sol, followed by drying and calcination at 600ºC for 3 h. The boehmite (γ- AlO(OH) sol is prepared by the colloidal sol-gel route using aluminium-tri-sec-butoxide(ALTSB). 70 mol of double distilled water is heated till 90 °C and 0.5 mol of (ALTSB), is added dropwise, in a N_2 stream (1). The temperature of the reaction mixture should be 80 °C, to prevent the formation of bayerite ($Al(OH)_3$) (6). After the addition of (ALTSB), the reaction vessel is kept at 90°C to evaporate butanol, which is formed during the course of the reaction. The solution is then cooled to 60°C, and the reaction mixture is peptised with HNO_3 to a pH of 2.8. The mixture is stirred vigorously throughout the reaction. The reaction mixture is refluxed for 20 hours at 90 °C resulting in a homogeneous and stable 0.5 molar boehmite sol solution. During 20 hours of refluxing the pH increases to 3.5. If the sol is peptised to a pH of 3.5 before the 20 hours of refluxing, the final pH will be about 4.4 resulting in fast aggregation of boehmite particles (1).

The membranes are coated with a silica sol by dip coating. The membranes are placed in a N_2 furnace and heated to 400-600 °C for 3 h, with a heating and cooling rate of 0.5 °C/min. The result is a silica membrane with a pore size of around 0.5 nm and a thickness of 30 nm. For further details, the reader is referred to reference (1).

2.3. Experimental techniques

2.3.1. Particle sizing

Photon Correlation Spectroscopy (PCS), also known as Dynamic Light Scattering (DLS) or Quasi-Elastic light scattering (QELS), is a method to measure Brownian motion of particles in suspension and relates this to the size. The Brownian motion is the random movement of particles due to the bombardment by the solvent molecules that surround them. The larger the particle, the more slowly it moves. This random motion causes the intensity of light scattered from the particles to form a moving speckle pattern. This movement can be detected as a change in intensity with time with suitable optics

and a photomultiplier. DLS is used to determine the size of particles in the range of approximately 2-1000 nm suspended in organic or aqueous solution (7).

The higher the temperature, the more rapid will be the movement. When the temperature goes up, the viscosity decreases and the Brownian motion speeds up, so this helps in getting better signal to noise ratios.

If the viscosity goes up, the movement will be slowed. In the PCS experiment, a particle in a light beam scatters light into space. The scattered light interferes with the original light beam. This creates the well know speckle pattern in space. If the particle moves, the interference will show a Doppler effect. The difference in frequency is low enough to be captured by a photo-detector. This creates an electric current pulse for each photon it receives. The Doppler frequency contains all velocity information of the particle.
The parameter calculated by DLS technique is defined as the translational diffusion coefficient (D). The particle size is then calculated from the translational diffusion coefficient (D).The relation between the size of a particle and its speed due Brownian motion is defined in the Stokes- Einstein equation. The hydrodynamic diameter d(H) is the effective diameter of the particles in the medium.

$$d(H)= kT/3\pi\eta D \qquad [1]$$

where k = the Boltzmann constant, T = absolute temperature, η= viscosity, and D = translational diffusion coefficient of particles.
PCS instruments consist of a laser, normally He-Ne, which acts as the light source. Then a detector with a photomultiplier, captures the scattered photons and sends the information to a computer.

2.3.2. Surface area and Porosity

Gas adsorption measurements are used for determining surface area and pore size distribution of a variety of different solid materials, such as industrial adsorbents, catalysts, ceramics and building materials (8).

Adsorption is the enrichment of one or more components in an interfacial layer. Physisorption occurs whenever an adsorbable gas (the adsorptive) is brought in contact with the surface of the solid (the adsorbent). The pore filling mechanisms are dependent on the pore shape and are influenced by the properties of the adsorptive and by the adsorbent-adsorbate interactions. The whole of the accessible volume present in micropores may be regarded as adsorption space and the process which then occurs is micropore filling.

Physisorption in mesopores takes place in two or less distinct stages (monolayer-multilayer adsorption and capillary condensation). For physisorption, the monolayer capacity (nm) is usually defined as the amount of adsorbate needed to cover the surface with a complete monolayer of molecules. The surface coverage (θ) for both monolayer and multilayer adsorption is defined as the ratio of the amount of adsorbed substance to the monolayer capacity.

The surface area of the adsorbent (A_s) may be calculated from the monolayer capacity (n_m^a in moles), provided that the area (a_m) effectively occupied by an adsorbed molecule in the complete monolayer is known. Thus,

$$A_s = n_m^a . L . a_m \qquad [2]$$

where L is the Avogadro constant. The specific surface area (a_s) refers to unit mass of adsorbent: $a_s = A_s/m$.

The majority of physisorption isotherms may be grouped into the six types shown in Figure 2.7. The reversible Type I isotherm is concave to the p/p^o axis and n_a approaches a limiting value as $p/p^o \rightarrow 1$. Type I isotherms are given by microporous solids having relatively small external surfaces (e.g. activated carbons, molecular sieve zeolites and certain porous oxides), the limiting uptake being governed by the accessible micropore volume rather than by the internal surface area.

The reversible Type II isotherm is the normal form of isotherm obtained with a non- porous or macroporous adsorbent. This isotherm represents unrestricted monolayer- multilayer adsorption.

The reversible Type III isotherm is convex to the p/p^o axis over its entire range. In such cases, the adsorbate-adsorbent interactions play an important role.

Characteristic features of the Type IV isotherm are its hysteresis loop, which is associated with capillary condensation taking place in mesopores, and the limited uptake over high p/p^o. The initial part of the Type IV isotherm is attributed to monolayer-multilayer adsorption since it follows the same path as the corresponding part of a Type II isotherm obtained with the given adsorptive on the same surface area of the adsorbent in a non-porous form. Type IV isotherms are given by many mesoporous industrial adsorbents.

Type V isotherm is uncommon, it is related to type III isotherm in that the adsorbent-adsorbate interaction is weak, but is obtained with certain porous adsorbents.

Type VI isotherm, in which the sharpness of the steps depends on the system and the temperature, represents step wise multilayer adsorption on a uniform non porous surface. The stepwise height represents monolayer capacity for each adsorbed layer and in the simplest case remains constant for two or three adsorbed layers. Amongst the best examples of type VI isotherms are those obtained with argon or krypton on graphitised carbon blacks at liquid nitrogen temperature.

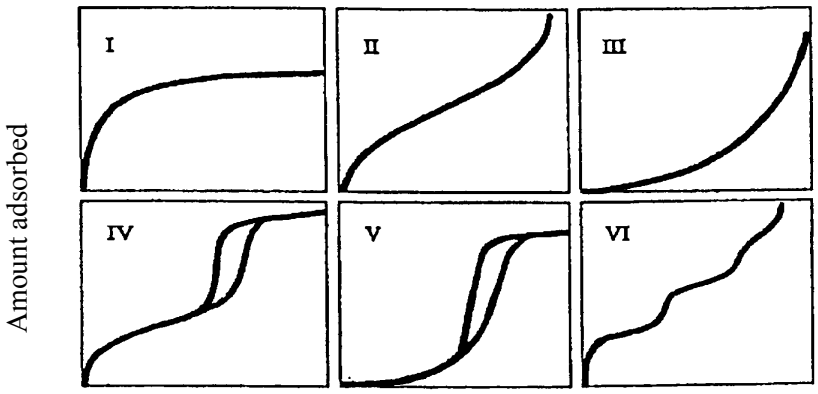

Figure 2.7 Type of physisorption isotherms

Adsorption/desorption isotherms of N_2 (77 K) and CO_2 (273 K) are determined by pretreating all materials by evacuation below 10^{-4} mbar at 473 K. Surface areas and *C*-values are determined by BET-3 fits (9, 10) of N_2 adsorption isotherms between $p/p_0 = 0$ and 0.5, according to:

$$n/n_m = C(p/p_0)/(1 - p/p_0) \times (1 - (N+1)(p/p_0)^N + N(p/p_0)^{N+1}) / (1 + (C-1)(p/p_0) - C(p/p_0)^{N+1}) \quad [3]$$

with n the gas adsorbed at relative pressure p/p_0, n_m the monolayer capacity of the surface, both in mol per g adsorbent, C a constant related to heat of adsorption and thus to the adsorbate-adsorbent interaction and N the number of adsorbed layers. From the 3-parameter fits of the isotherms (eq. 3), surface areas A were determined with:

$$A = n_m a_m N_A \quad [4]$$

in which a_m is the area occupied by a N_2 molecule in the completed monolayer, assumed to be 0.162 nm^2, and N_A Avogadro's number.

Mesopore size distributions are obtained from BJH fits (11) of the N_2 desorption isotherms between $p/p_0 = 0.35$ and 0.9. This method is based on Kelvin's equation, stating that condensation occurs in pores with radius r_K at a relative pressure p/p_0, which for cylindrical pores is represented by:

$$\ln(p/p_0) = -2 \gamma_s V_{mol} / RTr_K \quad [5]$$

with γ_s the surface tension of the liquid-vapour interface (8.85 mJ/m^2 for N_2), V_{mol} the molar volume of the condensed N_2 (34.7 cm^3), R the gas constant and T the temperature. During desorption, as the relative vapour pressure decreases, the larger pores are opened first. The t-layer remains after all pores

are opened, and desorbs subsequently. For a cylindrical pore, the relation between the real pore radius (r_p) and the Kelvin radius (r_K) is

$$r_p = r_K + t \quad [6]$$

where t is the thickness of the t-layer formed on the inner surface of the pores.

Total pore volumes were determined at $p/p_0 = 0.95$. In order to allow comparison of the different samples, the adsorbed amounts are expressed in terms of the volume of the adsorbed N_2 liquid, with a density of 0.8086 g/cm^3.

Surface areas from CO_2 adsorption isotherms are determined from fits according to the Dubinin method, modified by Kaganer (12) between $p/p_0 = 7x10^{-4}$ and $1.2x10^{-2}$, represented by:

$$\log n = \log n_m - D (\log p_0/p)^2 \quad [7]$$

with *D* an adsorbate-dependent constant. The surface area is subsequently calculated according to eq. (4), assuming the area a_m occupied by a CO_2 molecule is 0.179 nm^2.

2.3.3. Permporometry

Permporometry (13) is a method employed to determine the pore size distribution in the mesoporous membrane layers. Permporometry measures active pores only. The active pores are effective for gas diffusion, whereas passive pores are dead- end ones and do not contribute to gas diffusion. In applications, such as gas separation, only the active pores in porous media are important and a narrow size distribution of the active pores is essential.

Permporometry is based on the controlled blocking of pores by capillary condensation of a vapour phase and simultaneous measurement of the diffusional flux of a non-condensable gas through the remaining open pores. The condensable vapour chosen here is cyclohexane (the temperature of cyclohexane should be about 70 ºC), as it has a high evaporation rate and is inert to the membranes to be characterized, while oxygen is used as the non-condensable gas. When cyclohexane is brought in contact with a porous medium, several mechanisms of physisorption occur on the inner surface of the pores as the relative vapour pressure increases from zero to unity. First, a monomolecular layer is formed on the inner surface of the pores. As the relative vapour pressure increases further, a multi-molecular layer starts to form. This adsorptive layer of vapour phase on the inner surface of the pores is called the t-layer. When the relative vapour pressure rises further, capillary condensation occurs on the inner surface of the pores according to Kelvin equation, also described in the previous section, equation [5].

$$\ln P_{rel} = -\frac{\gamma_s V_{mol}}{RT}\left(\frac{1}{r_{K,1}} + \frac{1}{r_{K,2}}\right)\cos\theta \qquad [8]$$

P_{rel} is the relative vapour pressure of the condensable vapour, γ_s the surface tension of the liquid-vapour interface (N/m), V_{mol} the molar volume of the condensable vapour (m^3/mol), R the gas constant (J/mol K), T the temperature (K), θ the contact angle which the liquid makes with the pore wall, and $r_{k,1}$ and $r_{k,2}$ the Kelvin radii (m), which are the radii of curvature of the vapour-liquid interface under consideration. When it is assumed that the condensable vapour wets the membrane material completely, then θ=0. Assuming that the pores are cylindrical, $r_{k,1}$ and $r_{k,\,2}$ are equal to the Kelvin radius r_k of the cylinder, and Eq. (8) transforms into

$$\ln P_{rel} = -\frac{2\gamma_s V_{mol}}{RTr_K} \qquad [9]$$

The desorption process is used for measurement of the pore size distribution. As the relative vapour pressure decreases, the larger pores are opened first. The t-layer remains after all pores are opened, and desorbs subsequently. For a cylindrical pore, the relation between the real pore radius (r_p) and the Kelvin radius (r_k) is

$r_p = r_k + t$ [10]

where t is the thickness of the t-layer formed on the inner surface of the pores.

The above equation is also mentioned in the previous section, equation [6].

Permporometry is not valid for microporous materials (r<1.7 nm), but suitable for mesoporous systems.In this section a brief overview of the existing literature on permporometry is also presented. Permporometry study on the size distribution of active pores in porous ceramic membranes has been studied by Cao et al. (14). The authors studied the pore size distribution in γ- alumina membranes with pores ranging from about 2 nm to 10 nm. The ceramic membranes used for this study was La- doped γ-alumina membrane with porous α- alumina as the substrate.The authors used cyclohexane as the condensable vapour because it meets the requirements mentioned for a condensable gas (15, 16). Nitrogen was used as a carrier gas for the condensable gas. Oxygen gas was used to study gas diffusion through the membranes. The oxygen partial pressure varies with the relative vapour pressure of cyclohexane. In this method there is no overall pressure gradient across the membrane. The oxygen gas transport through the substrates is due to the oxygen gas concentration gradient across the sample. Therefore the oxygen gas transported through the substrates is assumed to be proportional to the oxygen differential partial pressure across the substrates in the pressure range measured (from 0 to 1 atm). The permporometry experiments reported by the authors were performed using the desorption process (14). This is because a shorter time is needed to equilibrate. The equilibrium time was 20-40 min for desorption process and much longer for adsorption ones.

Fain et al. (17) measured γ- alumina porous membranes using carbon tetrachloride as a condensable vapour, and measured pore size distributions as small as 2 nm.

Huang et al. (18) have measured pore size of γ- alumina membranes by changing permeation temperature at constant vapour pressure.

2.3.4. XPS (X-ray photoelectron spectroscopy)

XPS also known as electron spectroscopy for chemical analysis is an analytical technique that provides compositional information from the top few atom layers of the sample by probing it with a mono-energetic X-ray beam.

X-rays penetrate deep into the sample surface, exciting photoelectrons. However photoelectrons can travel only a short distance before their energy is modified due to interaction with neighbouring atoms. Only photoelectrons that escape with their original energy contribute to a peak in the spectrum. In practice such photoelectrons originate from atoms in near-surface layers. In the present study, XPS was carried out on supported γ-alumina membranes with a PHI Quantera Scanning ESCA microprobe with an analysis depth of 5-75 Å and a spatial resolution < 10 μm. The Si 2p, Al 2p and O 1s energy bands are analyzed and depth profiles of the concentrations of Si, Al and O inside the membrane were obtained by sputtering with Ar^+ at a sputter rate of 24 nm/min (3 ke V 2×2mm Ar+).

2.3.5. Solvent permeation experiments

Steady state liquid flux measurements are carried out using solvents in a dead-end nanofiltration cell on membranes.

1 Nitrogen cylinder
2 Pressure vessel
3 Pressure meter
4 Safety valve
5 Temperature meter
6 Solution release tap
7 Membrane
8 Low pressure side
9 Magnetic stirrer
10 Permeate flow
11 Beaker
12 Balance
13 Computer

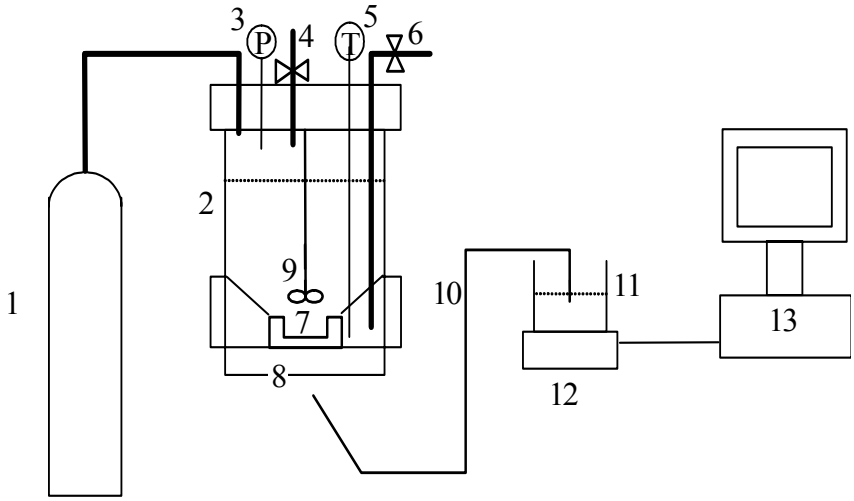

Figure 2.8 Schematic of a liquid permeation set up.

Flux is defined as the rate of permeation of feed components through unit area of membrane at unit time. The most commonly used flux unit in liquid permeation processes is kg/(m^2.h)

$J_i = m_i/(A_m . t)$ [13]

J_i is the flux of component "i" or the total flux and m_i is the mass of component permeated "i" or the total permeate weight through an effective membrane surface area (A_m) during time t. The volume of the cell in the set up used was 700 ml and the operating pressure range was kept at 2-14 bar (19). The stirring speed in the cell was kept constant at 200 rpm.

According to Darcy's law, when the transport mechanism obeys the viscous flow model, the flux is proportional to the applied pressure, irrespective of the type of liquid. The mathematical formulation of Darcy's law is

$j = -(k_m/\eta)\,\Delta p$ [14]

where J is the volumetric flux, η the bulk liquid viscosity, and ΔP the applied pressure difference across the membrane. The membrane permeability coefficient k_m of a single membrane layer with pore radius r is defined as

$k_m = \varepsilon r^2/8\tau L$ [15]

where ε is the porosity of membrane material, τ the tortuosity of the membrane layer, and L the membrane layer thickness. The above equation shows that k_m is a constant that depends only on the structural properties of the membrane material, not on the physical properties of the permeating liquid (20).

2.3.6. Gas Permeation

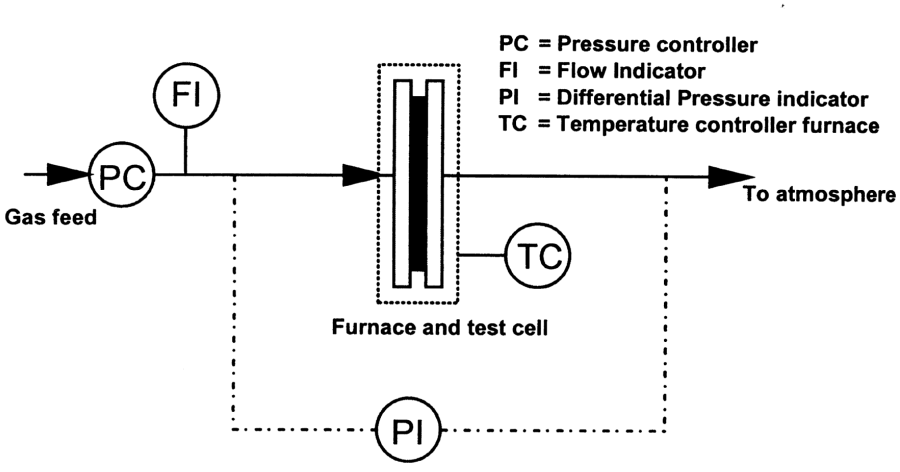

Figure 2.9 Schematic of a gas permeation set up

Figure 2.9 gives an experimental set up for permeance of gases. The membranes were dried for several hours at 200°C to remove adsorbed water from the micro pores (1). The membranes were placed in

permeance cells with the micro porous top layer at the feed side. The pressure difference over the membrane is adjusted by an electronic pressure controller. The mass flow meters measure the gas flow through the membrane with maximum flow ranges of 25 or 100 cm^3/min (STP). The pressure over the membranes is measured with an electronic pressure transducer.

2.3.7. Pervaporation

In pervaporation the liquid mixture is placed in contact with one side of a membrane, while the other side is kept under vacuum. The driving force for the transport of components is a chemical potential gradient across the membrane. Separation of components takes place due to selective evaporation and subsequent diffusion of the most volatile and mobile components from the liquid feed (21).

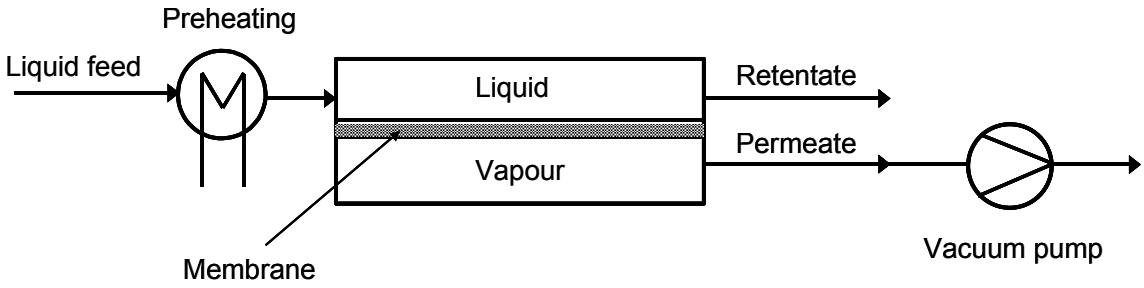

Figure 2.10 Schematic representation of the pervaporation process

A schematic representation of the vacuum pervaporation process is shown in Figure 2.10 (22). The feed flows along one side of the membrane and a fraction of the feed (permeate) passes through the membrane, leaving as vapor on the opposite side of the membrane. The permeate is collected after condensation in the liquid state. In order to increase process efficiency, the retentate, composed of the feed materials that do not pass through the membrane, is usually recycled to the feed container.

Pervaporation and vapour permeation technologies have better separation capacity and energy efficiency than competing distillation, adsorption and extraction technologies and their application may lead to considerable energy reductions (23). The main advantage of pervaporation over distillation is that it is independent of relative volatilities of components, and not limited by the vapor–liquid equilibrium.

Separation performance of a membrane is characterized by two parameters: flux and separation factor. Two types of selectivities are defined for a membrane: ideal selectivity and actual selectivity. The ideal selectivity is simply the ratio of fluxes of pure substances through the membrane J_i/J_j, and the actual selectivity α of a membrane in a binary system is defined as the ratio of concentrations of components *i* and *j* in the permeate to that in the feed:

$$\alpha = \frac{y_i / x_i}{y_j / x_j}, \qquad [16]$$

in which y and x are the fractions of components i and j in the permeate and feed, respectively.

The selectivity of a membrane is strongly influenced by two factors: the affinity of the membrane towards one (or more) component(s) of the feed, and the ease of diffusion of the permeating molecules through the membrane. The overall selectivity of a membrane can also be defined as the product of process selectivity, α_P and membrane selectivity, α_M:

$$\alpha = \alpha_P \cdot \alpha_M \qquad [17]$$

Either or both of these selectivities contribute to the preferential permeation of feed components through a given membrane. The separation factor of the process α_P is due to the differences in the vapour partial pressures of the feed components, e.g., in ethanol-water mixtures the vapour will be enriched with ethanol because its higher partial vapour pressure at a given temperature, so $\alpha_P < 1$. The vapour mixture then goes through the membrane, which has an intrinsic selectivity α_M. Therefore, the choice of proper membrane materials is a crucial factor for a specific separation. However, a material with high affinity towards one component of the feed may also lead to the higher selectivity. The operating parameters also influence the overall performance of a pervaporation process, in addition to the specific characteristics of the feed components and the membrane. These parameters include feed temperature, concentration of the components in the feed, and downstream pressure (24).

2.4. References

1) R. de Vos, High-Selectivity, High-Flux Silica Membranes for Gas Separation, PhD thesis, University of Twente, Enschede, The Netherlands, 1998.

2) C. Guizard, “Sol- gel chemistry and its application to porous membrane processing” pp. 227-258, Fundamentals of Inorganic Membrane Science and Technology, Vol., 4, Edited by A. J. Burggraaf and L. Cot, Elsevier Science, Amsterdam, 1996.

3) A. C. Pierre, “The Chemistry of Precursors solutions” pp. 11-89, in: Introduction to Sol- Gel Processing, Kluwer Academic Publishers group, Dordrecht, The Netherlands, 1998.

4) A. C. Pierre, “General Introduction” pp. 1-9, in: Introduction to Sol- Gel Processing, Kluwer Academic Publishers group, Dordrecht, The Netherlands, 1998.

5) M. J. van Bommel, T. N. M. Bernards and A. H. Boonstra, J. Non. Cryst. Solids, 128, 1991, 231-242.

6) B. E.Yoldas, J. Appl. Chem. Biotechnol., 23, 1973, 803-809.

7) Basic PCS training course, Malvern- Goffin- Meyvis.

8) K. S. W. Sing, D. H. Everett, R. A. W. Haul, L. Moscou, R. A. Pierotti, J. Rouquerol, T. Siemieniewska, Pure & Appl. Chem., 57, 4, 1985, 603-619.

9) S. Brunauer, P.H. Emmet, E. Teller, J. Amer. Chem. Soc., 60, 1938, 309.

10) S. J. Gregg, K. S. W. Sing, pp. 42, in Adsorption, Surface Area and Porosity, 2nd Ed., Academic Press, London, 1982.

11) E. P. Barrett, L. G. Joyner, P. P. Halenda, J. Am. Chem. Soc., 73, 1951, 373.

12) M. G. Kaganer, Zhur. Fiz. Khim, 33, 1959, 2202.

13) C. Eyraud, M. Betemps, J. F. Quinson, F. Chatelut, M. Brun, and B. Rasneur, Bull. Soc. Chim. France, 237, 1984, 9 -10.

14) G. Z. Cao, J. Meijerink, H. W. Brinkman and A. J. Burggraaf, J. Membr. Sci., 83, 1993, 221-235.

15) F. P. Cuperus, Characterization of ultrafiltration membranes: pore structure and top layer thickness, PhD. Thesis, University of Twente, The Netherlands, 1990.

16) F. P. Cuperus, D. Bargeman and C. A. Smolders, J. Membr. Sci., 71, 1992, 57-67.

17) D. E. Fain, "A dynamic flow-weighed pore size distribution", in: J. Charpin and L. Cot (Eds.), First Int. Conference on Inorganic Membranes, Montpelier, France, 1989, pp. 199-205.

18) P. Huang, X. Nanping, J. Shi, Y. S. Lin, J. Membr. Sci., 116, 1996, 301.

19) S. Roy Chowdhury, J. E. ten Elshof, N. E. Benes and K. Kiezer, Desalination, 144, 2002, 41.

20) S. Roy Chowdhury, Ordered and Disordered Porous materials for Nanofiltration application, PhD Thesis, University of Twente, Enschede, The Netherlands, 2005.

21) J. E. ten Elshof, C. Rubio Abadal, J. Sekulic, S. Roy Chowdhury, D. H. A. Blank, Micropor. Mesopor. Mater., 65, 2003, 197-208.

22) J. Sekuic, PhD thesis, Mesoporous and microporous Titania membranes, PhD thesis, University of Twente, Enschede, The Netherlands, 2004.

23) X. Feng, R.Y. M. Huang, Industrial & engineering chemical research, 36, 4, 1997, 1048-1066.

24) G. H. Koops and C. A. Smolders, pp. 249 – 273, Pervaporation membrane separation process, Edited by R.Y. M. Haung, Elsevier, Amsterdam, 1991.

Chapter 3 Hydrophobisation of mesoporous γ-Al_2O_3 with organochlorosilanes – efficiency and structure*

3.1. Abstract

γ-Al_2O_3 materials with small mesopores are hydrophobised by reactions with organochlorosilanes in liquid media. The structure of the modified materials is studied by means of physisorption and high-resolution SEM. A good measure of the decrease in surface polarity can be obtained from BET-fits of the N_2 isotherms. It was found that many pores become blocked by using chlorosilanes with bulky organic groups, while a more open structure is preserved for methylchlorosilanes. Using toluene as a solvent leads to a higher extent of modification than ethanol, as observed for methylchlorosilanes. Multifunctional organochlorosilanes (i.e. with 2 or 3 Cl-groups) are more reactive but also give rise to blockage of some of the microporous part as a result of polymerisation reactions. Mono- and difunctional methylchlorosilanes give the best results for alumina materials with small mesopores, preserving an open structure and leading to homogeneous modification. Modification with methylchlorosilanes in toluene leads to the lowest surface polarity. The results give clues for optimising the procedures for hydrophobisation of porous materials with small mesopores.

* H.L. Castricum, A. Sah, M.C. Mittelmeijer-Hazeleger, and J.E. ten Elshof, Microporous and Mesoporous Materials, 83, 1–9 (2005).

3.2. Introduction

Porous alumina is employed as an adsorbent for a range of applications, including chromatography, heterogeneous catalysis and membrane technology. Characteristics that contribute to its applicability include chemical as well as a high mechanical and thermal stability. Alumina is frequently used as a catalyst carrier, as its high strength makes it resistant to erosion, guaranteeing a long catalyst lifetime. Moreover, the surface can be made either acidic or basic by simple treatments. The highly porous γ-alumina phase has the largest range of applications of the aluminas, and is commonly used for hydrotreating, hydrocracking, hydrogenation, reforming and methanation. In membranes, γ-Al_2O_3 can be used either as an intermediate layer between an α-alumina support and a selective microporous top-layer or as a selective mesoporous layer on a support (1-3). As the surface is typically occupied by a large number of hydroxyl groups, enabling strong H-bonding with water, γ-Al_2O_3 is hydrophilic by nature. Whereas crystalline microporous silicas such as silicalite are hydrophobic due to their specific structure, amorphous SiO_2 is also highly hydrophilic (4,5). Employment of microporous and mesoporous amorphous silica and alumina in wet atmospheres will thus lead to rapid filling of the pores, which impairs the applicability in moist gas mixtures. Under severe conditions, hydrothermal stability becomes an important factor, as water may 'dissolve' M-O-M bonds (M=Al,Si), which will eventually give rise to another physical structure. In the case of membranes and chromatography, this leads to destruction of the separation functionality and thus limits the operating conditions under which they can be applied.

Adsorption of water can be inhibited if surface hydroxyl groups are replaced by hydrolytically stable groups with a hydrophobic character, such as alkyl or phenyl. For silica, one approach is to build in this organic functionality by in situ hydrolysis and condensation of alkoxide precursors with hydrophobic side groups, such as organosilanes or bridged silsesquioxanes (6). By this method, de Vos et al. were able to prepare hydrophobic silica layers using a combination of tetraethoxysilane and methyltriethoxysilane as the hydrophobisation agent, which resulted in a microporous silica membrane with methyl groups incorporated in the silica structure (7). However, as such hybrid precursors do not exist for alumina, the most obvious approach for mesoporous materials is post-modification by grafting the internal pore surface with hydrophobic groups. One of these possible hydrophobisation methods is a chemical reaction between chloride groups of an organochlorosilane with the surface hydroxyl groups. A thermally stable chemically bound layer is thus formed, which imparts the desired hydrophobicity. Agents with long organic tails have a significant effect (8), as only one bond with the solid material is needed for the creation of a large hydrophobic surface, shielding several OH-groups at a time. However, application of these reagents may be limited for materials with small pore sizes due

to steric hindrance. Multifunctional organosilanes, i.e. with two or more reactive groups, may undergo more extensive coupling with the OH-groups, and may thus especially reduce the number of vicinal OH-groups that are responsible for the strongest hydrophilic interaction (4,5,9). However, they may also react with each other, thereby forming a polymeric layer with only a small number of covalent bonds to the surface, which can however be quite effective in surface hydrophobisation (10,11). Various reports exist on successful modification of unsupported materials such as used for chromatography (12-15) and of composite materials such as membranes, e.g. by fluorinated silanes (16-18), chloro- and alkoxyorganosilanes (19-20). For catalyst preparation, a large number of post-modification procedures with various functional groups have been studied, e.g. (21). In selected systems, catalyst activity can be enhanced by hydrophobisation of the surface (22,23). Few studies, however, exist on preservation of the structure (24,25), especially for alumina. Nevertheless, structural preservation is an important additional requirement if separation applications are considered, which is even more so the case for materials with small mesopores.

Infra-red (IR) characterisation of membranes showed that the extent of grafting depends on the nature of the silanes used and was achieved most effectively with multifunctional agents. The N_2 adsorption and desorption isotherms showed a decrease in surface area and micropore volume for membranes silylated with $Me_2Si(OEt)_2$ or $MeSi(OEt)_3$, indicating that the pore wall had been covered by grafted moieties (26). Van Gestel (8) reported the effect of surface modification of γ-Al_2O_3/TiO_2 multilayer membranes with difunctional (2 chloride groups) C1 and C8 silanes for applications involving non-polar organic solvents. The highest hydrophobicity for mesoporous membranes was obtained with C8 silanes, which supports the view that silanes with long organic tails are advantageous. For microporous membranes, the authors concluded that silane coupling reactions took place in pores situated at the outer membrane surface, while reactions at the internal surface were sterically hindered for both C1 and C8 silanes.

In a simultaneous study (11), we investigated the modification of γ-alumina membranes with various organochlorosilanes by means of XPS and DRIFTS and reported the permeability of the membranes towards both polar and nonpolar liquids. In order to enhance understanding of the observed effects, we study the structural changes induced by modification of the unsupported materials, which can be characterised well by sorption techniques. γ-Al_2O_3 was used with a pore size of about 4 nm. In concordance with ref. (11), we applied a series of monofunctional, difunctional and trifunctional organochlorosilanes with organic groups of different sizes, in order to assess the influence of functionality and size of the silane on the extent of grafting and on the structure. Easily applicable liquid phase silination with the addition of a nucleophile (water) was chosen for its high reactivity at

low temperatures (24). Several procedures were followed to study the effect of the solvent and of H_2O addition. Surface and pore modification were studied by N_2 and CO_2 physisorption, TPO-MS, and SEM.

3.3. Experimental

3.3.1. Materials preparation

Mesoporous γ-alumina flakes were prepared from a boehmite sol, which was dried and subsequently calcined at 873 K in air, as described in detail in ref. (27). Chlorotriphenylsilane ($(C_6H_5)_3SiCl$, CTPhS, 96% purity), ter*t*-butylchlorodimethylsilane ($(CH_3)_3CSi(CH_3)_2Cl$, tBCDMS, 97% purity), chlorotrimethylsilane ($(CH_3)_3SiCl$, CTMS, 99% purity), dichlorodimethylsilane ($(CH_3)_2SiCl_2$, DCDMS, 99% purity) and trichloromethylsilane ($(CH_3)SiCl_3$, TCMS, 97% purity) were all obtained from Aldrich. The γ-alumina materials were hydrophobised by immersing them for a period of 12 h (unless stated otherwise) in 2-5 wt.% solutions of the above-mentioned precursors. An average 4 g of material was prepared at a time. The procedures are summarised in Table 1.

Table 1: Preparation procedures for modified γ-Al_2O_3 flakes.

	Silane	Solvent	Temperature (K)	Time (h)
A1	$(CH_3)_3CSi(CH_3)_2Cl$	Toluene	298	24
A2	$(CH_3)_3CSi(CH_3)_2Cl$	Toluene + 5 wt% H_2O	323	12
A3	$(C_6H_5)_3SiCl$	Toluene	298	24
A4	$(C_6H_5)_3SiCl$	Toluene + 5 wt% H_2O	323	12
A5	$(CH_3)_3SiCl$	Toluene + 5 wt% H_2O	323	12
A6	$(CH_3)_3SiCl$	Ethanol + 5 wt% H_2O	298	12
A7	$(CH_3)_2SiCl_2$	Ethanol + 5 wt% H_2O	298	12
A8	$(CH_3)SiCl_3$	Toluene + 5 wt% H_2O	323	2.5

In all cases, an excess of silane was present in order to enable full hydrophobisation of the Al_2O_3 surface, i.e. reactions could take place with all OH-groups in the material. As the reaction rates of the precursors under different conditions vary, some differences in preparation time were followed. The chlorosilanes with large organic groups (tBCDMS, CTPhS) and the multifunctional TCMS are more soluble in toluene than in water or alcohols. These precursors were allowed to react with the alumina surface in toluene with 5 vol% water (samples A2, A4 and A8). The systems were refluxed at 323 K in

order to enhance dissolution of the precursors. A8 was refluxed for just 2.5 h due to the comparatively high reactivity of TCMS. Alternatively, tBCDMS and CTPhS were dissolved in pure toluene - without water - and the reaction was carried out at room temperature for 24 h (A1 and A3). CTMS and DCDMS were dissolved in ethanol with 5 vol% water at room temperature (A6 and A7), while the influence of the solvent on modification by CTMS was further studied by dissolving this agent in toluene with 5 vol% water, again at 323 K (A5). After removal from the solution, the alumina flakes were rinsed 5 times with ethanol and dried at 473 K for 1 h in a flow of N_2 (100 ml/min, purity 99.999%) with heating/cooling rates of 0.5 K/min.

3.3.2. Materials characterisation

Thermogravimetric Analysis-Mass Spectrometry was carried out in a Setaram TG 85 thermobalance. The weight was recorded as a function of temperature during heating in synthetic air (20% O_2 in N_2, 99.999% purity, 60 ml/min). Initial masses were typically 150 mg. Heating was carried out at 10 K/min from room temperature to 1073 K (held for 30 min). A correction for the temperature-dependency of the buoyancy was performed. Analysis of reaction products was simultaneously carried out by means of a quadrupole mass spectrometer. In this way, carbon-containing molecules and fragments could be identified in the off-gas, which assisted in estimating the extent of surface modification.

Adsorption/desorption isotherms of N_2 (77 K) and CO_2 (273 K) were determined on a CE-Instruments 1990.

High resolution Scanning Electron Microscopy was carried out on a LEO Gemini 1550 FEG-SEM at a voltage of 2.0 kV.

3.4. Results and Discussion

3.4.1. Extent of modification

By heating in synthetic air, a weight loss was observed by TGA-MS for all materials. The weight loss is due to desorption of physisorbed water and dehydroxylation on one hand and to oxidation and decomposition of organic groups on the other. The latter contribution could be observed from the MS signals of CO_2 and other organic components, and evidences that modification of the alumina surface with silanes was successful. However, both the weight loss as observed by TGA and the release of organic species – including CO_2 – as observed by MS took place over a broad temperature range. As a consequence, it was not possible to distinguish between the contributions of dehydroxylation and that

of desorption and oxidation of organic fragments by means of the MS response. However, by considering the weight losses above 473 K (the pre-treatment temperature for N_2 physisorption), and comparing these to the weight loss of as-calcined unmodified γ-alumina, a good impression of the total extent of modification could be obtained such that the various modification procedures can be compared. These data are expressed in percentages of the end mass (i.e. after calcination in air at 1073 K) in Table 2.

Clearly, the weight loss for calcined – unmodified – γ-alumina is small, and no organic components were detected. Modification with the bulky tBCDMS and TCPhS and also with CTMS/toluene has led to a roughly similar amount of organic groups in the alumina. Moreover, the rate of oxidation was at a maximum around the same – high – temperature, i.e. 720 K, so it can be assumed that the organic surface structures were tightly bound.

Table 2: Analytical data (relative weight change above 473 K, pore volume at p/p_0= 0.95, N_2 surface area, C-value of the BET fit, CO_2 surface area, mean pore diameter and mean mesopore diameter from BJH fit) for γ-alumina materials (pure and modified with tert-butylchlorodimethylsilane, chlorotriphenylsilane and chloromethylsilanes). Liquid phase: toluene or EtOH (indicated).

Sample	Silane, conditions	$\Delta m/m_{end}$ (%)	v_p (cm^3/g)	$A(N_2)$ (m^2/g)	C	$A(CO_2)$ (m^2/g)	Mean d_p (nm)	d_p BJH (nm)
A	None	4	0.319	258	96	154	4.94	4.19
A1	$(CH_3)_3CSi(CH_3)_2$ Cl	27	0.141	216	157	121	2.62	3.6
A2	$(CH_3)_3CSi(CH_3)_2$ Cl	27	0.124	229	104	155	2.17	3.23
A3	$(C_6H_5)_3$ SiCl	26	0.047	70	-	150	2.67	-
A4	$(C_6H_5)_3$ SiCl	28	0.127	220	154	139	2.32	3.36
A5	$(CH_3)_3$ SiCl	28	0.230	276	79	131	3.33	4.07
A6	$(CH_3)_3$ SiCl, EtOH	7	0.297	249	181	154	4.66	4.00
A7	$(CH_3)_2$ $SiCl_2$, EtOH	9	0.289	268	150	142	4.33	3.99
A8	(CH_3) $SiCl_3$	12	0.224	216	89	-	4.16	3.81

Thermal analysis of methylethoxysilanes by Alami Younssi showed a maximum at similar temperatures (26). The smaller extent determined for TCMS can be associated with the short

preparation time (2.5 h as compared to at least 12 h for the other silanes) which has deliberately been held in view of the high reactivity of TCMS (11). The extent of modification with DCDMS and CTMS in EtOH was much more limited. The bonds between the silanes and γ-Al_2O_3 were earlier found to be stable towards water exposure (11), which was evident from an unchanged silane concentration present on the surface as observed by DRIFT Spectroscopy.

3.4.2. Physical structure

Adsorption/desorption isotherms were determined for both pure and silinated γ-alumina. N_2 isotherms are shown in Figure 1 and the corresponding analytical data are given in Table 2.

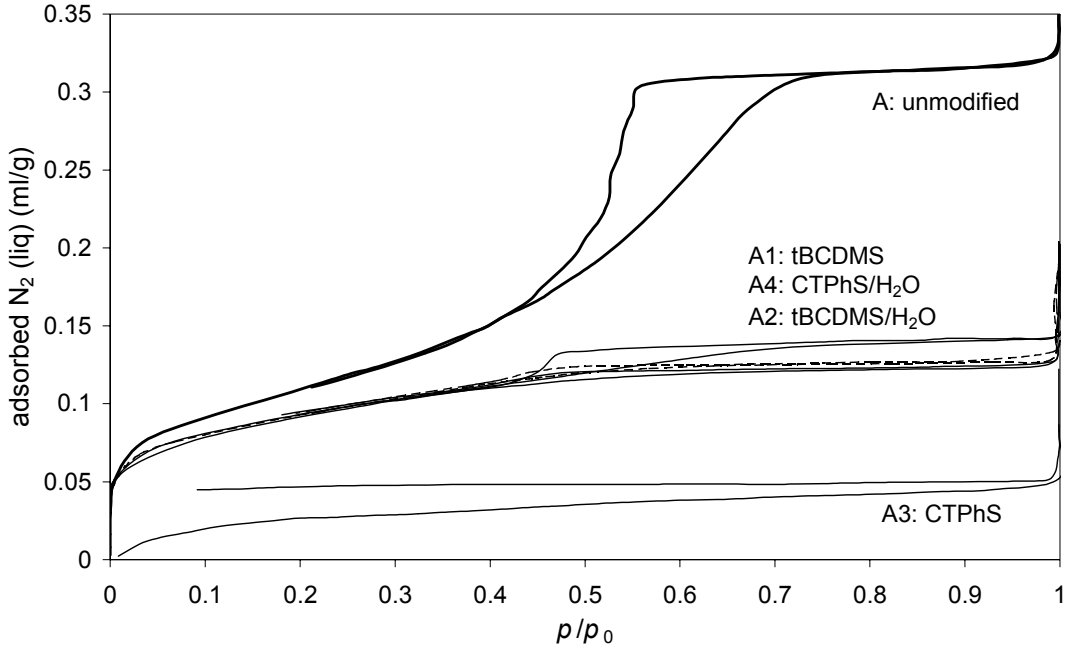

Figure 1a

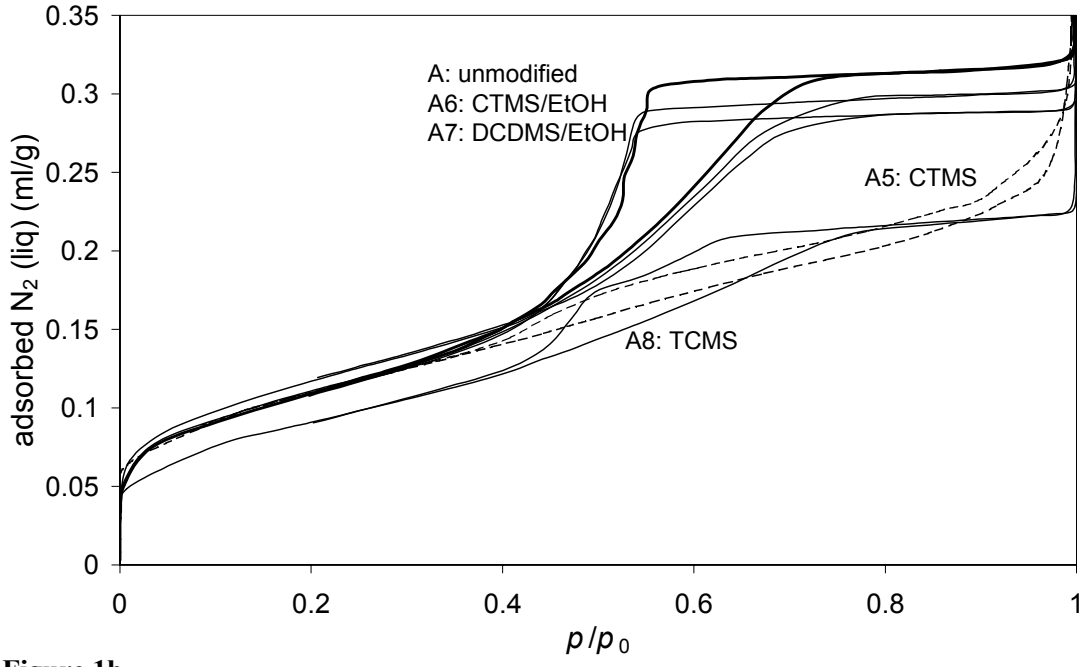

Figure 1b

Figure 1*:* N_2 physisorption isotherms for pure γ-alumina and materials modified with tert-butylchlorodimethylsilane and chlorotriphenylsilane (a) and with chloromethylsilanes (b). The dashed curves refer to samples A4 and A5.

The isotherms of unmodified γ-Al_2O_3 and the methylsilane-grafted materials indicate monolayer-multilayer adsorption (28). The steep desorption branches correspond to a type IV b for samples A and A6-A8, with some percolation effects. This is typically associated with materials with narrow necks and a relatively low level of pore connectivity. The isotherm of sample A5 is more of the type II b, which is typical for aggregated plate-like particles with non-rigid slit-shaped pores, suggesting some change in the pore structure. Samples A1-A4 exhibited much more limited capillary condensation, and the isotherms even tend towards the microporous type I b.

All pore volumes were smaller after grafting with silanes, notably of the tBCDMS and CTPhS-modified materials (A1-A4). Grafting with methylsilanes in ethanol only had a limited effect on the pore volume (A6-A7), but a toluene environment led to a more extensive decrease for CTMS (A5) and TCMS (A8). This is also in line with the larger amounts of organic species found in these materials.

For CTPhS in pure toluene (A3), equilibrium could not be reached within a reasonable period (i.e. within 1-2 h) during N_2 physisorption, which results in entirely non-overlapping adsorption and desorption branches. The low N_2 surface area determined is also related to the extremely slow adsorption process. Adsorption of CO_2 (table 2), on the other hand, gives a surface area in the same order as those of the other samples, although the precise values differ with a (constant) factor with

respect to those obtained with N_2 adsorption, which is most likely related to differences in the mechanism of micropore filling. For CO_2 adsorption, equilibrium is reached more quickly, which can well be explained by the higher temperature during adsorption. As the organic chains are far less rigid at 273 K than at 77 K, this will enable easier passage of the gas molecules towards the inner pores. Remarkably, the extent of modification of this sample is about equal to that of a sample modified at 323 K in an environment with water added (A4), which does not exhibit such extensive pore blockage.

We may thus conclude that pore blockage was determined by the distribution of the silanes, which may be different under other conditions, rather than by the extent of modification. For the materials prepared at room temperature without water, the silanes did not dissolve entirely into the liquid. Moreover, the water that was pre-adsorbed on the surface instead of separately added water may have acted as a nucleophile. As a more direct reaction between the Cl-groups and OH suffers from more steric hindrance than one between two OH groups, this would make reactions in the inner pores even less probable. These differences may have had an effect on the final distribution of the silanes on the surface, such that blockage of the pores occurred, impairing passage of N_2 molecules at 77 K.

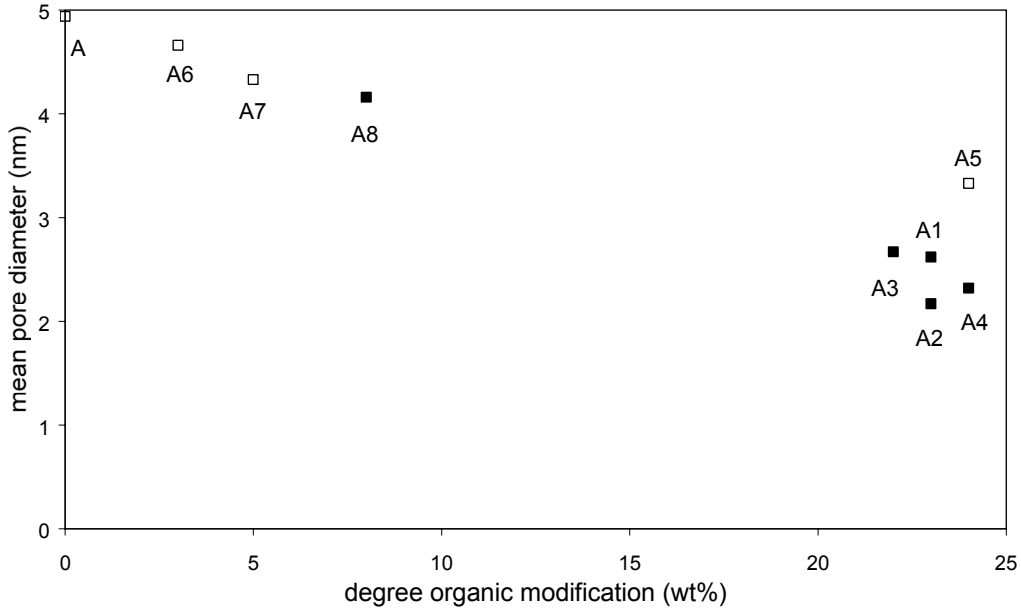

Figure 2*:* Relation between mean pore diameter and extent of modification (corrected for the mass loss of A). The open and closed (except A3) symbols relate to the series addressed in the text.

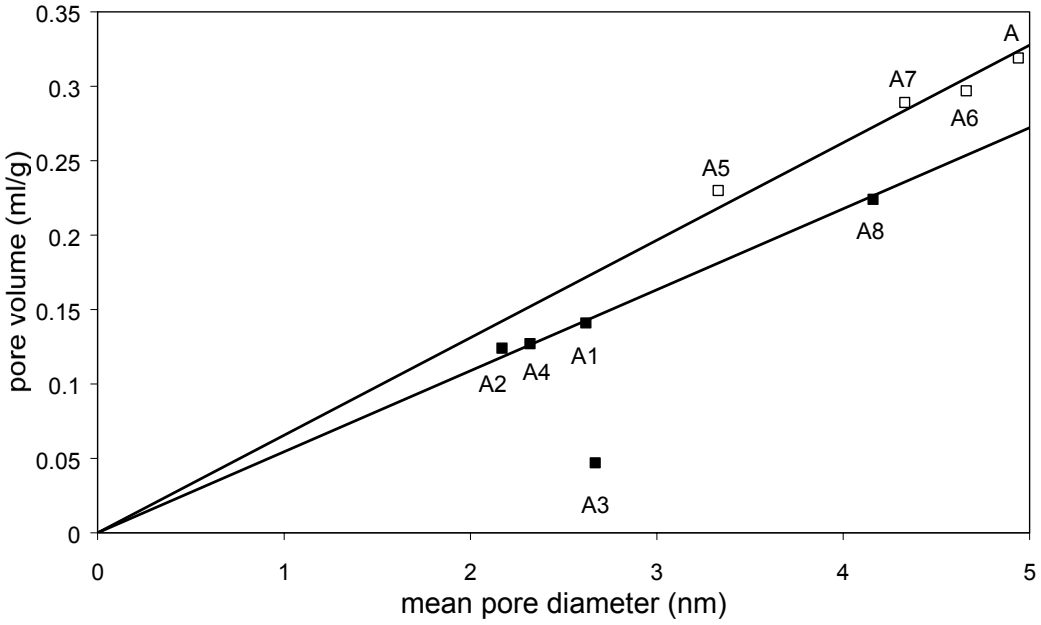

Figure 3*:* Relation between pore volume and mean pore diameter (calculated from pore volume and surface area using eq. 6).

The N_2 surface areas of the other modified materials are just somewhat smaller after modification, and vary only slightly. Clearly, the decrease in pore volume is not necessarily accompanied with a smaller surface area. This is an indication that the pore size distribution has decreased to smaller values. Assuming cylindrical pores, the mean pore size can be estimated with the relation:

$$d_p = 4\, v_p / A \qquad [6]$$

with d_p the pore diameter, v_p the pore volume and A the surface area. A relation can thus be perceived between the extent of modification (corrected for the mass loss observed for sample A) and the decrease of the mean pore diameter, as shown in Figure 2.

Figure 3 shows that there is a roughly linear relation between the pore volume and the mean pore diameter, which indicates that the changes in surface area are small indeed. The odd point is related to sample A3, for which no reliable isotherm could be obtained. Two different trendlines can be distinguished, one related to samples A, A5, A6 and A7 and the other related to samples A1, A2, A4 and A8.

For A3 no equilibrium was reached; this sample has a very low pore volume. The open and closed (except A3) symbols relate to the series addressed in the text. Linear relations are indicated by the trendlines.

In order to be more comparable to the first series (the original material and the DCDMS and CTMS-modified samples), the latter one should have smaller pore diameters than have been calculated now. If globular pores are assumed, the relation is $d_p = 3\ v_p / A$, resulting in smaller mean pore diameters with the same values for v_p and S. It is thus expected that for these samples the shape of the pores has become more globular with respect to the original γ-Al_2O_3. In practice, this means that inhomogeneous modification or pore-clogging took place, which was clearly most extensive for A3. Although less clearly observable, a similar difference between these series can be noticed in figure 2. For the first series (open symbols), extrapolation of the data would give a zero average pore diameter at about 71 wt% modification, for the second one (closed symbols), this would be around 45 wt%. The larger effect of modification on the mean pore diameter for the second series is another indication of more extensive pore plugging and thus of inhomogeneous modification.

For alumina modified with bulky silanes, capillary condensation was strongly suppressed, indicating significant loss of mesopores (larger than 2 nm). In addition, the lower amounts adsorbed at low p/p_0 indicate loss of the volume of the microporous part of the pore distribution. Mean mesopore sizes were determined, as far as they could be assessed, from BJH fits of the N_2 desorption isotherms (table 2), assuming no percolation effects. The mean mesopore diameters are in line with the trend in the total pore volumes and consequently with the estimated mean pore diameter. No mesoporosity could be observed for sample A3 as no equilibrium had been reached. Grafting with both DCDMS and CTMS in ethanol hardly led to loss of mesoporosity. We may conclude that these agents give rise to a very homogeneous decrease of the pore size, which has also been found earlier for difunctional methylsilanes in mesoporous solids (8). More extensive loss of mesoporosity is found for CTMS and TCMS in toluene. For CTMS, even another isotherm type is found, indicating slit-shaped non-rigid pores. This may be associated with strong modification of the pores with (flexible) organic groups, although without leading to extensive pore clogging. Modification with TCMS led to a bimodal mesopore size distribution, corresponding to a decrease of the number of pores with sizes around 5 nm, and, more obviously, to loss of microporosity (again visible from the lower amount adsorbed at low p/p_0). As the size of TCMS is about the same as that of CTMS, extensive polymerisation is the most likely explanation for both differences. This results on one hand in selective mesopore modification (mostly of the larger pores) and, on the other, in blockage of the passage of N_2 molecules at 77 K towards part of the micropores. From XPS measurements on membranes treated in similar ways, this was already postulated (11), and the current results give further substantiation. It was also found before that the bulky silanes were mainly deposited on the outer surface. Both structural effects have been confirmed here as these treatments led to inhomogeneous modification.

For all methylsilanes, steric hindrance is limited, so these reactants can enter into the pores most easily during grafting. It is expected that especially CTMS leads to direct and homogeneous modification of

the alumina surface, as only direct attachments to the surface can be formed and no polymeric networks as for DCDMS and TCMS. However, modification also seemed to be quite homogeneous for DCDMS. In a future study, the structural effects of modification with dimethyl and trimethyl chlorosilanes will be compared more systematically for porous materials with a range of pore sizes.

With SEM, clear differences were found between the unmodified and modified γ-Al_2O_3 materials. For the original unmodified alumina, porosity was visible with pore sizes below 10 nm, as well as irregular structures on a scale of about 100 nm, including structures with a fibrous morphology (Figure 4a). This sample suffered from excessive contrast, though. For the slightly CTMS-modified sample A6 (Figure 4b), contrast of the large structures was moderate, and as a consequence the small mesopores and the fibrous structures were more clearly visible. The material that was most 'closed' to adsorption, i.e. sample A3, merely displayed a hazy image (Figure 4c), under which the surface structure was poorly resolved. Moreover, the sample suffered from severe charging, which is another indication of strong surface modification.

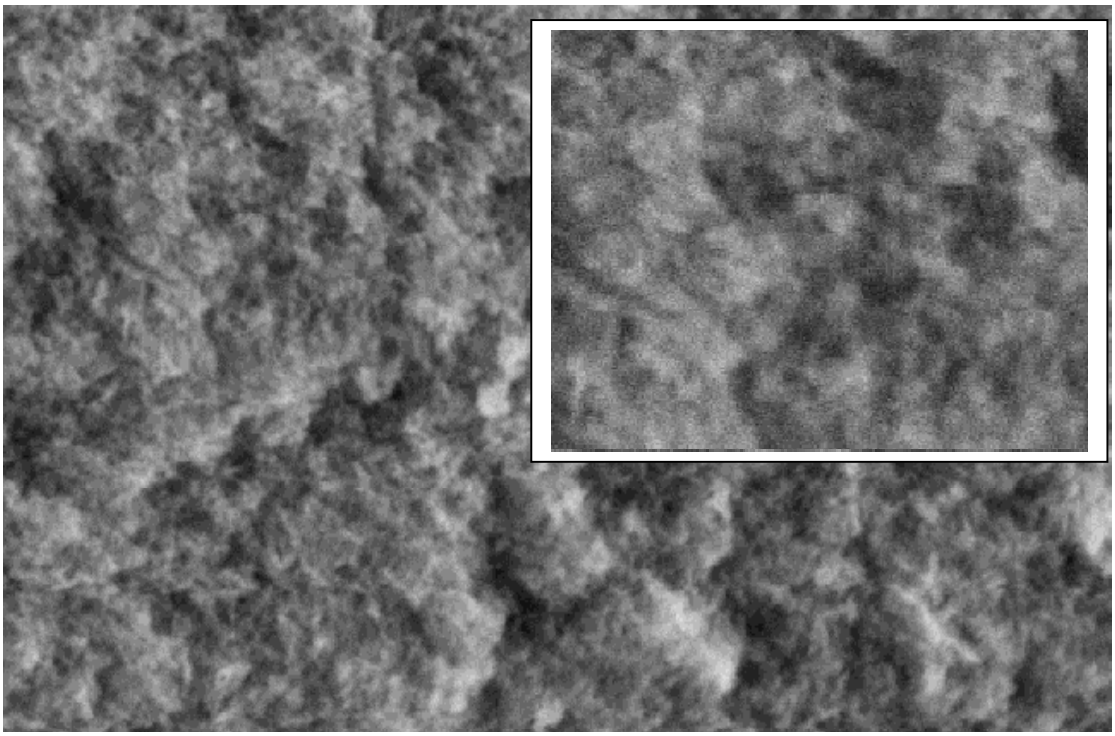

Figure 4a

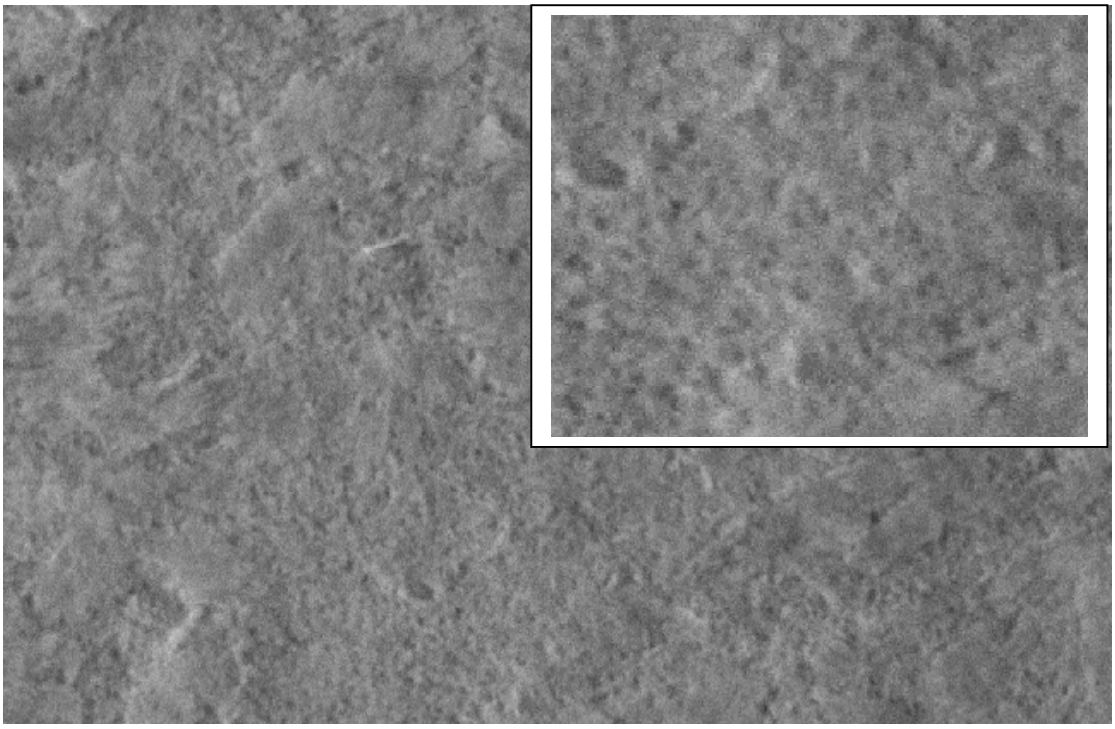

Figure 4b

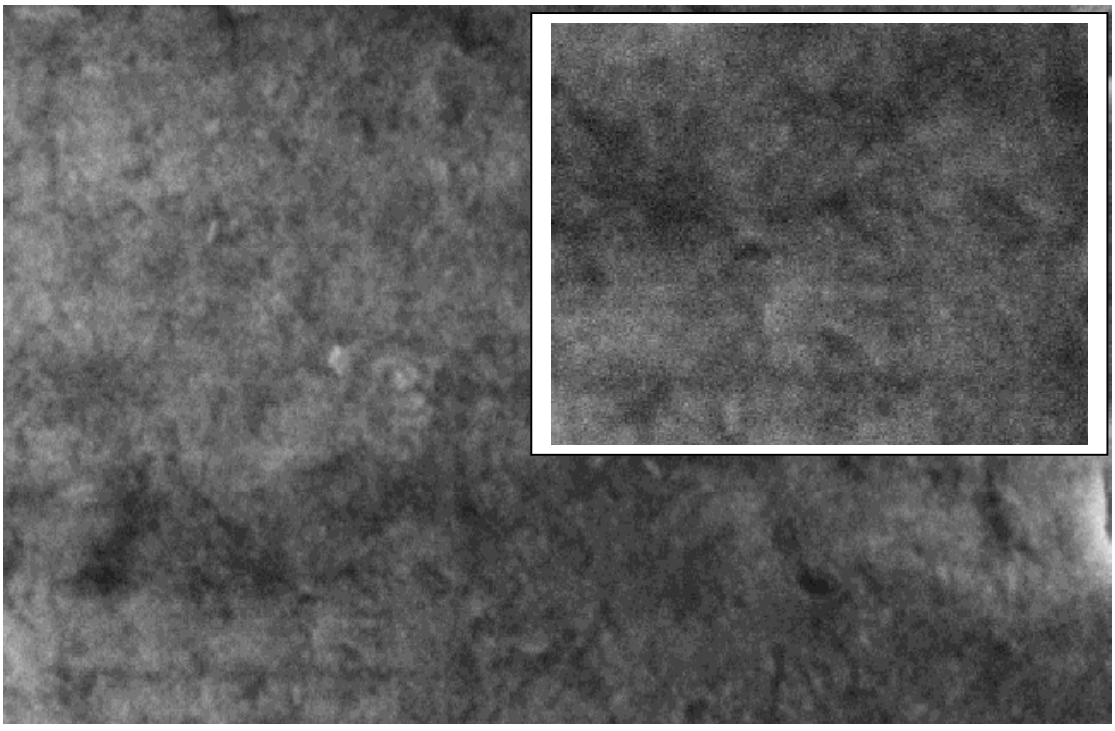

Figure 4c

Figure 4: SEM Micrographs of (a) unmodified alumina A, and of modified aluminas (b) A6 and (c) A3. In the insets, parts of the micrographs have been enlarged twice.

3.4.3. Hydrophobicity and surface polarity

After silination, all materials were calcined in N_2 at 473 K. Still, pre-treatment by evacuation at 473 K was very slow, indicating that large quantities of water were again present. During the evacuation procedure, most water could be removed, but re-exposure to ambient air again led to significant amounts of adsorbed water, which became evident from a weight loss below 473 K of several per cent of the total mass, as determined from TGA. This is an indication that, despite modification, the bulk of most materials had remained hydrophilic. This also became clear from the three-phase contact angles with water: these were too small for formation of a stable water drop, and could therefore not be assessed reliably, even after modification. Possibly, the water droplet interacts with the underlying layers and not only with the top layer. However, a hydrophobising effect of similar treatments has been observed from the ratio of permeabilities of (nonpolar) toluene and (polar) water, which increased slightly with the extent of modification from 0.6 for pure γ-Al_2O_3 to 1.1 for alumina modified by TCMS (11).

From the *C*-values of the BET fits, which are an indication of the strength of the adsorbate-adsorbent interaction, more information on the surface polarity was obtained. As the N_2 molecule interacts quite strongly with polar surface groups (e.g. OH-), high values indicate a hydrophilic surface. Clearly, CTMS/toluene and TCMS led to materials with the lowest *C*-values and thus have the most hydrophobic surfaces. Unmodified alumina also exhibits a rather low value, but this can be explained by the high pre-treatment temperature of 773 K, which also leads to a lower hydroxyl content and is therefore not directly comparable. Exposure to the water-containing liquids following the same procedures, but without silanes, gave *C*-values of around 180, showing a clear difference with most of the modified samples.

Adsorption isotherms of Ar did not reveal differences in *C*-values between the samples. The values were low in all cases (around 40), which could be anticipated, as Ar is a noble gas that is not involved in polar interactions. The adsorption / desorption isotherms of Ar further led to similar conclusions as for N_2 and did not provide additional structural information.

3.5. Conclusions

For γ-Al_2O_3 with a pore diameter of about 4 nm, we have shown that modification with especially chloromethylsilanes is very effective. The pore size and pore volume remained largely preserved and modification was most homogeneous, as no steric hindrance of bulky groups occurred in the small mesopores. For CTMS, toluene as a solvent led to a much higher extent of modification than ethanol.

Both CTMS and DCDMS were found to be suitable for homogeneous modification without extensive blockage of the pores. Application of TCMS led to polymerisation and thus to blockage of both micro- and mesopores. Inhomogeneous modification was also found for silanes with bulky alkyl groups, leading as well to loss of both microporosity and mesoporosity with respect to N_2 adsorption. Modification with these reagents occurred predominantly at the outside of the material. The distribution of the deposited silane on the material was found to be dependent on the homogeneity of the silane/solvent mixture. Factors that contributed to the homogeneity were temperature and whether or not water was added to the toluene solvent. Variation of the solvent and preparation procedures can be applied for further fine-tuning of the extent of modification. For high-temperature applications in membranes, post-modification of the external membrane surface with silanes with bulky organic groups after CTMS-modification of the membrane bulk can be envisaged to further increase permeance of nonpolar vs polar molecules.

3.6. References

1) R.M. de Vos, H. Verweij, Science 279 , 1998, 1710.

2) H. Verweij, J. Mater. Sci. 38, 2003, 4677.

3) S. Roy Chowdhury, K. Keizer, J.E. ten Elshof, D.H.A. Blank, Langmuir 20, 2004, 4548.

4) R.K. Iler, The Chemistry of Silica, Wiley & Sons Inc., New York, USA, 1979.

5) L.T. Zhuravlev, Colloids Surf. A 173, 2000, 1.

6) K.J. Shea, D.A. Loy, Chem. Mater. 13, 2001, 3306.

7) R.M. de Vos, W.F. Maier, H. Verweij, J. Membr. Sci. 158, 1999, 277.

8) T. Van Gestel, B. Van der Bruggen, A. Buekenhoudt, C. Dotremont, J. Luyten, C. Vandecasteele, G. Maes, J. Membr. Sci. 224, 2003, 3.

9) L.R. Snyder, J.W. Ward, J. Phys. Chem. 70, 1966, 3941.

10) J. Wood, R. Sharma, Langmuir 10, 1994, 2307.

11) A. Sah, H.L. Castricum, A. Bliek, D.H.A. Blank, J.E. ten Elshof, J. Membr. Sci. 243, 2004, 125.

12) K. Unger, Angew. Chem. Int. Ed. 11, 1972, 267.

13) K. Unger, D. Nyamah, Chromatographia 7, 1974, 63.

14) M. Novoty, L.S. Bektesh, K. Grohman, J. Chromatogr. 83, 1973, 25.

15) C. Stella, S. Rudaz, J.L. Veuthey, A. Tchapla, Chromatographia 53, 2001, S132.

16) S. Ohnishi, T. Ishida, V.V. Yaminsky, H.K. Christenson, Langmuir 16, 2000, 2722.

17) C.P. Tripp, R.P.N. Veregin, M.L. Hair, Langmuir 9, 1993, 3518.

18) K.-H. Song, J.-H. Song, K.-R. Lee, Sep. Purif. Technol. 30, 2003, 169.

19) L.A. Belyakova, A.M. Varvarin, Colloids Surf. A 154, 1999, 285.

20) C.P. Tripp, M.L. Hair, Langmuir 8, 1992, 1120.

21) J.H. Clark, D.J. Macquarrie, J. Chem. Soc., Chem. Commun. 1998, 853.

22) A. Corma, M. Domine, J.A. Gaono, J.L. Jorda, M.T. Navarro, F. Rey, J.P. Pariente, J. Tsuji, B. McCulloch, L.T. Nemeth, J. Chem. Soc., Chem. Commun. 1998, 2211.

23) M.D. Skowronska-Ptasinska, M.L.W. Vorstenbosch, R.A. van Santen, H.C.L. Abbenhuis, Angew. Chem. Int. Ed. 41, 2002, 637.

24) N.R.E.N. Impens, P. van der Voort, E.F. Vansant, Micropor. Mesopor. Mater. 28 1999, 217.

25) M.C. Capel-Sanchez, L. Barrio, J.M. Campos-Martin, J.L.G. Fierro, J. Colloid Interface Sci. 277, 2004, 146.

26) S. Alami Younssi, A.Iraqi, M.Persin, A. Larbot, J. Sarrazin, Sep. Purif. Technol. 32, 2003, 175.

27) N. Benes, A. Nijmeijer, H. Verweij, in: N.K. Kanellopoulos (Ed.), Recent Advances in Gas Separation by Microporous Ceramic Membranes, Elsevier, Amsterdam, 2000, p. 335.

28) K.S.W. Sing, D.H. Everett, R.A.W. Haul, L. Moscou, R.A. Pierotti, J. Rouquerol, T. Siemieniewska, Pure Appl. Chem 57,1985, 603.

Chapter 4 Hydrophobic modification of γ-alumina membranes with organochlorosilanes*

4.1. Abstract

Mesoporous γ-alumina membranes were chemically modified with several organochlorosilanes. XPS with depth profiling and permporometry experiments were used to study the local organosilane concentrations and their effect on the pore structure. It was found that the penetration of long chain chlorosilanes into the mesopores was sterically hindered and that grafting was not as effective as for short chain organosilanes. Membranes modified with monofunctional organosilanes showed a smaller Kelvin radius than unmodified γ-alumina membranes as observed by permporometry, indicating that methyl groups resided inside the pores. For membranes modified with di- and tri-functional organosilanes larger Kelvin radii were observed, indicating that polymerized silane networks only block the smaller pores. Another reason for the dilation of the structure may be leaching due to the acid environment induced by the chlorosilanes. The permeation of solvents was affected by the hydrophobic modification of the surface and the internal pore walls.

* A. Sah, H.L.Castricum, A. Bliek, D.H.A. Blank and J.E. ten Elshof, Journal of Membrane Science, 243 125-32 (2004).

4.2. Introduction

The strategy, employed in the present paper, is to post-modify a mesoporous inorganic membrane by grafting the internal pore surface with organosilanes. This process is illustrated in Figure 1. A hydrolysable group of the organosilane undergoes coupling with the hydroxyl groups of the mesoporous layer, forming a chemically bound monolayer initially, which imparts the desired hydrophobicity. Organosilanes with two or more hydrolysable groups can undergo further coupling with other organosilanes, forming a polymeric layer.

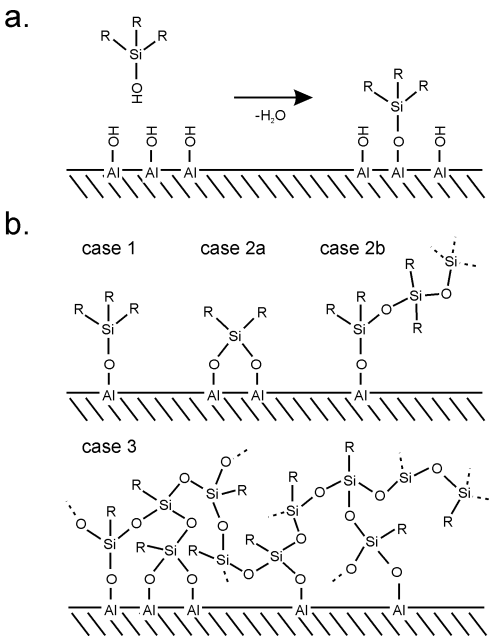

Figure 1. a) Schematic diagram showing monolayer deposition of a monofunctional hydrophobing agent. b) Surface structures of organosilanes grafted on hydroxyl-terminated surfaces. **Case 1**. Monofunctional precursor anchoring to a hydroxyl site. **Case 2a**. Difunctional precursor anchoring to two hydroxyl sites. **Case 2b**. Difunctional precursor forming a polymerized chain. **Case 3**. Trifunctional precursor forming a polymerized layer on a hydroxyl-terminated surface.

Picard et al. (1) reported the hydrophobic features of a mesoporous zirconia membrane grafted with fluorinated silanes. The membrane was impregnated by solutions of $C_6F_{13}C_2H_4Si(OMe)_3$ and $C_8F_{17}C_2H_4Si(OEt)_3$. Liquid permeation studies on the zirconia membranes showed a decrease in liquid permeability for the grafted membranes as compared to the ungrafted one. It was concluded that the grafting time is important to increase the hydrophobicity of the samples, while the differences in length of the hydrophobic tails had no influence.

Work on grafting γ-alumina membranes with Me_3SiCl, $MeSi(OMe)_3$, and $Me_2Si(OEt)_2$ organosilanes was reported by Alami Younssi et al. (2). The surface properties of γ-alumina membranes were modified in order to change the selectivity of the membranes towards chemical solutes of different polarities. Infra-red (IR) characterization of the membranes showed that the grafting depended on the nature of the silanes used and was achieved most effectively with multifunctional silanes. The N_2 adsorption and desorption isotherms showed a decrease in specific area and microporous volume for the membrane grafted with $Me_2Si(OEt)_2$ or $MeSi(OEt)_3$, indicating that the pore wall had been covered by grafted moieties. Modification of the surface properties of the membrane was confirmed by pervaporation tests on different binary mixtures of solvents. Both solvent fluxes and membrane selectivity depended on grafting conditions.

Dafinov et al. modifed γ-alumina membranes by alcohol chemisorption (3). The layer of chemisorbed alcohols was found to be stable up to 200°C, and imparted hydrophobic characteristics to the membrane, as was seen by a decrease in water permeability. Castro et al. studied the permeability of polyvinylpyrrolidone-modified porous silica membranes (4). Hydraulic permeability measurements showed that the permeability was determined by the configuration of terminally anchored polymer chains. Due to the affinity of the polymer for water, the hydrophilic PVP brush layer expanded, preferentially allowing the passage of water over oil. Caro et al. reported silylating the γ-alumina surface with octadecyltrichlorosilane (5).

Van Gestel et al. reported the effect of surface modification of γ-Al_2O_3/TiO_2 multilayer membranes for applications involving non-polar organic solvents (6). The effect of silane treatment ($(CH_3)_2SiCl_2$, $C_8H_{17}CH_3SiCl_2$) on the properties was found to depend on the pore size of the membrane (microporous, microporous-mesoporous, mesoporous) and on the silane reagent used. For microporous membranes it was shown that silane coupling reactions took place in pores situated at the outer membrane surface, while reactions at the internal membrane surface in the microporous structure were sterically hindered. Liquid permeability tests with hexane and water on mesoporous membranes indicated that silanes could be successfully introduced in the pore structure of the membrane. The degree of hydrophilic/hydrophobic modification, characterized by the permeability ratio of water/hexane was found to improve with increasing calcination temperature and increasing alkyl chain length, due to the formation of larger mesopores in the membrane structure and a more hydrophobic environment in the modified pores, respectively.

In the present paper a series of monofunctional, difunctional and trifunctional organochlorosilanes with organic groups of different sizes are used to study the influence of the nature and size of the

modifying agent on the extent of grafting. The effect on surface and pore modification is studied in detail by diffuse reflectance IR measurement, x-ray photoelectron spectroscopy (XPS) with depth profiling, and permporometry measurements. Solvent permeation experiments are used to study the selectivity of the grafted membranes towards liquids differing in polarity.

The work gives an insight into the phenomenon of grafting occurring in the membrane surface and inside the pores, as seen by the characterization techniques. The effect of the number of functional groups of the precursor in forming a polymerized layer, and the consequent chemical modification of the membrane is discussed.

4.3. Experimental

4.3.1. Membrane preparation

The γ-alumina membrane consists of a macroporous α-alumina support and a thin mesoporous γ-alumina layer. The α-alumina supports were made by colloidal filtration of well-dispersed 0.4 μm α-alumina particles (AKP-30, Sumitomo). The dispersion was stabilized by peptizing with nitric acid. After drying at room temperature, the filter compact was sintered at 1100ºC. Flat discs of 39 mm diameter and 2.0 mm thickness with a specific surface area of ~15 m^2/g were obtained after machining and polishing. The porosity of these supports is ~35%, and the pore diameter is 80-120 nm. Mesoporous γ-alumina membranes of ~0.5 μm thickness were prepared by dip coating the above mentioned porous α-alumina supports in a boehmite sol, followed by drying and calcination at 600ºC for 3 h. After calcination, the γ-alumina layers have a specific surface area of ~250 m^2/g. For further details, the reader is referred to ref. (7).

Triphenylchlorosilane ($Si(C_6H_5)_3Cl$, 96% purity), t-butyldimethylchlorosilane ($t\text{-}C_4H_9(CH_3)_2SiCl$, 97% purity), trimethylchlorosilane ($(CH_3)_3SiCl$, 99% purity), dimethyldichlorosilane ($(CH_3)_2SiCl_2$, 99% purity) and trichloromethylsilane ($(CH_3)SiCl_3$, 97% purity) were obtained from Aldrich. The stacked γ/α-alumina membranes were hydrophobically modified by immersing them for periods of 2-12 h in 2-5 wt% solutions of the above mentioned precursors. Triphenylchlorosilane and t-butyldimethylchlorosilane systems were refluxed at 50°C for 5 hours, as it enhances the dissolution of the precursors. It was found that the long chain chlorosilanes (t-butyldimethylchlorosilane, triphenylchlorosilane) as well as the multifunctional chlorosilanes are more soluble in toluene than in water or alcohols. The solvent used to dissolve a particular organosilane was selected on the basis of organosilane solubility and γ-alumina grafting efficiency.The organosilanes t-butyldimethylchlorosilane, triphenylchlorosilane, dichlorodimethylsilane, and trichloromethylsilane

were therefore dissolved in water-saturated toluene, while the other precursors were dissolved in ethanol with 5 wt% water. After removal from the solution the membranes were rinsed 5 times with ethanol to remove any unreacted chemicals. The grafted membranes were calcined at 200ºC for 1 h in pure N_2 atmosphere with heating/cooling rates of 0.5ºC/min.
For comparison, some γ-alumina powders were prepared by treating them with the respective precursor solutions in a similar manner as the membranes.

4.3.2. Membrane characterization

Permporometry (8) was employed to determine the pore size distribution in the mesoporous membrane layers.

Diffuse reflectance infra-red fourier transform spectroscopy (DRIFTS) experiments were carried out using a BIORAD FTS-45A infrared spectrometer, with a SPECAC "The Selector" P/N 19900 series DRIFTS. The IR spectra were processed with WIN-IR (a BIORAD software program).

The chemical stability of grafted organosilanes on γ-alumina was determined by soaking grafted γ-alumina powder in water for 4 h at room temperature. The powders were then heated in N_2 at 200ºC for 1 h with a heating and cooling rate of 0.5ºC/min to remove residual water. The organosilane concentrations on freshly grafted powders and soaked powders were compared by DRIFTS experiments.

Steady state liquid flux measurements were carried out using water, iso-propanol, 2-butanol, and toluene in a dead-end nanofiltration cell on grafted γ-alumina membranes. The volume of the cell is 700 ml and the operating pressure range was kept at 2-14 bar (9)**.** The stirring speed in the cell was kept constant at 200 rpm. Subsequent liquid permeation experiments on the same membrane were carried out in a sequence that started with the most hydrophobic (toluene) and ended with the most hydrophilic (water) solvent. Prior to the experiments, the membranes were left overnight in isopropanol to leach out any condensed water from the membrane mesopores (10).

4.4. Results and discussion

Diffuse reflectance IR specta of grafted γ-alumina powders were recorded. For the membranes, the surface concentration of the grafted silanes was too low to be detected by DRIFTS. Characteristic peaks associated with the organic side groups of the trichloromethylsilane on γ-alumina powders were observed, as seen from figure 2. The characteristic peaks can be attributed to various methyl

vibrations. The peak at 2970 cm^{-1} is due to -CH_3 asymmetric stretching and the 1267 cm^{-1} peak corresponds to -CH_3 deformation. The 850 cm^{-1} peak can be attributed to the -CH_3 rocking mode, and the 800 cm^{-1} peak is typical for the Si-C stretching mode (11). The Si-O-Si appears at 1130-1000 cm^{-1} (12, 13, 14). This indicates that a polymerized layer of methylated silanes has formed. In the case of the difunctional precursor $Si(Me)_2Cl_2$ the Si-O-Si peak was not observed, which may possibly indicate that both hydrolysable chlorine groups are utilized in forming bonds with the hydroxyls of the γ-alumina surface. For the monofunctional precursors, triphenylchlorosilane, trimethylchlorosilane, t-butyldimethylchlorosilane, the characteristic methyl, butyl and phenyl peaks were not detected. As the signal comes from one single monolayer in this case, the concentrations may have been too low to be detected by the instrument.

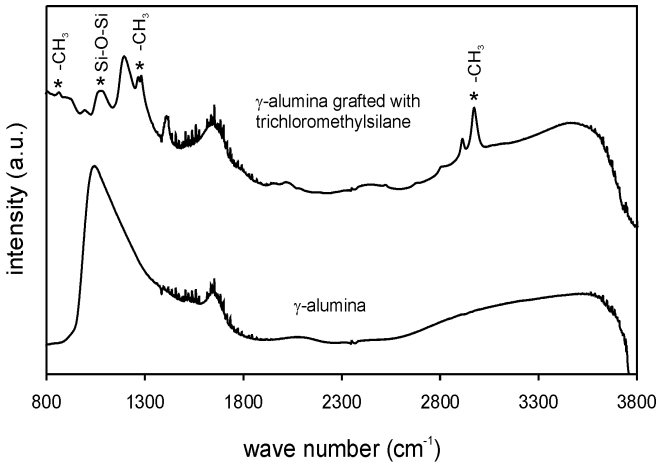

Figure 2 DRIFTS spectra of γ-alumina powder grafted with trichloromethylsilane.

Compositional information on the Al and Si atomic concentrations as a function of depth were obtained by XPS. Figure 3 shows an XPS spectrum of the surface of a γ-alumina membrane grafted with chlorotrimethylsilane.

The XPS data clearly show the presence of Si on the surface, indicating that grafting of the hydrophobic precursor was successful (case 1 in Figure 1b). A trace of Cl can also be observed, indicating that not all Cl had been washed out. In the case of silanes with large organic side groups (phenyl, butyl) silicon was only observed on the outer surface of the membrane, while silanols with 1-3 methyl groups were grafted both on the internal mesopore surface and on the external surface of the membrane. Probably, chlorosilanes with long chain hydrocarbon end groups (alkyl and aryl) cannot enter the 4.5-7 nm diameter mesopores easily due to steric hindrance and grafting was therefore not as effective as for precursors with methyl end groups (6).

In the XPS depth profiles shown in Figure 4, three regions can be distinguished: (i) the outer surface layer, with high concentrations of Si, (ii) the γ-alumina layer, until 300-400 nm depth, and (iii) the α-alumina support at 400 nm depth and more.

Different behavior is seen for different hydrophobing agents: while the monofunctional tri-methyl silane precursor reached a ~1 % Si concentration inside the γ- alumina pores, the concentration of the difunctional dimethyl silane remained much lower in the γ-alumina layer. There are two possible reasons to explain this phenomenon. First of all, it may be related to the fixed number of hydroxyl groups that are present on the inner pore surface of γ-alumina. While the monofunctional trimethyl silane precursor requires one OH group for covalent attachment to the alumina surface, the difunctional precursor may bond with two active OH sites (case 2a in Figure 1b). And as the total number of OH sites is limited, this type of behavior would effectively result in lower Si concentrations for the grafted difunctional precursor when all hydroxyl groups have been consumed. Secondly, the difunctional silane may also partially polymerize into linear chains inside the mesopores (case 2b in Figure 1b), which may possibly block the pores and hinder diffusion of similar precursors into the mesopores, also leading to lower Si levels inside the γ-alumina layer. Another possible explanation may be that DDMS is very reactive towards itself, giving PDMS particles that are washed out, leaving hardly any DDMS inside the alumina layer.

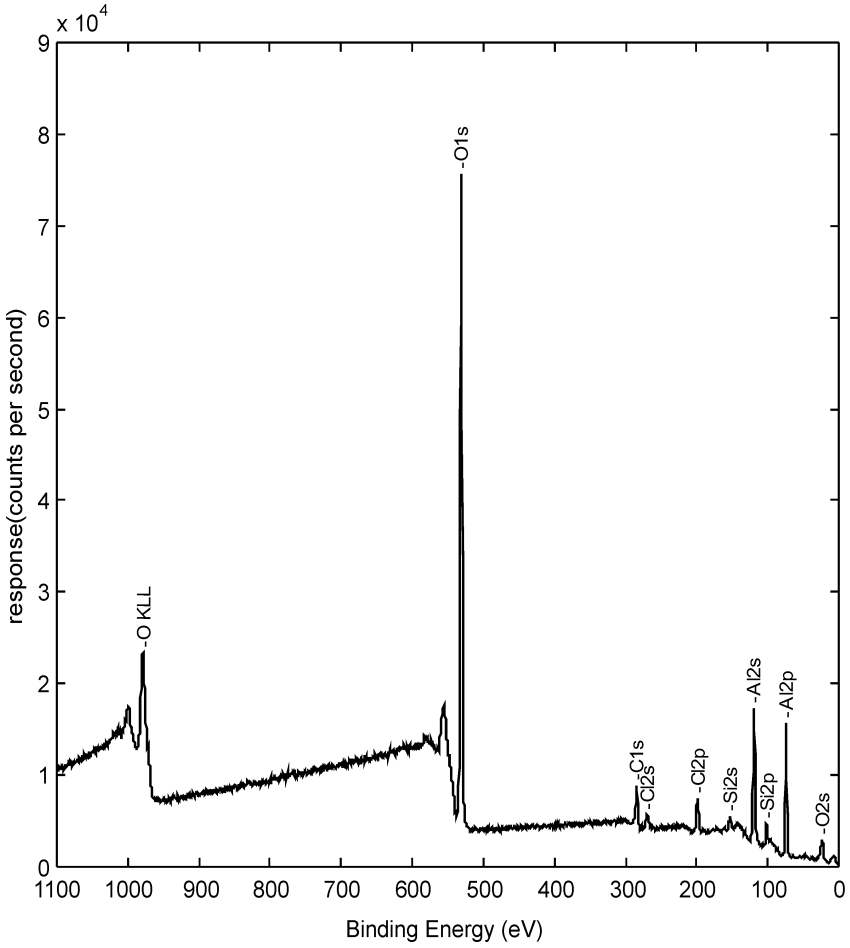

Figure 3 XPS results of a γ- alumina membrane grafted with trimethylchlorosilane.

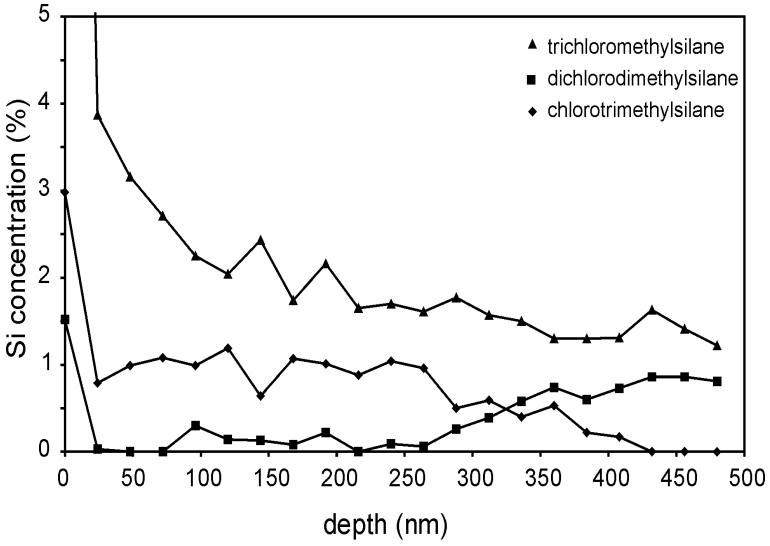

Figure 4 XPS depth profile showing Si atomic concentration as function of depth inside the membrane.

A high concentration of silicon was also observed in the system that had been treated with trichloromethylsilane. This is most likely due to the formation of a polymerized multilayer of organosilane being formed on the surface, as was observed directly by DRIFTS in the form of a Si-O-Si peak. In this case, after the condensation with the hydroxyls of the γ-alumina layer has taken place, there will still be one or two hydrolysable groups available for further coupling with other precursor molecules (case 3 in Figure 1b). Hence, for this precursor the silane concentration can reach relatively high values in both the γ and α alumina layers.

On the other hand, silicon was hardly detected in the α-alumina support layer that had been treated with the trimethyl silane compound, while a relatively high concentration was present in the support layer that had been treated with the dimethyl silane precursor. This strongly suggests that the dimethyl silane precursor is grafted predominantly in the form of linear chains (case 2b in Figure 1b). As the pore size of the α-alumina support is much larger than that of γ-alumina, pore blocking as a result of grafting will probably not occur in the α-alumina support. In the α-alumina region, the Si concentration of the trimethylsilane precursor reaches very low levels, whereas the dimethylsilane precursor gives much higher values. This can be explained by taking into consideration that α-alumina has a very low specific surface area of ~15 m^2/g whereas the γ-alumina has a higher specific surface area of ~250 m^2/g. The number of OH groups on an alumina surface is limited to ~5 per nm^2 so that even when all available sites in the α-alumina support are grafted with trimethyl silane, the Si atomic concentration will still be low. But as the possibility of linear polymerization without pore blocking exists for the difunctional precursor, a higher concentration can be realized in the α-alumina support.

The molar concentration of Si per unit real surface area for mono-, di- and trifunctional precursors at the outer membrane surface and inside the γ-alumina mesopores as determined by XPS are listed in Table 1.

Table 1: Silicon concentration (per unit true surface area) on the outer γ-alumina surface and inside the mesopores as calculated from XPS depth profiles.

Precursor	Surface concentration (mol/ m^2)	Mesopore surface concentration (mol/m^2)
trimethylchlorosilane	$7.3 \cdot 10^{-6}$	$2.0 \cdot 10^{-6}$
trichloromethylsilane	$5.1 \cdot 10^{-5}$	$2.9 \cdot 10^{-6}$
dichlorodimethylsilane	$3.7 \cdot 10^{-6}$	$5.2 \cdot 10^{-7}$
triphenylchlorosilane	0	0
t-butyldimethylchlorosilane	$2.5 \cdot 10^{-8}$	0

The very high concentration of Si for the trichloromethyl silane precursor on the outer surface indicates the presence of polymerized silane network, which confirms the DRIFTS results.

Figure 5 shows the desorption curve of the permporometry process for di- and tri-chloromethyl silane grafted γ-alumina membranes, and an unmodified membrane.

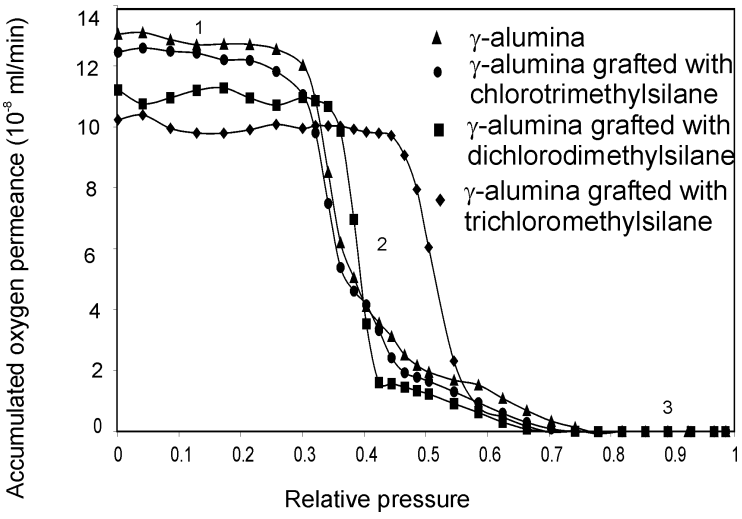

Figure 5 Accumulated oxygen permeation versus relative cyclohexane vapour pressure curve for γ-alumina membrane grafted with di- and tri- chloromethylsilane.

The figure shows the oxygen flux through open pores versus the relative vapour pressure of cyclohexane. At a relative vapour pressure of unity (region 3 in the figure), all pores are blocked. The accumulated oxygen permeation can be larger than zero only if there are some very large pores or cracks in the membrane, which is not the case here, indicating that our membrane preparation

procedure was very successful. Region 2 is the capillary condensation regime, where the Kelvin pore size distribution is calculated from the change of the oxygen permeation flux with changing pore radius. In region 1 all pores are open and only t-layer desorption is assumed to occur. The onset of capillary condensation for the membranes grafted with dichlorodimethylsilane occurred at a lower cyclohexane pressure than in the trichloromethylsilane-grafted membrane, which indicates that its Kelvin radii are smaller. Furthermore, the oxygen flux in region 1 and at zero cyclohexane pressure decreases in the order γ-alumina > dimethyl silane modified > methyl silane modified. This suggests that partial pore blocking for diffusing O_2 species occurs in the modified membranes.

Figure 6 shows the pore size distributions of the tri-, di- and mono-methyl chloro silane-modified membrane, and an unmodified γ-alumina membrane as calculated from the data of Figure 5.
It is seen that grafting with chlorotrimethylsilane leads to a decrease in the pore size, indicating that the hydrophobic precursor has penetrated into the pores and formed a monolayer. The Kelvin radius decreases from 2.3 nm for the ungrafted γ-alumina membrane to 2.0 nm for the grafted one. In contrast, the pore size distribution of the dichlorodimethylsilane-modified membrane shows an average Kelvin radius of 2.5 nm, while the trichloromethylsilane-modified membrane has an average Kelvin radius of 3.4 nm. The larger pore sizes in these latter cases may be explained if it is assumed that only the smaller pores become blocked with the polymeric silane networks. Acid leaching may also be involved here in increasing the pore diameter. As a result, oxygen can diffuse only through the remaining open larger pores.

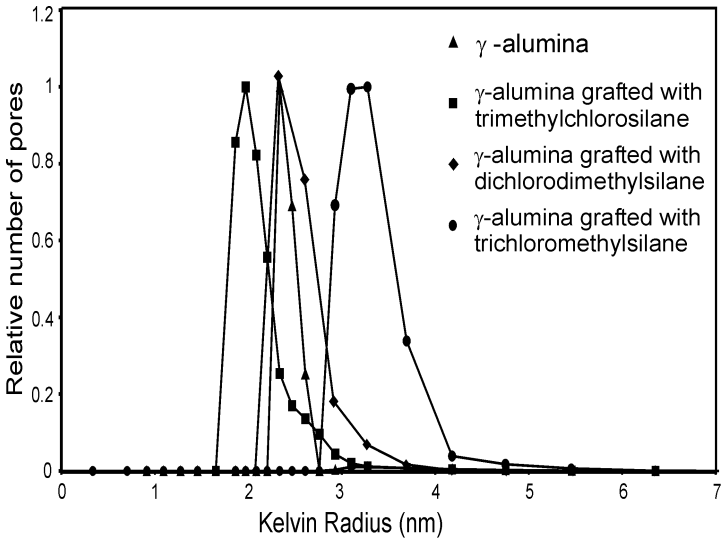

Figure 6 Normalized pore size distribution of γ-alumina membranes grafted with mono-, di- and trichlorosilanes by permporometry.

Under the assumption that all pores are cylindrical in shape, the t-layer was estimated from the total decrease in oxygen flux in region 1 of Figure 5 (15). Estimates of the t-layer thicknesses indicated a thickness of ~0.5 nm for the ungrafted and chlorotrimethylsilane grafted membranes, a thickness of ~0.8 nm for the dichlorodimethylsilane grafted membrane, and ~1.5 nm for the trichloromethylsilane grafted membrane. Although a thickness of ~0.5 nm for the t-layer thickness is physically reasonable, the latter two values are not. This indicates that the assumption of t-layer adsorption on cylindrical pore walls does not hold in these cases. It is most likely that the dicholorodimethylsilane and trichloromethylsilane-grafted membranes have seemingly thicker t-layers because of the polymerized silane chains or 3D network inside the pores, which facilitate the physisorption of cyclohexane by Van der Waals interactions. In such cases t-layer adsorption may occur not only on the pore walls but also by association with the silane network, which effectively results in higher levels of cyclohexane adsorption than would be expected on the basis of adsorption on the pore walls only.

Liquid permeation experiments were carried out on the grafted γ-alumina membranes with water, isopropanol and toluene. Liquid fluxes were measured as function of the applied pressure. Figure 7 shows a representative example of these results.

In all cases the volumetric flux j varied linearly with the pressure applied over the membrane Δp, and the permeability constants k_m were determined from Darcy's law,

$$j = -(k_m/\eta)\,\Delta p, \qquad [4]$$

where η is the solvent viscosity. The permeability coefficients k_m are listed in Table 2.

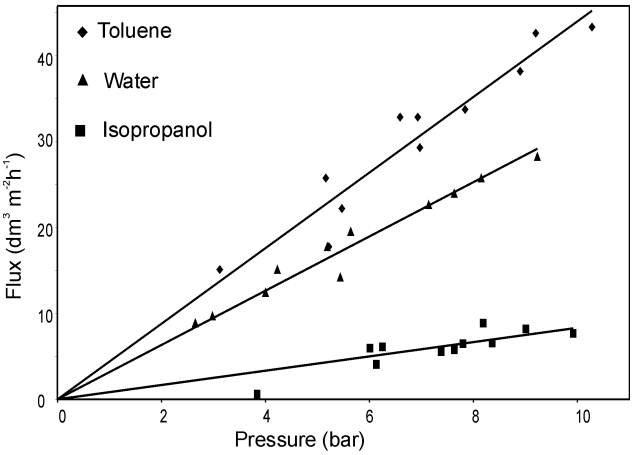

Figure 7 Flux versus pressure for different solvents on a γ-alumina membrane grafted with trimethylchlorosilane.

Table 2 Permeability constants k_m (10^{-14} m) for different solvents on γ-alumina membranes grafted with various precursors.

Precursor	Toluene	Isopropanol	Water
None	0.62	0.67	1.03
trimethylchlorosilane	0.68	0.53	0.78
trichloromethylsilane	0.048	0.041	0.044
dichlorodimethylsilane	1.63	1.55	1.57

Very low permeabilities were observed for the membrane grafted with trichloromethylsilane. Most likely this is due to the polymerised layer of organosilane that formed on the surface and inside the γ-alumina pores as seen by XPS and DRIFTS. The polymerised multilayer provides an initial barrier for the solvents to pass through. The more hydrophobic character of this membrane in comparison with the other ones is indicated by its higher toluene/water permeability ratio. The other membranes show much higher permeabilities than the trichloromethyl modified membrane, and they were all roughly in the same range. Because permeabililty differences up to 35-40% for a specific solvent are often observed even between similar membranes form the same batch of material (2), no definite conclusions can be drawn from the observed differences, and it is therefore preferred to compare results for various solvents on a particular membrane (16). In general, the toluene/water permeability ratio appears to increase slightly upon grafting, but remains below unity, which indicates a low level of hydrophobic modification.

Hence, among all precursors only the trichloromethylsilane precursor imparted a predominantly hydrophobic character, since only this membrane has a larger permeability coefficient for toluene than for water. The hydrophobic character is due to the polymerised organosilane network that had formed on the outer surface and inside the γ-alumina mesopores. However, the liquid permeability of this membrane was very low in comparison with the results obtained on the other membranes. It appears that two effects are operating: (1) porosity reduction of the γ- alumina layer due to the presence of organosilane groups, leading to a decreased permeability, and (2) chemical modification of the outer membrane surface and the internal pores, offering a hydrophobic environment inside the pores. As the results of this study show, the permeation of solvents is influenced by a combination of these two effects, so that a higher degree of modification also leads to a lower permeability. These results are in accordance with previous work done by Picard et al. (1) on zirconia membranes grafted with fluorinated silanes, where the same trend was observed. Furthermore, the results of Alami Younssi et al. (2), who concluded that the extent of grafting depends on the nature of the silanes used, and that

hydrophobic modification is achieved most effectively with multifunctional silanes, are also confirmed by the findings of this paper.

The DRIFTS results in Figure 8 show the characteristic peaks of the trichloromethylsilane grafted powders, before and after treatment with water.

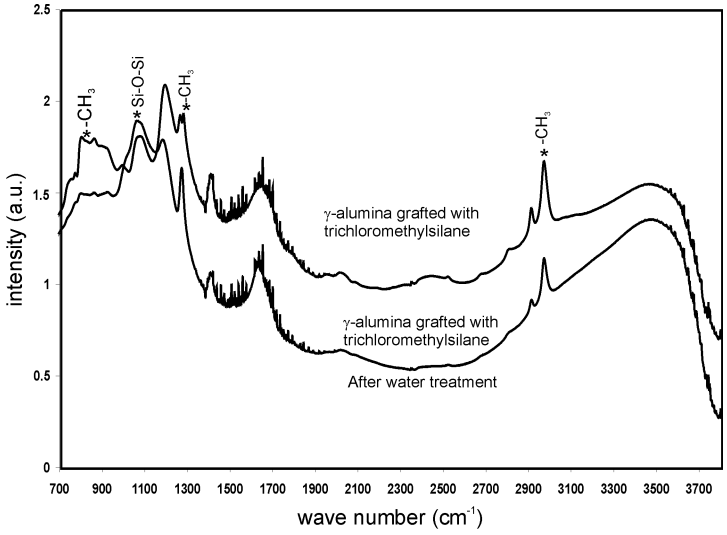

Figure 8 DRIFTS spectra for γ-alumina powders grafted with trichloromethylsilane, before and after treatment with water.

As can be seen from the results the trichloromethylsilane precursor binds strongly to the γ-alumina surface and is able to resist the effect of extended exposure to an aqueous medium.

4.5. Conclusions

It was seen that varying degrees of hydrophobicities were achieved by the use of different precursors. Depending on the side chain lengths and also on the functionality of the precursors, the degree of hydrophobation varied. The triphenyl and t-butyldimethyl silane precursors are bulky and steric hindrance dominated the efficiency of the grafting process. In the case of the monofunctional trimethylchlorosilane, methyl groups were effectively chemisorbed inside the pores, but the extent of modification was not sufficient to impart a hydrophobic environment for hydrophobic solvents. The trichloromethylsilane modified membrane had a predominantly hydrophobic character, as was seen by liquid permeation, XPS and DRIFTS, due to the polymerised organosilane network that was formed on the outer surface and inside the γ-alumina mesopores. The surface concentration on the membrane and

also the extent to which the hydrophobic moiety enters the pores determines the permeability towards solvents and gases.

4.6. References

1) C. Picard, A. Larbot, F. Guida-Pietrasanta, B. Boutevin, and A. Ratsimihety, Sep. Purif. Technol. 25, 2001, 65.

2) S. Alami Younssi, A.Iraqi, M. Persin, A. Larbot and J. Sarrazin, Sep. Purif. Technol. 32, 2003, 175.

3) A. Dafinov, R. Garcia -Valls, J. Font, J. Membr. Sci. 196, 2002, 69.

4) R. P. Castro, Y. Cahen, and H.G. Monbouquette, J. Membr. Sci. 84, 1993, 151.

5) J. Caro, M. Naoek, and P. Kolsch, Micropor. Mesopor. Mater. 22, 1998, 321.

6) T. Van Gestel, B. Van der Bruggen, A. Buekenhoudt, C. Dotremont, J. Luyten, C. Vandecasteele, and G. Maes, J. Membr.Sci. 224, 2003, 3.

7) R. M. de Vos, Hydrophobic Silica Membranes, PhD Thesis, University of Twente, Enschede, the Netherlands, 1998.

8) C. Eyraud, M. Betemps, J.F. Quinson, F. Chatelut, M. Brun, and B. Rasneur, Bull. Soc. Chim. France 9-10, 1984, I-237.

9) S. Roy Chowdhury, J. E. ten Elshof, N. E. Benes and K. Kiezer, Desalination, 144, 2002, 41.

10) S. Roy Chowdhury, R. Schmuhl, K. Keizer, J. E. ten Elshof and D. H. A. Blank, J. Membr.Sci. 225, 2003, 177.

11) J. Joo, T. Hyeon and J. Hyeon-Lee, Chem. Commun., 2000, 1487.

12) D.R. Anderson in: A. Lee Smith (Ed.), Analysis of Silicones, Wiley, New York, 1974, Chapter 10.

13) L.J. Bellamy, The Infra-red Spectra of Complex Molecules, 3rd ed., Chapman and Hall, London, 1975, Chapter 20.

14) A. Lee Smith, Spectrochim. Acta, 16, 1960, 87.

15) G. Z. Cao, J. Meijerink, H.W. Brinkman, and A. J. Burggraaf, J. Membr. Sci. 83, 1993, 221.

16).C.Guizard,A.Ayral,A.Julbe,Desalination,147,2002,275.

Chapter 5 Development of sol-gel derived microporous organosilica hybrid materials

5.1. Abstract

A novel hybrid inorganic organic sol was prepared by cocondensation of alkoxide precursors with hydrophobic side groups, namely organosilanes $RSi(OR')_3$ and bridged silsesquioxanes, $(R'O)_3$-R''-$Si(OR')_3$. The motivation for this work was the current state of the art hydrophobic microporous material, which is based on methyl triethoxysilylethane (MTES) and tetraethoxysilane (TEOS) and has reported a CH_x:Si ratio between ~0.3 and 0.5. Higher loadings of methyl groups led to a collapse of the siloxane network. In the present chapter, the development of a new hybrid material with a CH_x:Si ratio of 1 is described. Structurally it is based on a combination of the bridged silsesquioxane precursor 1,2-bis(triethoxysilyl) ethane (BTESE, $(EtO)_3$-Si-CH_2-CH_2-Si-$(OEt)_3$) and MTES. It is shown that the particle size and morphology of the sol can be tuned by changing the main reaction parameters, [BTESE]/[MTES], pH, hydrolysis ratio, and reflux time. Microporous organosilica hybrid powders with micropores of 0.24-0.28 nm diameter were obtained after calcination in N_2. It was shown that it is possible to adjust the sol in order to influence the pore size characteristics.

5.2. Introduction

Loy et al. have studied the sol gel chemistry of bridged polysilsesquioxanes $(EtO)_3$-Si-R-Si-$(OEt)_3$ (1). Hybrid organic-inorganic materials with extensive cross linking can be prepared from molecules that contain a variable organic group attached to two or more trifunctional silyl groups via carbon-silicon bonds, which are non hydrolyzable. Sol-gel polymerization of such poly(trialkoxysilyl) monomers leads to network materials called bridged polysilsesquioxanes. The bridging moiety allows the development of the full potential of both organic and inorganic components in polymers with diverse properties. These hybrids contain a wide range of organic and inorganic ratios without phase separation. With low molecular weight bridging groups, the ratio of silica to organic material is approximately equal. A greater control over morphology can be obtained under these conditions utilizing bis- or tris(trialkoxysilanes) as the starting precursors for hybrid materials.

Bis(trialkoxysilyl) monomers are hydrolysed and condensed under relatively mild conditions that are typical for sol-gel polymerizations. Monomers can be dissolved in an organic solvent and the polymerizations are initiated with the addition of aqueous acid or base. An excess of water is usually used (>3 H_2O per Si). Alkoxide groups attached to silicon atoms are hydrolysed to silanols that subsequently condense with each other or with ethoxysilanes to give rise to a siloxane network, as illustrated in Scheme 1.

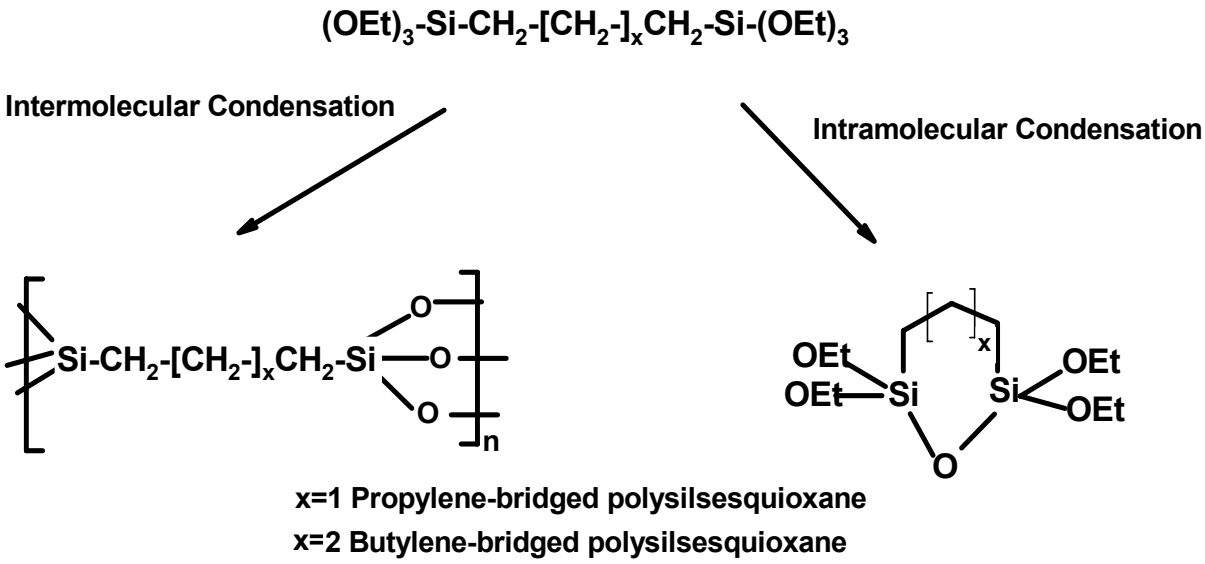

Scheme 1. Intermolecular and intramolecular pathways for the hydrolysis and condensation of 1,3-bis(triethoxysilyl)propane and 1,4-bis(triethoxysilyl)butane (2). Where x represents number of methylene groups ($–CH_2$) in the skeleton.

As hydrolysis and condensation proceed, highly branched polysilsesquioxanes grow in size, leading to an increase in viscosity of the solution. Before gelation is reached, the sol containing the growing polymers can be cast as thin films or drawn into fibres. If left undisturbed polymerization of most bridged monomers leads to gels within a few hours. Sol-gel polymerizations of bis(trialkoxysilyl) monomers are in almost all respects similar to those of purely inorganic precursors such as TEOS (tetraethoxysilane). The main difference is that bridged polysilsesquioxanes form gels at lower concentrations than sol-gel polymers derived from tri- and tetra-ethoxysilanes.

Sol-gel polymerizations of monomers with two triethoxysilyl groups, $(EtO)_3Si\text{-}R\text{-}Si(OEt)_3$, give hydrocarbon bridged polysilsesquioxanes which are cross-linked polymeric gels (2). However, when such α, ω- bis(triethoxysilyl)alkanes ($R=\text{-}[CH_2]_n\text{-}$, n=2-14) are polymerized, the flexible alkylene-bridging group may allow intramolecular reactions that produce cyclic (di)silsesquioxanes, in addition to intermolecular condensation which leads directly to polymers and gels. This is illustrated in detail in Scheme 1.

The acyclic and cyclic silsesquioxanes are different in their structure and reactivity. Depending on whether polymerization proceeds via intramolecular or intermolecular pathway, the architecture of the resulting polymer varies. It was found from mass spectrometry and ^{29}Si NMR spectroscopy that the length of the alkylene bridging group has a profound effect on the degree of cyclization and polymerization of α, ω- bis(triethoxysilyl)alkanes and thus on the formation of polymeric gels. Since the intramolecular pathway does not contribute to the formation of polymeric networks necessary to form gels, cyclization reactions slow or even prevent gelation. Under basic conditions, where the rates of hydrolysis and condensation of alkoxysilanes have been shown to increase with the extent of reaction, all α, ω- bis(triethoxysilyl)alkanes react to form polymeric gels within a few hours. But under acidic conditions, where the reaction rates decrease with extent of reaction, there was a strong dependence of gelation times on the length of alkylene group.

Gelation times measured in months were observed with monomers with shorter alkylene bridging groups (n=2-4) because of the formation of stable six-and seven-membered bicyclic disilsesquioxanes (n=3-4) and cyclic dimers (n=2), as shown in Scheme 2. In a bicyclic disilsesquioxane two silsesquioxane species first condense and then couple to form two cyclic rings. In a cyclic dimer, intramolecular cyclic structures are first formed which then couple together.

Loy et al. studied the cyclization phenomena during the synthesis of alkylene-bridged polysilsesquioxanes for monomers with short alkylene bridges of 2-4 carbons.
The cyclic products were found to inhibit the polymerization of the monomers under acidic conditions. The ethylene-bridged monomer formed an unusual bicyclic dimer **4** which consisted of two fused

seven membered organosiloxane rings (3). The mass spectrum of the reaction products of 1,2-bis(triethoxysilyl)ethane **1** with 1 equivalent of water under acidic conditions showed that the products were predominantly the bicyclic dimer **4** and its hydrolysis products.

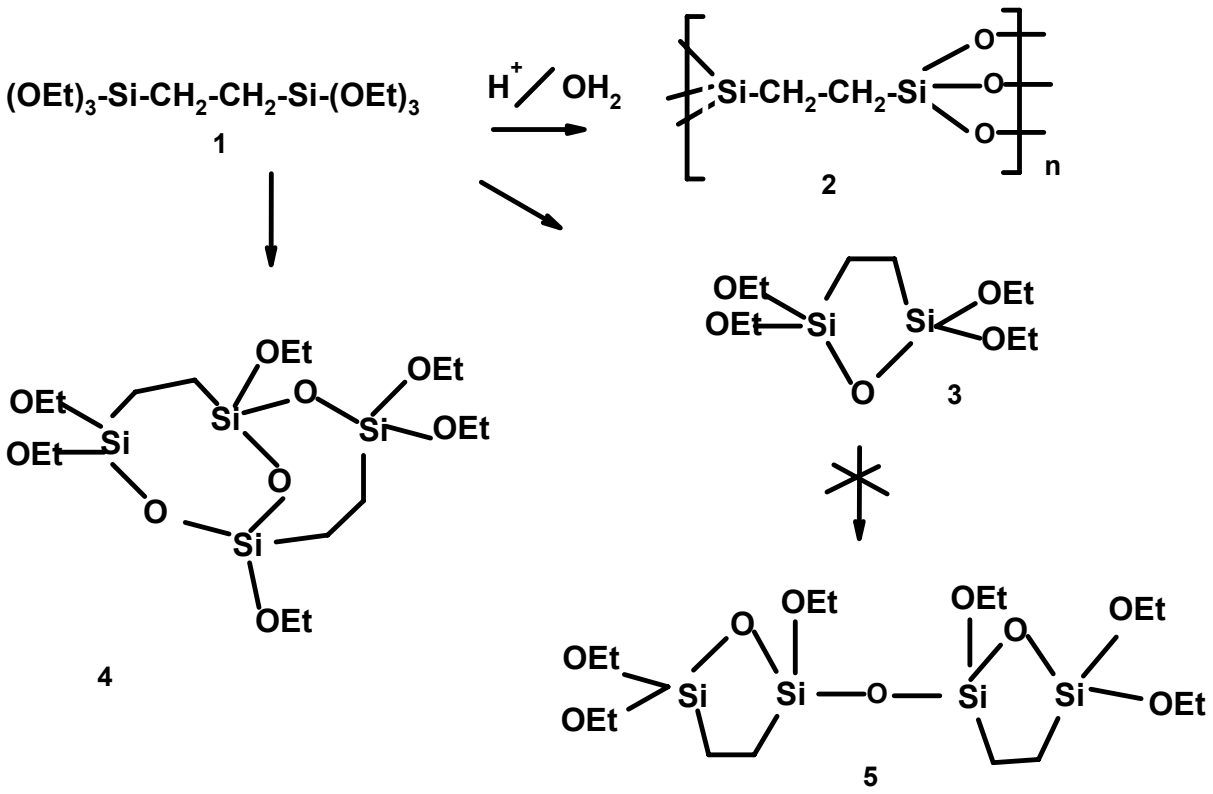

Scheme 2. Reaction paths for the hydrolysis and condensation of 1,2-bis(triethoxysilyl)ethane **1** into a polymeric network **2**, an unreactive cyclic dimer **3**, or a bicyclic dimer **4**.

In the present study the experimental efforts are focused on the development of a microporous organic-inorganic hybrid material with a high loading of organic components. The final goal is to develop stable sols that are suitable for microporous thin film formation on membranes.

The ethylene-bridged precursor 1,2-bis(triethoxysilyl)ethane, $(EtO)_3$-Si-CH_2-CH_2-Si-$(OEt)_3$ (BTESE) is used because of the length of the bridging group. The number of bridging carbon groups has an influence on the cyclic structures formed, and on gelation, which ultimately influences the microstructure of the material. Shea et al. found that the pore diameters of the gels increased with the increase in length of the carbon bridge (4). For the formation of microporous materials with pore sizes in the range of single molecules it is therefore more desirable to use BTESE, with a bridging group containing only two carbon atoms.

We employed a combination of MTES and BTESE for the sol-gel reaction. The average alkoxide functionality (number of hydrolysed alkoxies per precursor) *f*, is given by equation 1,

$$f = (\{\rho_{BTESE} \times c_{BTESE}\} + \{\rho_{MTES} \times c_{MTES}\})/ (c_{BTESE}+c_{MTES}) \quad [1]$$

where ρ_{BTESE} and ρ_{MTES} are the number of hydrolysable alkoxy groups in BTESE and MTES, respectively, and c_{BTESE} and c_{MTES} are the concentrations of BTESE and MTES, respectively. The presence of MTES brings down the average alkoxide functionality in solution, so that the formation of fast growing, anomalously large particles is inhibited. It also lowers the statistical chance that two bridged monomers will couple and undergo condensation into unreactive dimers. Hence it helps in the uniform growth of the polymeric network.

The influence of reaction parameters like the hydrolysis ratio $[H_2O]/([BTESE]+[MTES])$, the molar ratio of the starting precursors, [BTESE]/[MTES], the ratio of acid to precursor $[H^+]/([BTESE]+[MTES])$, and reflux time on the growth and pore characteristics of the resulting materials was studied. The techniques used for characterization of the sol and unsupported powders were nuclear magnetic resonance (NMR) and Mass Spectrometry to study the molecular structure of the sols, Dynamic Light Scattering for particle size measurements on sols, adsorption studies (N_2, CO_2, C_2H_2) for pore size distributions, and atomic adsorption spectroscopy (AAS) for the chemical stability of sols.

5.3. Experimental

5.3.1. Synthesis

The precursor BTESE (1,2-bis(triethoxysilyl)ethane, purity 96%, Aldrich) was distilled before use to remove traces of impurities and water. MTES (methyl-triethoxysilyl ethane, purity 99 %, Aldrich) was used as-received. Ethanol was dried before use with molecular sieve beads of sodium aluminium silicate with pore sizes of 1.0 nm. The precursors were separately dissolved in ethanol. MTES/ethanol was added to BTESE/ethanol. The reaction mixture was stirred with a magnetic stirrer in an ice bath. Water was mixed with acid solution (HNO_3, 65 wt %, Aldrich). Half of the acid/water mixture was added to the precursor mixture, and the sol was allowed to reflux at 60˚C for 3 h. The remaining half of the acid/water mixture was added after 1.5 h, allowing the reaction mixture to be stirred with a magnetic stirrer in an ice bath. This stepwise addition of the acid/water mixture suppresses multiple hydrolysis of precursor alkoxide groups, thus helping the uniform growth of particles in the sol.

The range of the concentration of the reactants are as follows:
[BTESE]/[MTES]=(0.25-3), $[H_2O]/([BTESE]+[MTES])$=(1-7), $[H^+]/([BTESE]+[MTES])$=(0.025-0.2). The reaction parameters of sol A are [BTESE]/[MTES]=1, $[H_2O]/([BTESE]+[MTES])$=2, and $[H^+]/([BTESE]+[MTES])$=0.1. Sol C has the same composition as Sol A, except that it was refluxed for 7 h. Sol B has a higher hydrolysis ratio $[H_2O]/([BTESE]+[MTES])$=4.

Powders were obtained by drying the sols in a petri dish. As a standard heat treatment, all powders were calcined at 300˚C for 3 h in a N_2 atmosphere, with 0.5˚C/min heating and cooling rates. Thermogravimetric analysis (TGA) in flushing nitrogen was done on the unsupported powders, to study the burnout of organic groups. The experiments were performed in a N_2 stream with a heating rate of 0.5 ˚C/min up to to 600 ˚C. The instrument was a Setaram MTB 10-8 Microbalance (Setaram, Lyon, France).

5.3.2. Characterization Techniques

NMR

^{29}Si Nuclear Magnetic Resonance on sols was carried out on a Bruker 500 MHz NMR in a 10 mm tube with a spinning frequency of 8 Hz. Pulse duration was 10 μs (~45° pulse), with a repetition rate of 2.5 s. Deconvolution of the spectra to assess the degree of condensation was carried out with WINNMR. A volume of 6 ml of sol was used in the measurements. The sols were stored and measured at -80°C. Cr(acac) (0.1 wt %) was added to decrease the magnetization rate of the silicon nucleus.

Particle size measurements

Particle size measurements were carried out in a Malvern Zetasizer 3000HSa. The zetasizer was used to determine the size of particles suspended in the ethanol-based sols in the particle size range of approximately 2-1000 nm. Particle sizes measured below 2 nm can be considered as approximate values. All measurements were done on freshly prepared sols unless stated otherwise.

Mass Spectrometry

Mass Spectra of sols were taken on a FINNIGAN MAT-95 double focussing instrument. The spectra were taken with Fast Atom Bombardment ionisation and 3-Nitro benzyl alcohol as matrix. The sols were analysed as prepared.

N_2, CO_2 and C_2H_2 adsorption

Adsorption/desorption isotherms of N_2 (77 K) and CO_2 (273 K) and C_2H_2 (273 K) on dried calcined powders were determined on a CE-Instruments Milestone 200 (5). All materials were pre-treated by evacuation to below 10^{-4} mbar at 473 K. Continuous corrections were being made for variations in the atmospheric pressure p_o (6, 7). Surface areas were determined from the adsorption isotherms by the Dubinin method, modified by Kaganer, between $p/p_0=2\times10^{-5}$ and 1×10^{-2}, as represented by

$$\log n = \log n_m - D (\log p_o/p)^2 \quad [2]$$

where n is the gas adsorbed at relative pressure p/p_o, n_m the monolayer capacity of the surface, both in moles per gram of adsorbent, and D an adsorbate-dependent constant. Surface areas A were determined with

$$A=n_m a_m N_A, \quad [3]$$

in which a_m is the area occupied by a molecule in the completed monolayer and N_A is Avogadro's number. The value of a_m is assumed to be 0.162 nm^2 for N_2, 0.179 nm^2 for CO_2 and 0.204 nm^2 for C_2H_2 (8).

Density measurement

Volume and Density measurements were performed by gas pycnometry.

A gas pycnometer operates by detecting the pressure change resulting from displacement of gas by a solid object. An object of unknown volume V_{sample} is placed into a sealed chamber of known volume V_{cell}. After sealing, the pressure within the sample chamber is measured P_1. Then an isolated reference chamber of known volume $V_{expansion}$ is charged to a pressure P_2, which is greater than that of the sample chamber. A valve isolating the two chambers is opened and the pressure of the system is allowed to equilibrate (9).

The pore volume was calculated as follows: $\rho = m/V$.

The mass m of the sample is a known quantity.

$V_{sample}=V_{cell}-V_{expansion}/ (\{P_1/P_2\}-1)$

Where P_1 is the applied pressure, P_2 is the final pressure, V_{sample} is the volume of the sample.

Helium typically is the gas used because it readily diffuses into small pores.

Densities of bulk materials were measured by a Multivolume Pycnometer 1305 at room temperature using He as filling gas. The (dried) powder samples were flushed with dry He until the measured volumes remained unchanged and no water was present in the pores. Particle densities were determined from the volumes by immersing the fragments in mercury, which measurement includes the pore volume (6).

Atomic adsorption spectroscopy

To determine the chemical stability of the hybrid powders in terms of solubility, samples of 0.11 g of powder were soaked in aqueous solutions (volume 10 ml) with pH between 1.5 and 13 for 24 h at room temperature. A 0.05M nitric acid solution was used. The liquid was then analysed for Si by atomic adsorption spectroscopy (AAS, Unicam Spectra AA 939, Solaar). The gas used was nitrous oxide / acetylene. For the element of interest, Si, the detection limit of AAS is 0.3 mg/l.

5.4. Results and discussion

5.4.1. NMR studies

Figure 1a shows the ^{29}Si NMR spectra of sol A taken after 5 min. and 45 min. of reaction. It was difficult to obtain quantitative data of the mixed MTES/BTESE sols, because of overlapping spectral lines. The condensed species show spectral lines at lower field (-50 to -65 ppm) whereas the spectral lines of the hydrolysed species are at higher field end (-50 to -40 ppm).

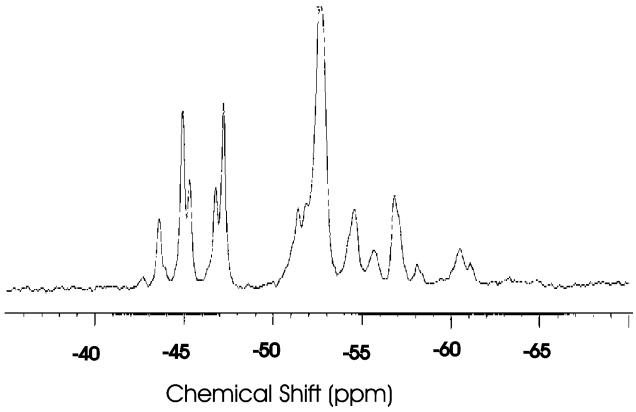

5 min

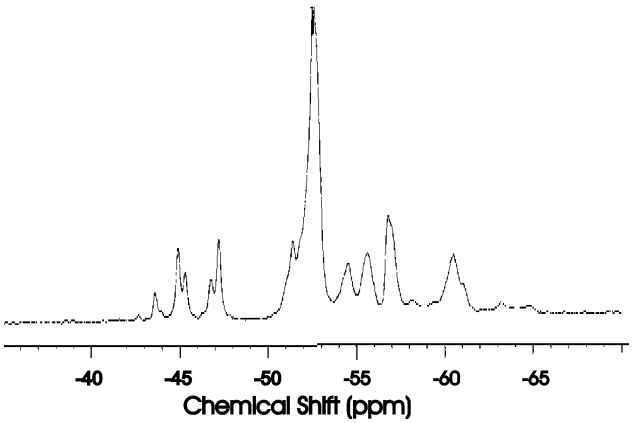

45 min

Figure 1a NMR spectra for co-condensation of BTESE/MTES, after 5 min and 45 min of reaction. Water addition was done in two steps, second addition took place after 1.5 h.

At the start of reaction, the peaks of hydrolysed species developed gradually, indicating the hydrolysis of monomeric species. After 45 minutes, condensed species had formed predominantly from the hydrolysed monomers. Figure 1b shows the evolution of the spectra after water addition after 95 min.

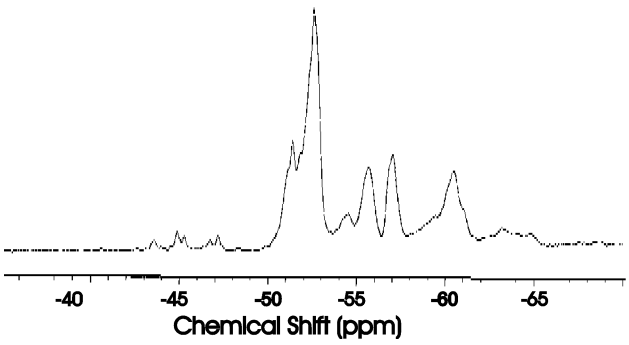

90 min

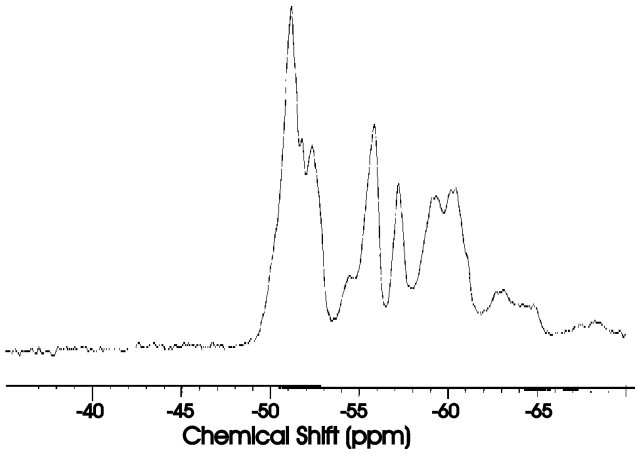

Water added 95 min

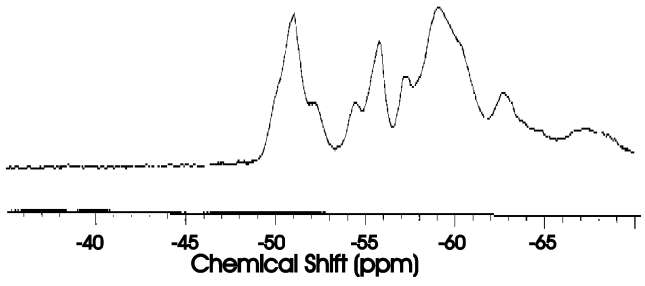

3 h

Figure 1b NMR spectra for co-condensation of BTESE/MTES after 90 min, 95 min and 3 h of reaction. Water addition was done in two steps, second addition took place after 1.5 h.

A change in the spectra was found after the 2nd addition of water, indicating that partly condensed species hydrolyse further and monomeric species condense. After 3 hours there are predominantly condensed species as the peaks broaden. The study provides insight into the fact that a two-step addition of water is critical for a uniform and more homogeneous growth of the sol. During the first step of water addition, hydrolysis of monomers takes place which then start to condense to form a siloxane network. The second step of water addition helps in the further hydrolysis of dimeric species, as well as condensation. Figure 1c shows the spectra after 3 h for a sol in which water was added in a single step at the start of the reaction.

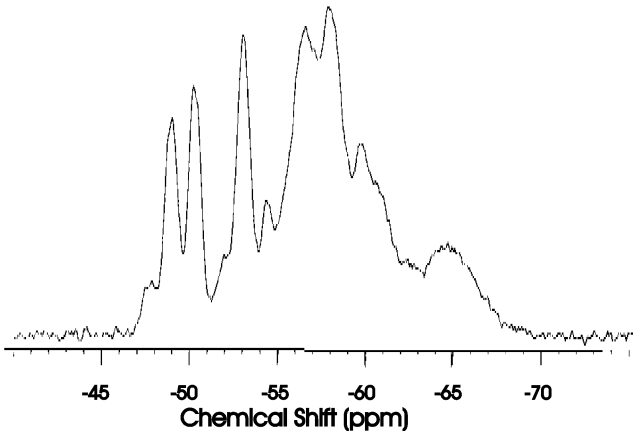

Figure 1c NMR spectrum for co-condensation of BTESE/MTES after 3 h of reaction.
Water was added in a single step at the start of reaction.

The occurrence of peaks at higher field -50 to -40 ppm indicates that non-hydrolysed dimers and trimers are still present at the end of the reaction (after 3 h). Castricum et al. found that hydrolysis proceeds at the same rates for MTES and BTESE, hence additional hydrolysis will have occurred in both precursor molecules. Over time, condensation was found to proceed gradually, with more extensive hydrolysis observed in the course of condensation. The rate of condensation per Si atom was slightly lower for BTESE (it was similar to that of TEOS), but the fact that BTESE contains 6 hydrolysable groups compensates for the lower condensation rate. The NMR results indicate that a polymeric network is formed in the case of BTESE and MTES, with BTESE as the matrix. These results will be discussed in more detail elsewhere by Castricum et al. (8)

5.4.2. Mass Spectrometry

Mass spectrometry (MS) on sols was carried out to determine the main species present in the sol. Figure 2 shows the MS spectrum of sol A as a function of mass/charge (m/z) ratio. The spectra are taken over a wide range of molecular weights (0-2500 g/mol). The main peaks due to hydrolyzed and

condensed products were observed at m/z=302, 345, 390, 487, 509, 643, 786, 933, and 1007. The peaks indicate the presence of intermediates of considerable stability. A clear periodicity is observed in the spectrum from 390 onwards, as the maxima appear at molecular weight differences of ~130-140 g/mol.

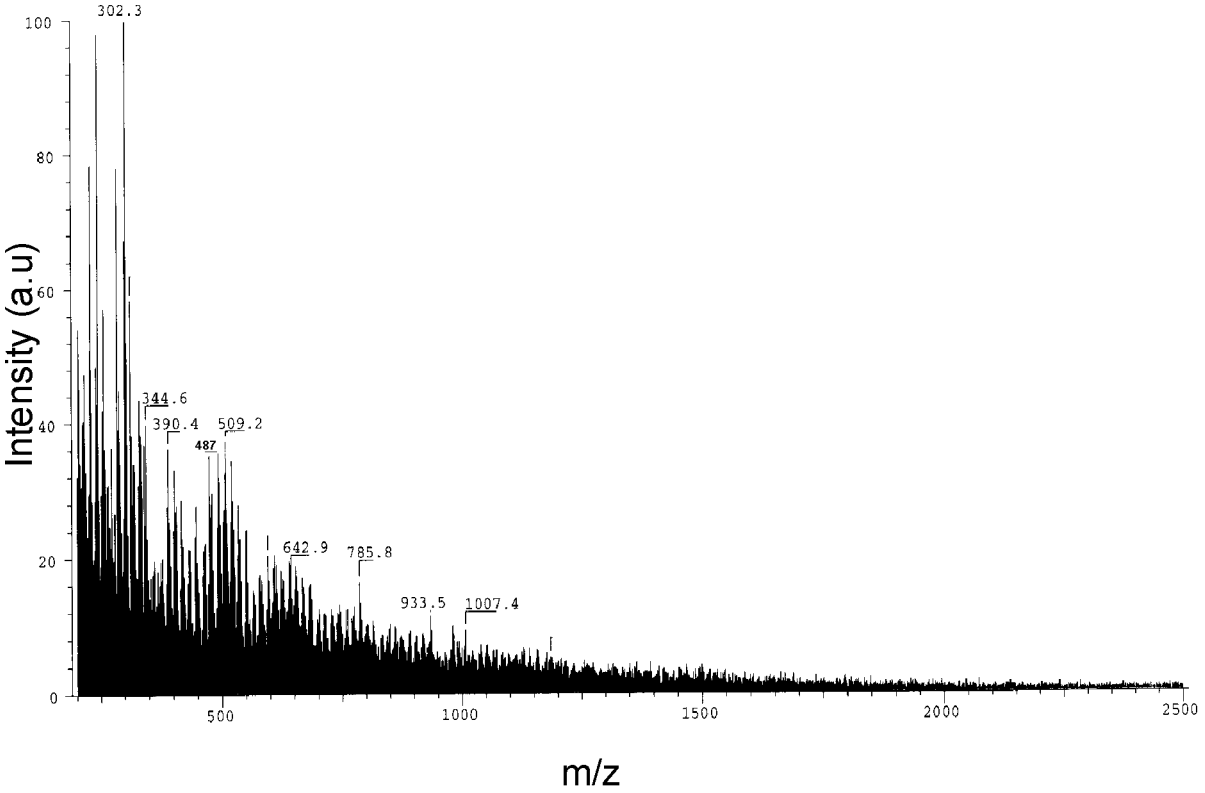

Figure 2 Mass spectroscopy spectrum of sol A.

The weight of a unit of the fully condensed species $–CH_2\text{-}SiO_{1.5}\text{-}$ is 66 g/mol. So each new maximum indicates a particle with a weight of about 1 condensed BTESE ($–SiO_{1.5}\text{-}CH_2–CH_2\text{-}SiO_{1.5}\text{-}$) or 2 condensed MTES ($–CH_2\text{-}SiO_{1.5}\text{-}$) species larger. Since it seems unlikely a priori that MTES species would become incorporated in growing sol particles only in pairs, the low molecular weight material probably consists mostly of BTESE oligomers. The peak maxima at 509, 643, 786, and 933 represent unreactive complexes built up primarily of such BTESE units with unhydrolysed ligands. The peaks at higher m/z, i.e., 1500- 2500 g/mol represent heavier oligomer species which may contain both BTESE and MTES units.

Loy et al. (4) isolated the bicyclic dimer **4** of Scheme 2 at an m/z ratio of 487 by mass spectrometry. The intermediate **4** is stable (unreactive) and therefore does not get incorporated in the polymer chain. The mass spectra in Figure 2 does show a peak at m/z ratio of 487, indicating the presence of bicyclic BTESE intermediate **4** in the current system of study. It is seen from Figure 2 that intermediates (dimers, trimers, cyclic, hydrolysed or protonated species) formed in co-condensation of MTES and BTESE have molecular weights ranging from 250 to at least 2500 g/mol.

Figure 3 shows the low molecular weight fraction of the sol in more detail. Peak maxima in the range of molecular weights between 340- 480 g/ mol are numbered.

These peaks indicate the presence of isotopes. Isotopes are atoms of the same element having the same atomic number but with different masses due to different numbers of neutrons. The prominent peaks are occurring at a molecular weight difference of 2 g/mol. The element H has two stable isotopes, protium (abbreviated as ^{1}H) and deuterium (abbreviated as ^{2}H). A possible explaination to account for the difference could be deuteration of the complexes, in the sol, during hydrolysis and condensation reactions.

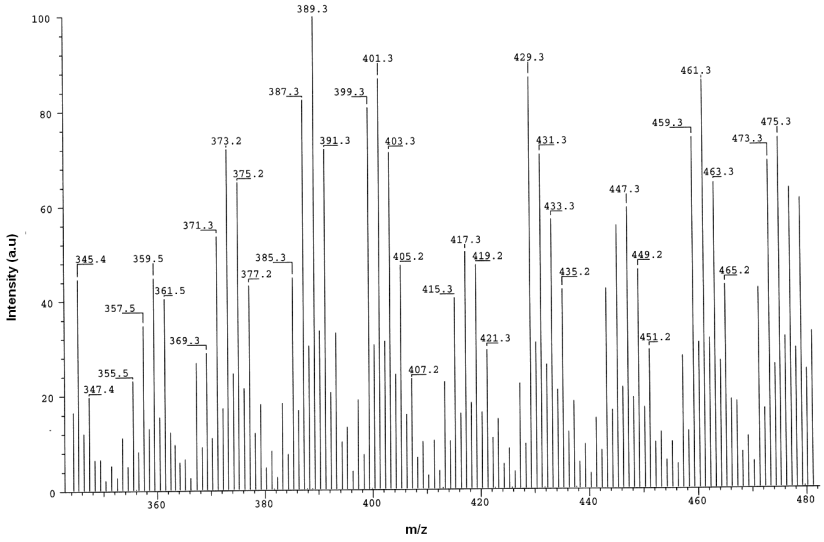

Figure 3 Mass spectroscopy spectrum for sol A for the range of molecular weights from 340-480 g/mol.

Figure 3 also shows peaks at a periodic difference of 28 g/mol. Some examples are (359.5 and 387.5), (373.2 and 401.2), (389.3 and 417.3), (401.3 and 429.3), (431.3 and 459.3), (447.3 and 475.3). In the hydrolysis and condensation of BTESE with MTES, the $–OC_2H_5$ group (45 g/mol) is replaced by –OH group (17 g/mol). The ethoxy group is the leaving group whereas the hydroxyl group is the incoming group. The difference in molecular weights of these two groups (28 g/mol) explains the above observation.

Campaniello et al. studied sols of methylated silica. These sols were prepared by acid catalysed reaction of precursors TEOS and MTES. Gel permeation chromatography was used to determine the particle size distributions. In Gel permeation Chromatography, the particle size is expressed in molar mass, while in mass spectrometry a number distribution of molecular weights of ionized species is

obtained. The authors have reported average particle size around ≈1000 g/mol, respectively. The correlation of these Gel Permeation Chromatography results with that of the mass spectrometry spectra of the present sols, indicate a structural similarity between these two types of sols.

5.4.3. Sol stability

The sols formed were monitored by light scattering experiments after a period to investigate the influence of ageing. Figure 4 shows the particle size distribution of the hybrid inorganic-organic sol A as a function of time.

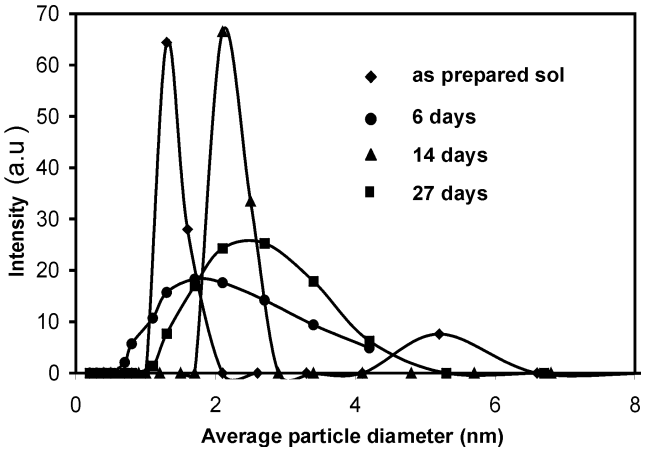

Figure 4 Particle size distributions of sol A as a function of ageing time.

There is gradual slight increase in the particle size from 1.4 nm to 2.5 nm over a period of 27 days. The sol exhibits particle growth with time but if stored at low temperature (5°C), it is useful for our particular interest, which is forming thin films on membranes.

5.4.4. Influence of pH

In order to obtain a microporous material the sol polymers must be able to interpenetrate considerably (10). Short slightly branched linear polymers are the most suitable for this purpose. These are formed predominantly in acid catalyzed sol-gel reactions where the alkoxy group is protonated and subsequently replaced by water according to an S_N2 reaction with the inversion of the silicon tetrahedron.

Under basic conditions, a nucleophilic hydroxyl anion attacks the silicon of the alkoxysilane. A pentavalent negatively charged intermediate is formed. Condensation of silanols in basic conditions takes place along the inner centers of oligomers, resulting in highly branched dense polymers. Such

materials are suitable when mesoporous systems are to be developed. Since the final aim is to prepare truly microporous materials with no mesopores present, all sol-gel reactions have been carried out in an acidic environment at pH ranges mentioned earlier.

Figure 5 shows the variation in particle size as the ratio of the acid/precursor is changed. The sol preparation conditions were the same as Sol A, with the acid concentration being varied each time. Freshly prepared sols were used.

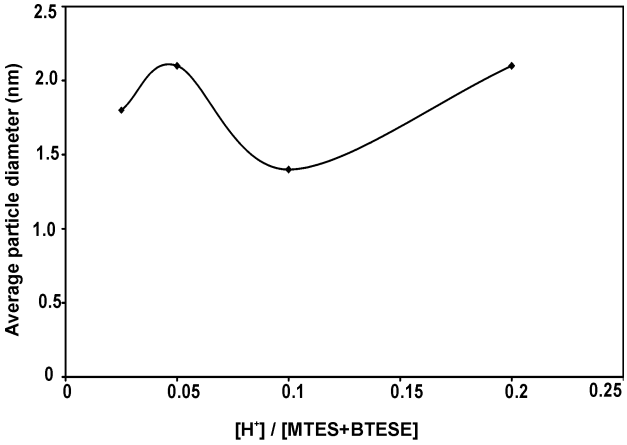

Figure 5 Influence of $[H^+]$/ [BTESE+ MTES] on the average particle diameter of sol A.

The preparation conditions are acidic and below the isoelectric point of silica of ~2.5. No significant differences in particle sizes are observed in the pH range 0.6 – 1.6.

5.4.5. Influence of molar ratio of [BTESE]/ [MTES]

Figure 6 shows the variation in particle size of sol A as the molar ratio [BTESE]/[MTES] is changed. The reaction conditions were the same as in sol A, with the [BTESE]/[MTES] ratio being changed each time.

The sol was analyzed as prepared. At [BTESE]/[MTES] =0.25, i.e., at a molar excess of MTES, the mean particle diameter is 7.7 nm. At [BTESE]/ [MTES] =1, the mean particle diameter is 1.4 nm. At [BTESE]/ [MTES] =3, i.e., at a molar excess of BTESE, the mean particle diameter of the sol was ~70 nm. The particle diameter of the sol appears to reach a minimum as the ratio of [BTESE]/ [MTES] is increased.

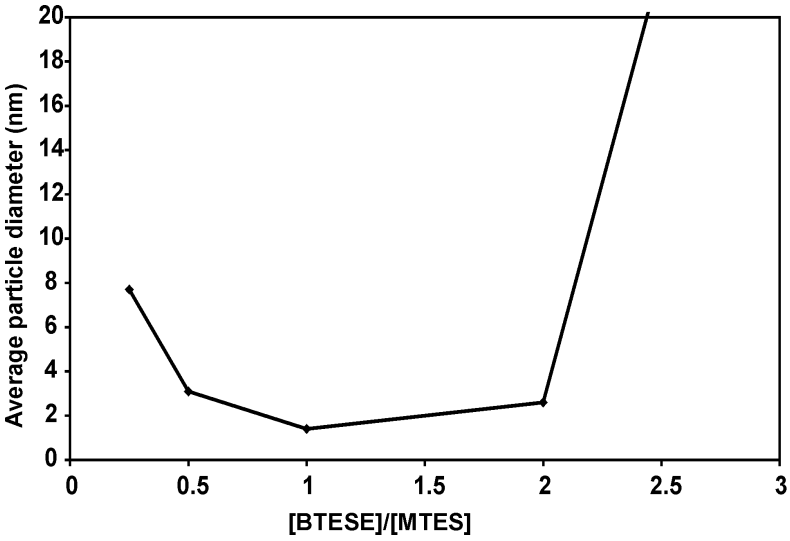

Figure 6 Influence of [BTESE]/ [MTES] ratio on the average particle diameter of sol A.

Apparently to keep a small particle size it is advantageous to mix BTESE and MTES in a roughly similar ratio. In Scheme 2 in the Introduction, various intermediates formed during hydrolysis and condensation of BTESE are shown. For instance, the intermediates **3**, **4** and **5** are stable complexes that do not get incorporated into the polymer chain easily. These intermediates may inhibit uncontrolled polymeric growth of a sol. The presence of MTES in approximately the same ratio helps in the linear growth of polymer chains in the sol in two ways: 1) it brings down the average alkoxide functionality in solution, so that the fast formation of large particles, which occurs easiest from nuclei with a large number of reactive groups, is inhibited; 2) It also lowers the statistical chance that two bridged monomers will couple to form unreactive complexes such as **4**. Of the various factors governing the reaction, the 1:1 mixture of BTESE and MTES, appears to be a preferred combination in the current circumstances.

5.4.6. Influence of hydrolysis ratio

Figure 7 shows the particle sizes upon variation of the hydrolysis ratio. The sol had the same reaction conditions as Sol A with the water concentration being varied each time. The hydrolysis ratio is defined here as the molar ratio of water to precursor (BTESE+ MTES).

For a 1:1 molar ratio of bridged precursor and MTES, the average monomer functionality defined earlier is 4.5. Complete hydrolysis can therefore occur at a hydrolysis ratio of 4.5 or more. Apparently, higher hydrolysis ratios do not lead to further growth of the particles; excess water is present in that case.

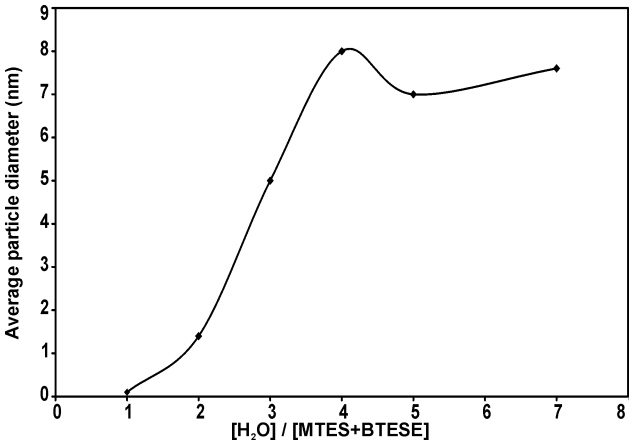

Figure 7 Influence of [H_2O]/ [BTESE+ MTES] on the average diameter of sol A.

Below the value of 4.5, the growth of particles appears to be limited by the available concentration of water and the formation of smaller particles is observed.

5.4.7. Influence of reflux time

Figure 8 shows the influence of reflux time on particle size of sol A.

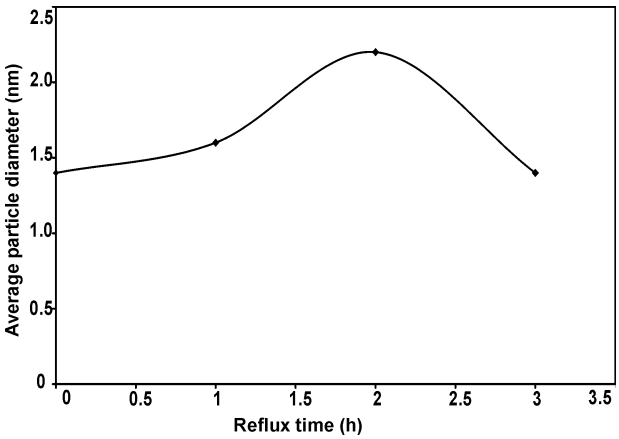

Figure 8 Influence of reflux time on the average diameter of sol A.

No appreciable difference in particle size is seen as reflux time increases from 0 to 3 h. Probably one of the reasons we do not see a difference in particle size is because the hydrolysis ratio was only 2, so that all water was completely consumed in the hydrolysis of the precursors, while it was insufficient for large sol particles to be formed. However, with SAXS morphological differences in the wet sols would be more evident.

5.4.8. Adsorption and density experiments

Figure 9 shows the weight loss upon calcination of the air-dried sol A as a function of temperature as found with TGA analysis.

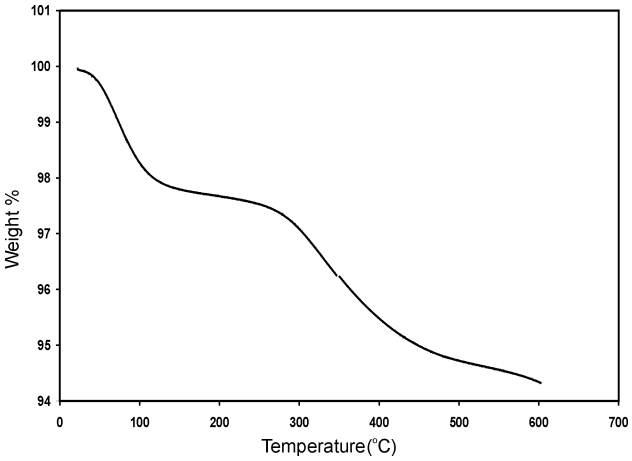

Figure 9 Weight loss of air-dried hybrid powder as a function of calcination temperature in N_2.

The sharp decline in weight till 100 ˚C indicates loss of residual physisorbed water. The second sharp decrease with an onset at 300 ˚C is attributed to decomposition of organic groups and further condensation (dehydroxylation) of the (organo)silica phase. At higher temperatures further decomposition of organic groups and densification of the silica with loss of hydroxyl groups occurs. Therefore, all powders discussed below were calcined at 300˚C in nitrogen.

Samples A, B and C (discussed in detail in the experimental section) were found to be closed towards N_2 physisorption. This suggests that the pore size is smaller than the size of N_2 (0.3 nm). As can be seen in Table 1, the surface areas determined by CO_2 adsorption (molecular diameter 0.28 nm) are of similar magnitude for all three samples, with somewhat higher values for sample C. With C_2H_2 (0.24 nm) as the probe molecule the surface areas were substantially larger than found with CO_2. As C_2H_2 has a smaller critical diameter than CO_2, larger quantities will be adsorbed in small micropores. This indicates that the hybrid gels have small pores with sizes between those of CO_2 (molecular diameter 0.28 nm) (11) and C_2H_2 (molecular diameter 0.24 nm). For pore size distributions or pore entrances with a mean just above the critical diameter of C_2H_2, this will result in a large difference in adsorption between C_2H_2 and CO_2, as was indeed observed here. A similar difference is found between surface areas determined by N_2 and CO_2 in the absence of micropore filling, as N_2 has a larger critical diameter than CO_2.

For measurement of the density, He with a critical diameter of 0.2 nm was used as a replacement gas. It was thus possible to probe the ultramicropores present. Of course the regions with pore sizes smaller than 0.2 nm could not be probed with He gas. He is the smallest probe molecule, however the density measurements took a long relatively time for equilibration, 1-2 minutes as compared to seconds in "normal" cases, indicating that the small pores allowed only slow transport of He molecules with a size of 0.2 nm. This is an indication of ultramicroporous character of the hybrid materials. The densities as listed in Table 1 are higher than that of pure MTES (ρ=1.32 g/cm^3).

In MTES, the –CH_3 group is incorporated in the pores of the siloxane network giving rise to regions where He gas does not approach. This is known as closed porosity. The hybrid BTESE-MTES samples are more open to He gas than MTES, which exhibits pockets of closed porosity (7), thus exhibiting higher densities.

Table 1 Specific surface areas from CO_2 and C_2H_2 adsorption on powders derived from sols A, B, and C. Density as determined by He method.

Sample	[BTESE]/ [MTES]	[H_2O]/ ([BTESE] + [MTES])	CO_2 surface areas (m^2/g)	C_2H_2 surface areas (m^2/g)	Density (g/cm^3)
A	1	2	340	1649	1.54
B	1	4	344	1340	1.50
C	1	2	552	2941	1.59

5.4.9. Chemical Stability of the hybrid powders

AAS was used to study the amount of Si that had leached out into the liquid phase.
Table 2 gives the weight % of Si present in the liquid after treatment with solutions of different pH. The hybrid powders are stable in the pH range between 1.5 and about 8. Sekulic et al. (12) investigated the chemical stability of amorphous silica by similar solubility tests with unsupported material at room temperature. They also used AAS to analyse the leached material. It was found that pure silica is stable in the pH range below 8, at least down to 2.

Table 2 Percentage of Si on total Si in the material leached out in solutions of different pH, for Sample A.

pH	Weight%Si
1.5	<0.006
2	<0.006
4.5	<0.006
5.5	<0.006
6.5	0.07
8.5	0.3
11.5	0.8
13	1.0

Apparently, the stability of the BTESE - MTES composite is very similar to that of pure silica. The reason for this is that in both materials the siloxane bridges Si-O-Si are the weakest bonds, being susceptible to hydrolysis by water.

5.5. Conclusions

From the above results, it is seen that the particle size and morphology of organosilica sols and powders can be tuned by changing the main reaction parameters, [BTESE]/[MTES], pH, hydrolysis ratio, and reflux time. Hence, depending on the application of interest it is possible to modify the pore size characteristics by tuning the sols. It has been shown to be possible to obtain a microporous hybrid powder starting from MTES and bridged silsesquioxane precursors.
Details of thin film formation on membranes with the sols described in this chapter will be discussed in Chapter 6.

5.6. References

1) D. A. Loy and K. J. Shea, Chem. Rev. 95, 1995, 1431-1442.
2) D. A. Loy, J. P. Carpenter, S. A. Myers, R. A. Assink, J. H. Small, J. Greaves, and K. J. Shea, J. Am. Chem. Soc. 118, 1996, 8501-8502.
3) D. A. Loy, J. P. Carpenter, T. M. Alam, R. Shaltout, P. K. Dorhout, J. Greaves, J. H. Small, and K. J. Shea, J. Am. Chem. Soc. 121,1999, 5413-5425.
4) K. J. Shea and D. A. Loy, Chem. Mater. 13, 2001, 3306-3319.
5) H.L. Castricum, A. Sah, M. C. M. Hazeleger, C. Huiskes, J. E. ten Elshof, to be submitted.

6) M. G. Kaganer, Z. F. Khim, 33, 1959, 2202.

7) S. J. Gregg, K. S. W. Sing, Adsorption, Surface Area and Porosity, 2nd Ed., Academic Press, London, 1982, 42.

8) H. L. Castricum, A. Sah, J. E. ten Elshof, D. H. A. Blank, to be published.

9) Volume and Density Determinations for particle technologists, Micrometrics Instrument Corp. 2/16/01.

10) B. N. Nair, W. J. Elferink, K. Keizer, and H. Verweij, J. Colloid Interface Sci. 178, 1996, 565-570.

11) M.C. Mittelmeijer-Hazeleger, H. de Jonge and A. Bliek, in Characterization of Porous Solids IV, Eds. B. McEnaney, T.J. Mays, J. Rouquérol, F. Rodriguez-Reinoso, K.S.W. Sing, K.K. Unger, The Royal Society of Chemistry, Cambridge, UK, 1996, p. 429.

12) J. Sekulic, M. W. J. Luiten, J. E. ten Elshof, N. E. Benes, K. Keizer, Desalination, 148, 2002, 19-23.

Chapter 6 Development of hybrid inorganic-organic silica membranes and study of transport properties.

6.1. Abstract

The transport of solvents and gases through γ-alumina supported membranes with hybrid silica microporous top layers is studied. The preparation of the hybrid silica sols of which the membrane top layers were prepared has been discussed in detail in Chapter 5. Coating experiments showed that when the particle size of the sol was very small, penetration of the sol particles into the underlying layers of the support occurred, and this had an effect on the flux of solvents in pervaporation tests. The flux of water and solvent was very low in that case. When larger sols were used, much less penetration was observed. SEM and XPS showed that the thickness of the hybrid films can be tuned by changing the sol parameters like the hydrolysis ratio, or by coating single or double layers. The calcined hybrid silica layer appeared to have a low surface tension, so that application of a second layer resulted in a non-uniform thickness because of lack of wetting of the surface. This is indicative of a hydrophobic surface. In the current composite membrane system of interest, α-alumina (macroporous)/γ-alumina (mesoporous)/hybrid silica (microporous), membranes were characterized by SEM, XPS, permporometry, gas permeation and pervaporation. In gas permeation experiments, H_2/O_2 showed a permselectivity of ~ 3, and a H_2/SF_6 permselectivity of ~100. Permeation experiments with H_2 as permeating species in the presence of water vapour at different partial pressures showed no decrease in permeance, indicating that adsorption of water vapour did not occur in the pores. This is an indication of the hydrophobic environment provided by the hybrid silica top layer. In pervaporation, for a 97.5 wt% n-butanol and 2.5 wt% water mixture, the membrane showed a separation factor of ~150 for at least 3 months at a temperature of 150°C.

6.2. Introduction

Based on the work of De Vos et al. discussed in Chapter 1, Campaniello et al. prepared methyl silica membranes from mixed MTES/TEOS sols and compared their behaviour with that of standard silica membranes, as described in detail in ref. (1).

The authors used acid-catalysed one step and two-step hydrolysis method to prepare the sols. The methyl silica sol was prepared by adding MTES towards the end of the reflux period of the pure silica sol. Methyl silica sols with various methyl concentrations were synthesized. In the two step hydrolysis method TEOS was prehydrolysed at the start of the reaction, before MTES was added, and a final addition of HNO_3 and H_2O was made. Membranes were prepared by dip-coating a mesoporous γ-alumina layer on 1 m long tubular α-Al_2O_3 supports, with a wall thickness of ~ 3 mm, as described elsewhere (2, 3). The separating layer was coated on the exterior of the tubular membrane (3). The membranes were heated in air at 250°C (methyl silica) or 400 ° C (pure silica) for 2 hours. Membranes were prepared from methyl silica sols with TEOS:MTES = 10:1 (10% MTES) and 10:3 (30% MTES). For the long term pervaporation tests with n-butanol/water mixtures at 95°C, the membranes were continuously kept on stream and the water content at the feed side was controlled to be 1-3 wt %. The authors found that the water flux for the pure silica membranes reduced to very low values within a week. This effect was attributed to pore blocking by water molecules that are bound to the internal pore surface. On increasing the $–CH_3$ content, the flux decline with time reduced. The $–CH_3$ groups make the surface more hydrophobic and a water molecule is less likely to be adsorbed on the inner surface. Another reason is that the larger pore sizes of the methyl silica membrane could prevent total blocking by water. The membranes with the highest $–CH_3$ concentration used in this study showed no appreciable degradation during the first 15 and 18 months of operation with n-butanol fluxes of ~10 and ~200 g m^{-2} h^{-1}, respectively. The authors concluded that incorporation of $–CH_3$ groups in silica membranes is a satisfactory method to obtain separating performances at temperatures up to 95°C, under the mentioned measurement conditions, for more than 18 months. At higher temperatures the separating layer undergoes changes in the structure and cannot give a high performance in separations.

This chapter describes the development of a composite microporous membrane α-alumina (macroporous)/γ-alumina (mesoporous)/hybrid silica (microporous). The hybrid silica top layer was prepared from BTESE {1,2-bis-(triethoxysilyl)ethane} and MTES (methyl triethoxysilylethane) precursors, and is described in detail in chapter 5.

6.3. Experimental

6.3.1. Membrane synthesis

Disk Shaped Membranes

Disk shaped γ-alumina membranes were prepared at the University of Twente, The Netherlands (4). The γ-alumna membranes were dip coated with hybrid silica sols that had been synthesized as discussed in the previous chapter. The membranes were coated with freshly prepared sols without dilution. A single layer of the microporous top layer was deposited. The dried membranes were calcined at 300˚C for 3 h in a N_2 atmosphere with 0.5˚C/min heating and cooling rates. The reaction parameters of sol A are as follows:
[BTESE]/[MTES]=1, $[H_2O]/([BTESE]+[MTES])=2$, and $[H^+]/([BTESE]+[MTES])=0.1$. Sol B has similar parameters, apart from a higher hydrolysis ratio, i.e., $[H_2O]/([BTESE]+[MTES])=4$. The γ-alumina supported membrane coated with sol A, was named Type A. The membrane coated with sol B, was named Type B. The preparation of Sols A and Sols B is described in detail in Chapter 5.

Tubular Membrane manufacturing

The tubular membranes were prepared at ECN, Petten, The Netherlands. The α-alumina macroporous support tubes which are used as the structural base for the actual membrane are made by ceramic paste extrusion process followed by sintering (2). The standard diameter of the support tube is ID/OD =8/14 mm, and the tubes can be obtained in a length up to 1 m. The tubular membranes consist of 2 α-alumina layers applied on the support tube by a film coat technique with an α-alumina colloidal suspension.The γ-alumina layer is applied by coating of a boehmite sol. After drying and heat treatment the boehmite transforms into γ-alumina (2). The silica membrane which is the top separation layer is prepared by means of sol-gel processing. The sol is coated onto the support followed by drying and calcination. All layers were applied on the outside of the tube.
The tubular membranes were coated with sol B, and calcined at 300 ˚C for 3 h in a N_2 atmosphere, with 0.5 ˚C/min heating and cooling rates.

6.3.2. Characterization Techniques

Permporometry

Permporometry (5) was employed to determine the pore size distribution in the microporous membrane layers. The principle of permporometry and occurrence of capillary condensation is described in detail in Chapter 2. An important point to be noted is the applicability of the Kelvin equation for characterization of nanoporous materials (pore diameter <2 nm). Strictly speaking, the Kelvin equation is only valid for membranes having pore sizes larger than 2 nm. The values should therefore be taken as approximations.

The condensable gas used in permporometry should possess certain characteristics. It should have a reasonable vapour pressure, a high evaporation rate and should be inert to the material being characterized. It should also possess good wettability and consists of small spherical molecules. CCl_4 could be an ideal candidate (6) but is also a very poisonous gas, and is therefore not used.
The type of vapour can affect the pore size distribution because of interaction with membrane surfaces (7). To date, the vapours applied for permporometry measurement have been water (8, 9), alcohols of various molecular weights (10,11), cyclohexane (11) and carbon tetrachloride (12), i.e., ranging from polar to non-polar liquids.

Carbon tetrachloride and hexane are considered to be appropriate vapours for the measurement of large pores, while water, methanol and ethanol are good for small pores (7).
The adsorption of vapour occurring before capillary condensation is another important factor affecting pore size determination (13). The adsorption of carbon tetrachloride and hexane, which are hydrophobic and non-polar molecules, is smaller than that of water and alcohols which are hydrophilic and polar in nature. It was found that the amounts of adsorbed methanol and ethanol on silica-zirconia composites were approximately ten times larger than that of cyclohexane at the same vapour pressure (13). For the case of water as a condensable vapour and membranes with relatively large pore sizes the Kelvin condensation diameter was nearly the same as the actual pore size or hardly affected by adsorption layer, since the molecular size of water is relatively small compared to alcohols. Alcohols with hydroxyl groups on one end and an alkyl group on the other absorb on the membrane surface with the silanols. Since the alkyl groups are relatively large, the effective pore size for nitrogen permeation is reduced compared to water (7).

Tsuru et al. (13) concluded that the properties of vapours (size and polarity) play an important role in measuring the pore size distribution of silica based inorganic membranes by nanopermporometry. The

vapour of water and non-polar compounds is suitable for measuring pore size distribution, and water vapour can be used to measure pore size distributions smaller than 1 nm.

In the current work, permporometry with cyclohexane as the condensable vapour and oxygen as the diffusional gas was carried out at the University of Twente, The Netherlands, on disk-shaped membranes. This setup can measure Kelvin radii down to about 1.7 nm, i.e. mesopores. The pressure on both sides of the membranes is kept constant, so that oxygen transport occurs only by diffusion. Permporometry with water vapour as the condensable gas and He as the diffusional gas at a temperature of 150°C was carried out at ECN, Petten, The Netherlands, on tubular membranes. With this set up, Kelvin radii in the microporous range can be estimated. The measurement is performed in a pressure gradient, i.e., helium transport occurs by molecular diffusion and pressure-driven transport.

SEM

Scanning Electron Microscopy was used to study the surface topography of membranes. The system was LEO 1550 FEG SEM, with a redesigned high efficiency in lens detector.

XPS

XPS was carried out on supported γ-alumina membranes with a PHI Quantera Scanning ESCA microprobe with an analysis depth of 5-75 Å and a spatial resolution < 10 μm. The Si 2p, Al 2p and O 1s energy bands were analyzed and depth profiles of the concentrations of Si, Al and O inside the membrane were obtained by sputtering with Ar^+ at a sputter rate of 40 nm/min (3 keV 2×2mmAr^+).

Gas Permeation

Membrane gas permeance was measured in the pressure-controlled dead-end mode in the temperature range of 50 to 300°C, described in detail in Chapter 2. Prior to the permeance measurements the membranes were dried for several hours at 200°C in the furnace of the setup to remove adsorbed water from the micropores (14). The disk-shaped membranes were placed in stainless steel permeance cells with a microporous top layer at the feed side. The pressure difference of 3.8 bar over the membrane was controlled by an electronic pressure controller. The gas flow through the membrane was measured by mass flow meters with a maximum flow range of 25 or 100 (ml/min STP).

Pervaporation

Pervaporation experiments on disk membranes were done in a laboratory scale pervaporation unit (15). The feed mixture contained in a 2 L heated vessel under a pressure of 2-3 bar, was pumped continuously through the feed compartment of the pervaporation unit, where it came into direct contact with the top layer of the membrane. The retenate was recycled to the feed vessel. The permeate side of the membrane was kept under near vacuum (6 mbar) with a vacuum pump. Steady state fluxes were determined by collecting the vapours at the permeate side in an ethanol-based cold trap and measuring the weight increase with time. The compositions of the feed and permeate were determined by Karl Fischer titration.

Pervaporation measurements on tubular membranes at temperatures ranging from 95°C to 150 °C were performed in a stirred vessel containing n-butanol water mixture. These experiments were carried out at ECN, Petten, The Netherlands. The pervaporation feed composition at 95 °C is 95%BuOH and 5%H_2O and at 150 °C it is 97.5% BuOH and 2.5%H_2O. The permeate pressure is in both cases 10 mbar. The feed pressure was the saturation vapour pressure of n-butanol at that particular temperature. At 95 °C, the feed pressure was equal to the atmospheric pressure. At 150 °C, the feed pressure was approximately around 5-6 bar.

6.4. Results and Discussion

SEM on membrane Type A, as shown in Figure 1a, showed a very thin hybrid silica layer of ~25 nm thickness.

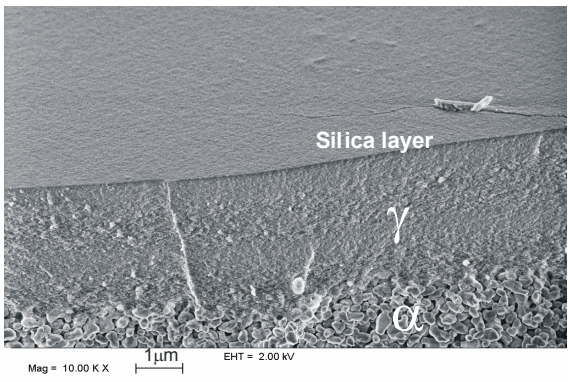

Figure 1a SEM picture of Type A membrane, with a single top hybrid silica layer of ~23 nm thickness.

A second hybrid silica coating step yielded an overall very thick hybrid silica layer of ~600 nm thickness, shown in Figure 1b. The sol spreads uniformly at the center but at the edges the liquid receded, forming globular structures on the surface. For a liquid to wet or adhere to the surface, the surface energy of the substrate must be greater than the surface tension of the liquid. Surface tension is a measure of the surface energy and it is the property by which liquids through contraction of the surface tend to bring the volume onto a shape having the least surface area. The higher the surface energy of the solid substrate relative to the surface tension of the liquid, the better will be the wettability and smaller the contact angle. Apparently, the underlying hybrid silica layer has such a low surface tension that the second wet layer does not spread. Hence there is no wetting. Figure 1c shows the SEM picture of the surface at the edges. The low surface tension of the hybrid silica layer is indicative of a hydrophobic surface.

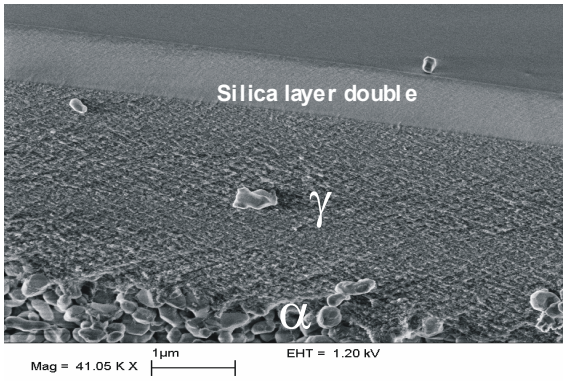

Figure 1b SEM picture of Type A membrane with a double-coated layer of hybrid silica. Picture taken at the center of the membrane.

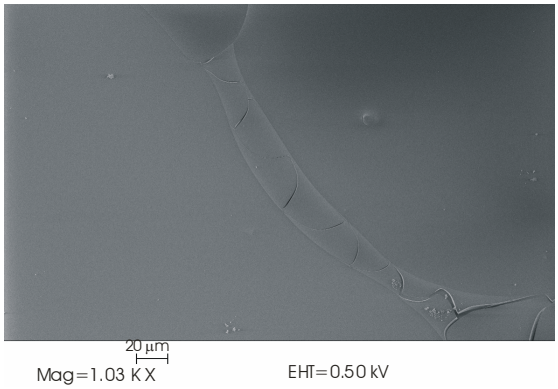

Figure 1c SEM picture of Type A membrane with a double-coated layer of hybrid silica. Picture taken near the edge of the membrane.

The layer thicknesses observed by SEM were confirmed by XPS. Figure 2a shows the atomic fractions of Si and Al as a function of depth inside single- and double-coated Type A membranes. The XPS

depth profiles confirm the observations made by SEM. Al is the majority cation up to the surface of the single-coated membrane in Figure 2a. Some silicon enrichment can be observed in the first 10-30 nm, but it seems that no well-defined hybrid silica layer has formed. The silica phase penetrated at least partly into the γ-alumina support. For the double-coated membrane, a separate Si-containing top layer can be recognized, and a substantial fraction of Al is observed at a depth of approximately 400 nm and further. This confirms the presence of a thick hybrid silica top layer seen by SEM. These strongly differing layer thicknesses of single- and double-coated Type A membranes may be explained by considering that the hybrid silica sol particles of Type A are ~1.4 nm in diameter, and may therefore penetrate into the ~6 nm diameter pores (14) of the underlying γ-alumina layer, probably as a result of capillary suction of that layer.

To prevent the penetration of the sol particles into the mesoporous γ- alumina layer, an alternative is to work with sols with a larger particle size. The sol Type B with average particle diameter of ~ 8 nm was used. Prior to deposition the sol was diluted 10 times in order to obtain thin, homogeneous layers. Figure 1d shows the corresponding SEM picture.

For the resulting single and double coated Type B membranes, the Si and Al concentrations were monitored with XPS. The XPS depth profile in Figure 2b shows that the Si concentration of the single coated membrane decreases to zero at a corresponding depth of 60-120 nm. Further into the membrane the Al concentration starts to rise, indicating the presence of the intermediate γ-alumina layer. The larger sized sol and dilution help in getting a uniform layer, which does not penetrate the support. For the doubly coated membrane, the XPS depth profile shows that the Si concentration decreases to zero at a corresponding depth of approximately 120-160 nm. This is roughly twice the thickness of a single coated layer.

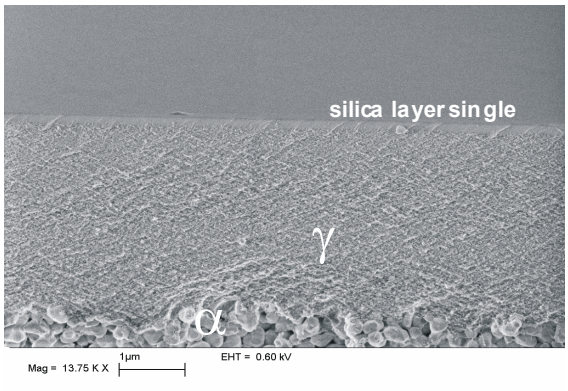

Figure 1d SEM picture of Type B membrane with a single top layer of ~120 nm.

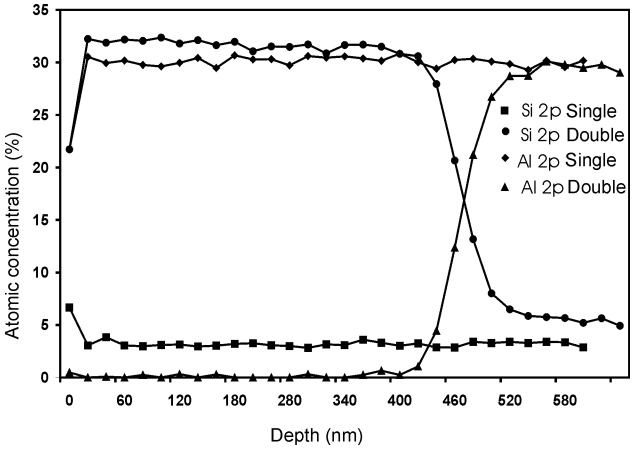

Figure 2a XPS depth profile of singly and doubly coated Type A membranes.

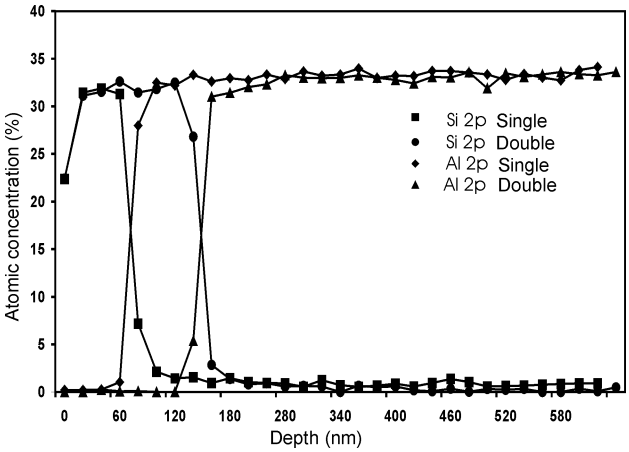

Figure 2b XPS depth profile of singly and doubly coated Type B membranes.

The Type A membrane showed zero oxygen flux with permporometry using cyclohexane as the condensable vapour. When the pores of the membrane are saturated with cyclohexane, oxygen molecules with a kinetic diameter of 3.46 Å (14) are not able to pass through the membrane. However, permporometry with water vapour as the condensable vapour and He as the diffusional gas can be employed to obtain an estimate of the pore size distribution of microporous layers. Water, being smaller and more polar than cyclohexane, can be used to block membrane micropores, while He with a kinetic diameter of 2.60 Å (14), can pass through smaller pores than oxygen.

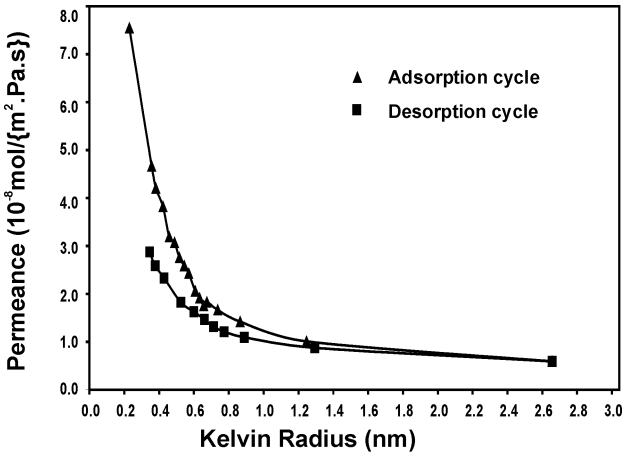

Figure 3a Permeance of He (mol/m^2.s.Pa) versus Kelvin radius (nm) for Type A membrane, for adsorption and desorption cycles.

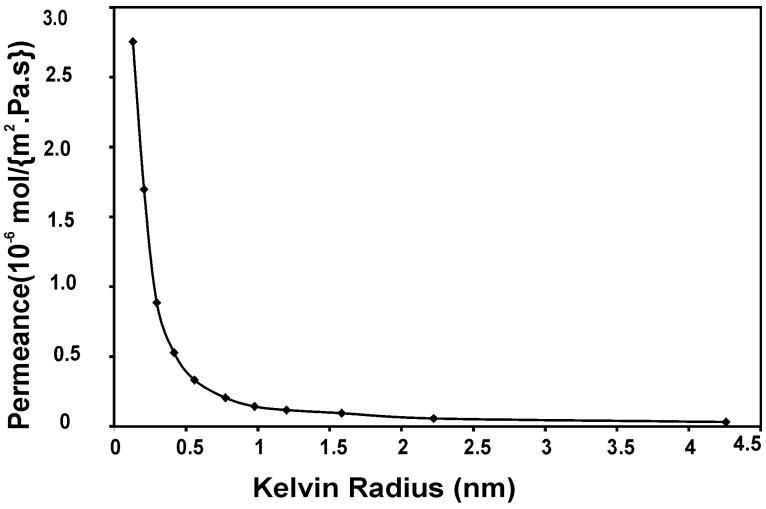

Figure 3b Permeance of He (mol/m^2.s.Pa) versus Kelvin radius (nm) for silica membrane using TEOS and MTES (30%) as precursor.

Permporometry experiments with water as the condensable vapour and He as the diffusion gas gave distributions for membrane Type A as shown in Figure 3a. Figure 3a gives a plot of the permeance of He gas versus Kelvin radius for the adsorption and desorption cycles, for membrane Type A. The theory of adsorption and desorption cycles has been discussed in Chapter 2. These pore size distributions compare well with the distribution of the MTES/TEOS-based silica membrane containing 30% MTES (1), which is shown in Figure 3b for the sake of comparison. The sol used in the latter case was prepared by using TEOS and MTES (30 mol%) as precursors, as described in ref. (1). The curves of the MTES/TEOS hybrid silica membrane and the Type A membrane do not differ significantly, except that the Type A membrane seems to be having more pores > 2 nm .

Permporometry characterization of microporous ceramic membranes has also been studied by Tsuru et al. (15). The authors evaluated nano-order pore size of membranes using this technique. Nitrogen was used as a carrier, and silica-zirconia ceramic membranes were used for study. The pore size distribution, based on Kelvin equation was evaluated over a range of 0.5-30 nm, using water as a condensable vapour. Vapours of methanol, ethanol, isopropanol, carbon tetrachloride, and hexane were also studied. For the case of relatively large pore sizes (larger than 1 nm), pore size distributions obtained by water vapour agreed very well with those by carbon tetrachloride and hexane. However, the pore sizes measured using alcohols were found to be smaller than those determined by water vapour.

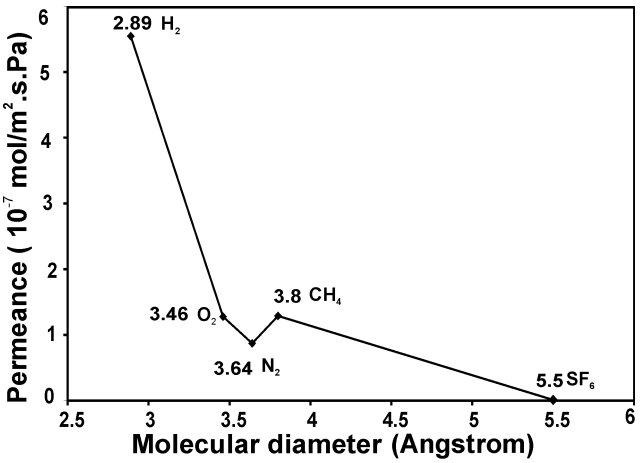

Figure 4 Gas permeance of H_2, O_2, N_2 CH_4, and SF_6 (mol/m^2.s.Pa) versus molecular diameter (Å) at 200°C for Type A membrane.

Figure 4 shows the permeance {mol/(m^2.s.Pa)} of a Type A membrane versus the molecular kinetic diameter of a series of dry gases at 200 °C. The mean molecular diameters of gases H_2, O_2, N_2, CH_4, and SF_6 are 2.89, 3.46, 3.64, 3.8, and 5.5 Å, respectively (14). The results indicate that the layer has a microporous nature, as there is a sieving mechanism for gases of different diameters. The gas SF_6 with the largest kinetic diameter of 5.5 Å has a zero permeance, so that the maximum pore size is smaller than this value. Molecular sieving refers to the complete blocking of transport of molecules with a certain size or shape and the free passage of smaller or differently shaped molecules. No relationship between the molecular mass and the permeance could be established, from which it can be concluded that Knudsen-type diffusion does not occur in this membrane. In Knudsen diffusion, the permeance of gases is inversely related to the square root of the molecular mass. De Vos et al. (16) prepared hydrophobic silica membranes using TEOS and MTES as precursors for gas separation. These membranes show very high gas permeance for small molecules, such as H_2, CO_2, N_2, O_2, and CH_4, and permselectivities of 20-50 for these gases with respect to SF_6 and larger alkanes like C_3H_8 and i-C_4H_{10}.

The authors have reported a very high permeance for N_2 and O_2 of 4×10^{-7} and 7×10^{-7} mol/(m^2.s.Pa), respectively.

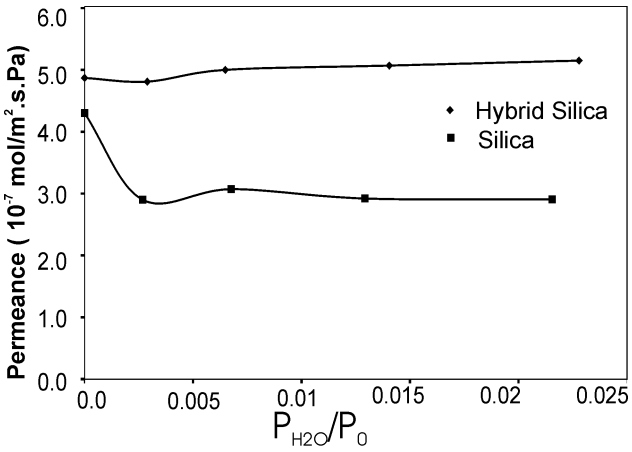

Figure 5 Permeance of H_2 versus P_{H2O}/P_0 for hybrid membrane Type A and normal silica.

Gas permeation experiments in the presence of water vapour were performed at 200 °C on the hybrid membrane Type A. Single H_2 gas permeation experiments were carried out with water vapour at defined partial pressures. As can be seen from the figure no appreciable decrease in permeation of H_2 is observed when the hybrid membrane Type A is exposed to water vapour. For the sake of comparison Figure 5 also shows the permeance of H_2 gas when exposed to water vapour for a normal silica membrane modified with fluorinated silane (17).
These results indicate a hydrophobic nature of the hybrid membrane as water vapour does not adsorb on the inner walls of the pores. Thus, the passage of H_2 molecules is not hindered by the presence of water vapour.

Pervaporation tests on single coated Type A disk membranes with a mixture of 95 wt% n-butanol and 5 wt% water at 75-95°C showed a negligible flux and virtually no selectivity. The low flux can be attributed to the penetration of the hybrid silica layer into the support, as confirmed with the XPS depth profile and SEM. The high transport resistance is the result of suffocation of the pores by the hybrid sol. Table 1 shows the fluxes of water and n-butanol, and the separation factors. The separation factors are especially low if we take into account the effects of preferential evaporation of water over butanol, so that a separation factor larger than unity is expected even if the membrane were not selective at all.

Table 1 Pervaporation data for Type A membrane at 75 and 95°C, for 95% n-butanol-5% water. Measurements were done at ECN, Petten, The Netherlands.

temperature(°C)	Water flux {g/(m^2.h)}	Butanol flux {g/(m^2.h)}	total flux{g/(m^2.h)}	water content permeate(%)	Separation factor
75	321	369	690	46	16
95	444	954	1398	32	9

Figure 6 shows the pervaporation results of a mixture of 95 wt% n-butanol–5 wt% water at 95 °C for Type B membrane. The Type B membrane, undiluted and single coated, showed a separation factor of 100 for 100 h without significant deterioration of performance. However, the fluxes are hardly larger than those of membrane Type A. In any case the hybrid Type B membrane is selective and is able to dehydrate butanol.

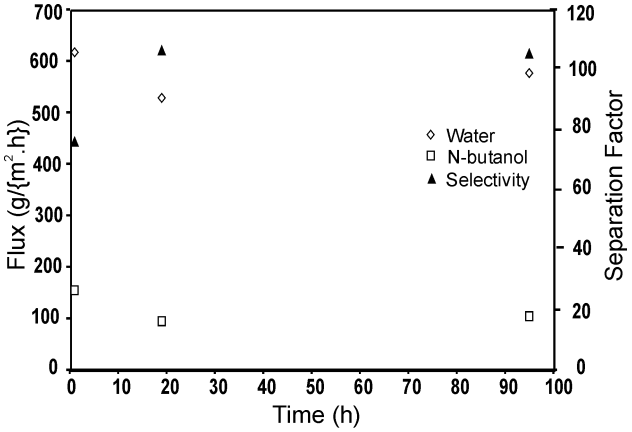

Figure 6 Flux and separation factor versus time for Type B membrane, for 95% n-butanol-5% water at 95° C.

For a 95% ethanol- 5% water mixture, membrane Type B showed flux and separation factors of 1.59 {kg/(m^2.h)} and 4.45, respectively at 75 °C. The separation factor is higher for the n-butanol-water mixture than the ethanol-water mixture, which can be explained by the larger kinetic diameter of n-butanol. Ethanol has a kinetic diameter of 0.52 Å (18). In addition ethanol is more hydrophilic than n-butanol, which explains the higher permeability of the membrane for ethanol. In order to compare how the hybrid silica membranes in this study compares with normal silica, the work of Sekulic et al. (19) is referred to. They found that for a 90/10 EtOH/H_2O system the total flux was1.0 kg/m^2 h and the separation factor was 800. For a 95/5 2-BuOH/H_2O system the total flux was 1.0 kg/m^2 h and the separation factor was 1000. These pervaporation fluxes and separation factors are reported at 80 °C.

Long Term Pervaporation Tests

For the economic application of inorganic membranes, we need to study their reliable, constant long term behaviour under relatively harsh conditions (1). Pervaporation tests were therefore carried out on tubular membranes at a temperature of 150°C, at which temperature normal silica and the MTES/TEOS-based silica (1) are not stable. Figure 7a and 7b show the separation factor and flux versus time for a tubular membrane coated with sol B, for a feed mixture of 97.5 wt% n-butanol and 2.5 wt% water mixture. The separation factor decreases from 300 to 50 in the first 20 days of operation. It then increased and remained constant at a value of ~150 for at least 3 months. The ability to function at a higher temperature, i.e., 150°C is remarkable, when it is compared with the relatively fast deterioration of conventional silica membranes at 95°C (1), and the deterioration of methyl silica above 130°C (1).

The seemingly strange trend of the separation factor with time as shown in Figure 7a, first a decrease, followed by an increase, may be due to the initial interaction of the solvent mixture with the hybrid silica network in the early stages of operation. As time progresses, the network seems to stabilize with respect to adsorption of solvents in the hydrophilic and hydrophobic parts and the separation factor increases and remains constant. Another interpretation could be that the hydrocarbon chains in the siloxane network are flexible. Under pressure, restructuring of the network takes place, resulting in compression. This results in a decrease in flux initially and then later then an increase in flux which becomes steady.

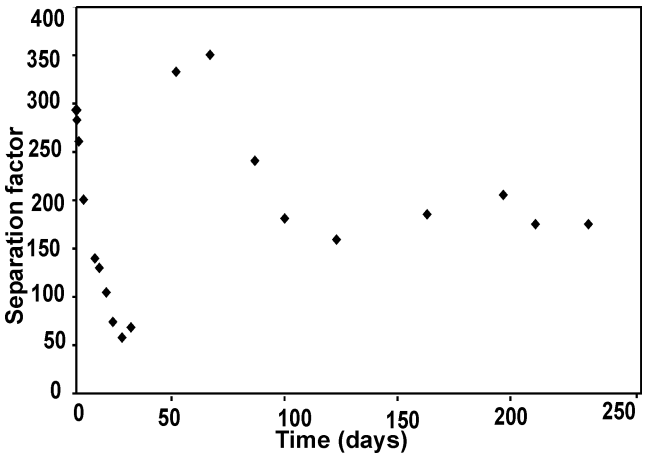

Figure 7a Separation factor versus time for tubular membrane coated with sol B, for 95% n-butanol-2.5% water at 150 ° C.

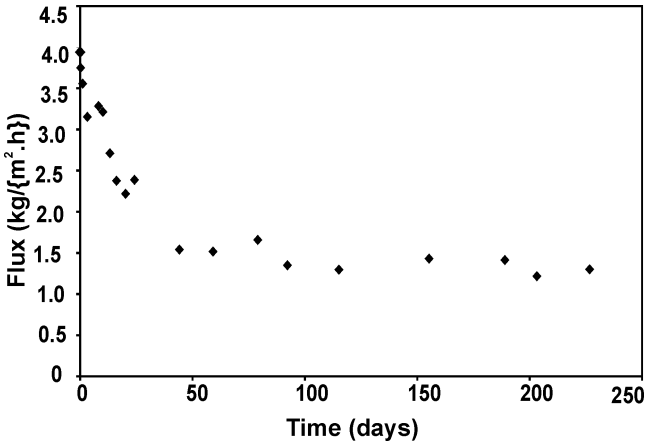

Figure 7b Flux versus time for tubular membrane coated with sol B, for 95% n-butanol- 2.5% water at 150 ° C.

6.5. Conclusions

The hybrid silica membrane made from BTESE and MTES precursors has proven to be successful in gas separation and dehydration of a mixture of 97.5% butanol – 2.5% water at a temperature of 150 °C. In comparison with conventional silica membranes, which operate at a maximum temperature of ~95 °C, this is a significant improvement of thermal stability. Gas separation experiments indicate a microporous membrane, as there appears to be a molecular sieving mechanism for gases of different diameters. The external surface and internal pore surface appear to be hydrophobic.

6.6. References

1) J. Campaniello, C. W. R. Engelen, W. G. Haije, P. P. A. C. Pex and J. F. Vente, Chem. Commun., 2004, 834-835.

2) H. M. van Veen, Y. C. van Delft, C. W. R. Engelen and P. P. A. C. Pex, Sep. Purification Technol., 22-23, 2001, 361-366.

3) B. C. Bonekamp, "Preparation of Asymmetric Ceramic Membrane Supports by Dip-Coating", Fundamentals of Inorganic Membrane Science and Technology, Vol.,4, edited by A. J. Burggraaf and L. Cot, Elsevier, Amsterdam, 1996.

4) R. M. de Vos, H. Verweij, J. Membr. Sci. 143, 1998, 37.

5) C. Eyraud, M. Betemps, J. F. Quinson, F. Chatelut, M. Brun, and B. Rasneur, Bull. Soc. Chim. France, 237, 1984, 9 -10.

6) D. E. Fain, "A dynamic flow-weighed pore size distribution", in: J. Charpin and L. Cot (Eds.), First Int. Conference on Inorganic Membranes, Montpelier, France, 1989, pp. 199-205.

7) M. G. Katz, G. Baruch, J. Membr.Sci., 58, 1986, 199.

8) M. Asaeda, S. Kitao, Key Eng. Mater., 61/62, 1991, 295.

9) M. Asaeda, T. Tsuru, Porous silica-zirconia membranes for separation of organic molecular mixtures by pervaporation, in: Proceeedings of the Fourth International Conference on Inorganic Membranes, Gatlinburg, USA, 1996, p. 68.

10) F. P. Cuperus, Characterization of ultrafiltration membranes: pore structure and top layer thickness, PhD. Thesis, University of Twente, The Netherlands, 1990.

11) F. P. Cuperus, D. Bargeman and C. A. Smolders, J. Membr. Sci., 71, 1992, 57-67.

12) G. Z. Cao, J. Meijerink, H. W. Brinkman and A. J. Burggraaf, J. Membr. Sci., 83, 1993, 221-235.

13) T. Tsuru, T. Hino, T. Yoshioka, M. Asaeda, J. Membr. Sci., 186, 2001, 257-265.

14) R. M. de Vos, Hydrophobic Silica Membranes, PhD Thesis, University of Twente, Enschede, the Netherlands, 1998.

15) J. Sekulic, J. E. ten Elshof, and D. H. A. Blank, Langmuir, 21, 2005, 508-510.

16) R. M. de Vos, W. F. Maier, H. Verweij, J. Membr. Sci., 158, 1999, 277-288.

17) V.Boffa, J. E. ten Elshof, D. H. A.Blank, to be submitted.

18) J. E. ten Elshof, C. R. Abadal, J. Sekulic, S. R. Chowdhury and D. H. A. Blank, Micropor. Mesopor. Mater., 65, 2003, 197-208.

19) J. Sekulic, J. E. ten Elshof, D. H. A. Blank, J. Membr. Sci., 254, 2005, 267-274.

Chapter 7 Conclusions and Recommendations

In this chapter, the work described in this thesis is discussed in a broader perspective. The goal of the work was to increase the hydrothermal stability of silica and at the same time tackle the problem of hydrophilicity facing silica based ceramic membranes. Two approaches have been followed, namely grafting and in situ synthesis for mesoporous and microporous layers, respectively.

7.1. Grafting

Grafting the underlying intermediate mesoporous membrane has been done with organochlorosilanes. The hydrocarbon group of the organochlorosilane imparts the desired hydrophobic character. Chapter 3 and Chapter 4 show the effects of modification of γ-alumina powders and supported membranes with methyl chlorosilanes. A detailed structural study on the grafted materials is provided. A drawback of the grafting procedure is that the pore sizes are effectively reduced due to the tail length of the organosilane. In case of multifunctional organosilanes there is multilayer deposition, due to the formation of a polymerized network. This leads to a strong increase of the transport resistance.
Grafting the intermediate mesoporous layer or the microporous top layer of a composite membrane system with organometallic precursors having an ethoxy, chloro, or a hydroxyl hydrolysable group are alternative routes. An interesting field of study could also be the use of fluorinated precursors, though they suffer from the drawback that they are usually available only with a long fluorohydrocarbon group, hence decreasing the pore size of the membrane system substantially.

7.2. In Situ Modification

Incorporation of the hydrocarbon group by in situ reaction of starting precursors was used for the formation of organofunctional silanes. By using the precursor 1,2–bis(triethoxysilylethane), having the bridging group $-CH_2-CH_2-$, organic groups are incorporated into the backbone of the network. The bridging group repeats itself periodically in the polymer chain. In the present work, the bridged precursor was used in combination with the precursor methyl tri-ethoxysilane.

In Chapter 5 the development of the hybrid sol was discussed. A nanosized organosilica sol was obtained, which exhibited considerable stability. In Chapter 6, pervaporation studies showed that a microporous hybrid membrane could be made, which was able to work at higher temperatures (150°C) than microporous silica, and was effective in dehydrating n-butanol for a longer period of time (>3 months). The external surface and internal pore surface appeared to be hydrophobic, from SEM and gas permeation experiments.

Adsorption studies on hybrid powders formed by a combination of 1,2-bis(triethoxysilyl)ethane and methyl triethoxysilylethane showed them to be impervious to nitrogen gas, but gave larger values with a smaller molecule like acetylene. An interesting field of study is to increase the porosity of the system by incorproration of surfactant group or an organic molecule, leading to the formation of periodic mesoporous organosilicas.Work has been done in this field. Theije et al. (1) have characterized mesoporous organosilica films for ultralow-k dielectrics. The authors used surfactants as templates in organosilicate matrixes, starting from tetraethoxysilane and methyltrimethoxysilane. Films containing 50-60% methyltrimethoxysilane in tetraethoxysilane and cetyl trimethylammonium bromide as a surfactant appeared most suitable as a low-k dielectric material.

The hybrid organosilica sols of 1,2-bis(triethoxysilyl)ethane and methyl triethoxysilylethane gave a lamellar MCM-50 type phase which collapsed upon calcinations, using cetyltrimethylammonium bromide (CTAB) as self-assembling surfactant. However, the porosity of the calcined system increased by approximately 30 %, while the system was still microporous. This could be a method to make microporous thin films with increased porosity and permeance.

Asefa et al. (2) have used cetyltrimethylammonium bromide to bring periodicity to a hybrid system of 1,2-bis(triethoxysilyl ethane) and TEOS (tetraethylorthosilicate). Powder X-ray diffraction patterns showed the presence of periodic arrangement of channels in a hexagonal geometry with a unit cell dimension a ≈ 47 Å. TEM images of the materials showed hexagonal symmetry mesopores with a pore centre-to-centre distance of ~ 45-50 Å. Nitrogen adsorption methods at 77K were found to be of type IV, which is characteristic of a mesoporous material. The average BET surface area was 637 g/m^2.

By adopting the above mentioned approaches we have brought about a hybrid character to an inorganic composite system i.e. we were able to obtain sol- gel derived hybrids as well as grafted organic groups into inorganic materials. A small decrease in hydrophilicity of the silica surface is a step towards energy saving and cost effective operations. A step forward could be to have a microporous silica layer on top of the grafted intermediate layer. In this way the hydrophilic character provided by the intermediate layer could be reduced.

7.3. Future outlook for hybrid materials

The hybrid materials show a combination of the characteristics of inorganic and organic materials (3). Hybrids of polymers bonded to an amorphous oxide sol-gel matrix weakly may have transparent, colorless, homogeneous characteristics with good mechanical properties. It is possible to tune the porosity as well as the hydrophilic/hydrophobic balance. Bifunctional alkoxysilanes R'R"$Si(OR)_2$ where R' and R" are alkyl or aryl groups make the oxide chain networks more flexible, but will also increase the average pore size as they are difunctional and thus act as chain extenders. Since alkyl and aryl groups are hydrophobic, polar solvents such as water or alcohol are not retained by the gel (3). Polyfunctional alkoxy silanes bring about a variable spacing between silicon atoms yielding materials with varying rigidity. Their specific surface area can go up to 1260 m^2/g (3).

Moreau et al. (4) synthesized a bis-urea silylated precursor which on acidic hydrolysis forms a self organized hybrid silica with lamellar order. They attributed the interactions of the urea groups to H bondings. Self organization by H-bonds is an attractive property of these materials. Hybrid solids are of importance in molecular recognition, catalysis, transport, electronic, optical and magnetic applications (4). In this context it is important to control and engineer the structure at the nanoscopic and macroscopic levels.

By using these bifunctional precursors, for membrane preparation applications we are able to fine tune the properties of the membrane as per requirements.
The synergy on combining inorganic organic materials holds great potential and needs to be harnessed in the future.

7.4. References

1) F. K. de Theije, A. R. Balkenende, M. A. Verheijen, M. R. Baklanov, K. P. Mogilnikov and Y. Furukawa, J. Phys. Chem B 107(18), 2003, 4280-4289.
2) T. Asefa, M. J. Maclachlan, N. Coombs and G. A. Ozin, Nature, 402, 1999, 867-870.
3) A. C. Pierre, "Applications of sol gel processing"; pp. 347-380, in: Introduction to Sol-Gel Processing, Kluwer Academic Publishers group, Dordrecht, The Netherlands, 1998.
4) J. J. E. Moreau, L. Vellutini, M.W. C. Man, P. Dieudonne, and J. Sauvajol, J. Am. Chem. Soc. 123, 2001, 7957-7958.

List of Publications

1) A. Sah, H.L.Castricum, A. Bliek, D.H.A. Blank and J.E. ten Elshof, "Hydrophobic modification of γ-alumina membranes with organochlorosilanes," Journal of Membrane Science, 243, 2004, 125-32.

2) H.L. Castricum, A. Sah, M.C. Mittelmeijer-Hazeleger, and J.E. ten Elshof, "Hydrophobisation of mesoporous γ-Al_2O_3 with organochlorosilanes efficiency and structure", Microporous and Mesoporous Materials, 83, 2005, 1–9.

3) H.L. Castricum, M.C. Mittelmeijer-Hazeleger, A. Sah, and J.E. ten Elshof, "Increasing the hydrothermal stability of mesoporous SiO_2 with methylchlorosilanes – a 'structural' study", Microporous and Mesoporous Materials, 88, 2006, 63-71.

Patent

A. Sah, H.L. Castricum, J. Vente, D.H.A. Blank, and J.E. ten Elshof, Microporous molecular separation membrane with high hydrothermal stability, European Patent EP 06100388.5.

Acknowledgements

The four years of PhD are like a journey, and it is the joys and moments shared together that make it a memorable experience. I will cherish the days spent at IMS.

Every new start of a project requires a mentor. Thank you Dave and Andre, for always being there and guiding me through the rough rides.

I have enjoyed the coffee breaks and all the birthday celebrations with the IMS colleagues.

I would like to thank my colleagues Jose, Monse, Jelena, Mai, Tijana, Krisztina, Beatrix, Sankho, Riaan, Fredric, Richard, Vittorio, Mattijn, Frank, Arjen M, Arjen J, Thang, Paul, Koray, Gerald for the help and cooperation always.

A special thank you for the technical help provided by Mieke, Cindy, Attila, Henk, Gerrit, Herman.

Thank you Marion for the help with the formalities and paper work.

I would like to thank Louis, Henny, Bernard, Guus, Henk Kruidhof for their co-operation.

Thanks for the SEM (Mark Smithers) and XPS measurements (Albert and Emiel).

I would like to end by thanking all IMS members, for being there.

Hessel, the discussions with you were very useful. Thank you for all the help.

My Indian friends Ruchira, Kanya, Sheela, Kavitha-Kiran, Vasughi, Pramod-Vishakha, and the others too, thank you for the times we spent together.

A thank you to my parents and sister for supporting me in all my endeavours.

Ashima .